Precision calibration of the DØ liquid argon calorimeter and algorithms of electron, photon and jet reconstruction

Jan Stark
Laboratoire de Physique Subatomique et de Cosmologie
Grenoble, France

for the DØ Collaboration

Calorimetry for High Energy Frontier, Paris, 22-25 April 2013

W boson mass

Today's measurements are precise enough to test the electroweak theory at the **loop level**.
At higher orders (including loop diagrams), the mass of the W boson can be expressed as:

$$M_W = \sqrt{\frac{\pi \alpha}{\sqrt{2} G_F}} \frac{1}{\sin \theta_W \sqrt{1 - \Delta r}}$$

Radiative corrections (Δ r) depend on M_t as $\sim M_t^2$ and on M_H as $\sim \log M_H$. They include diagrams like these:

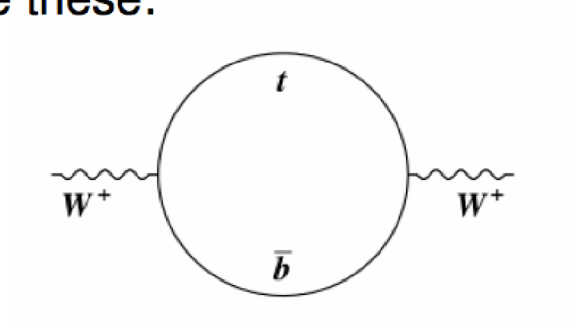

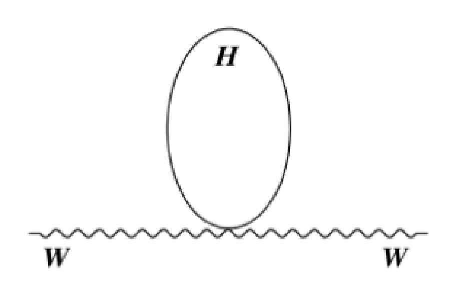

Precise measurements of M_W and M_t constrain SM Higgs mass.

Additional contributions to Δr arise in various extensions to the Standard Model, *e.g.* in SUSY:

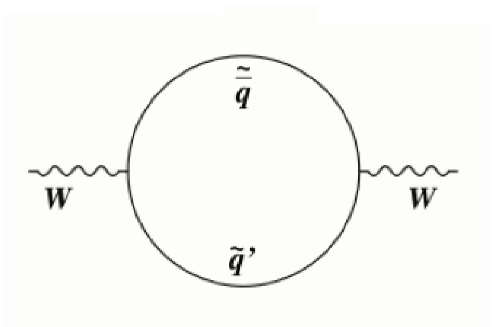

Current state of the art

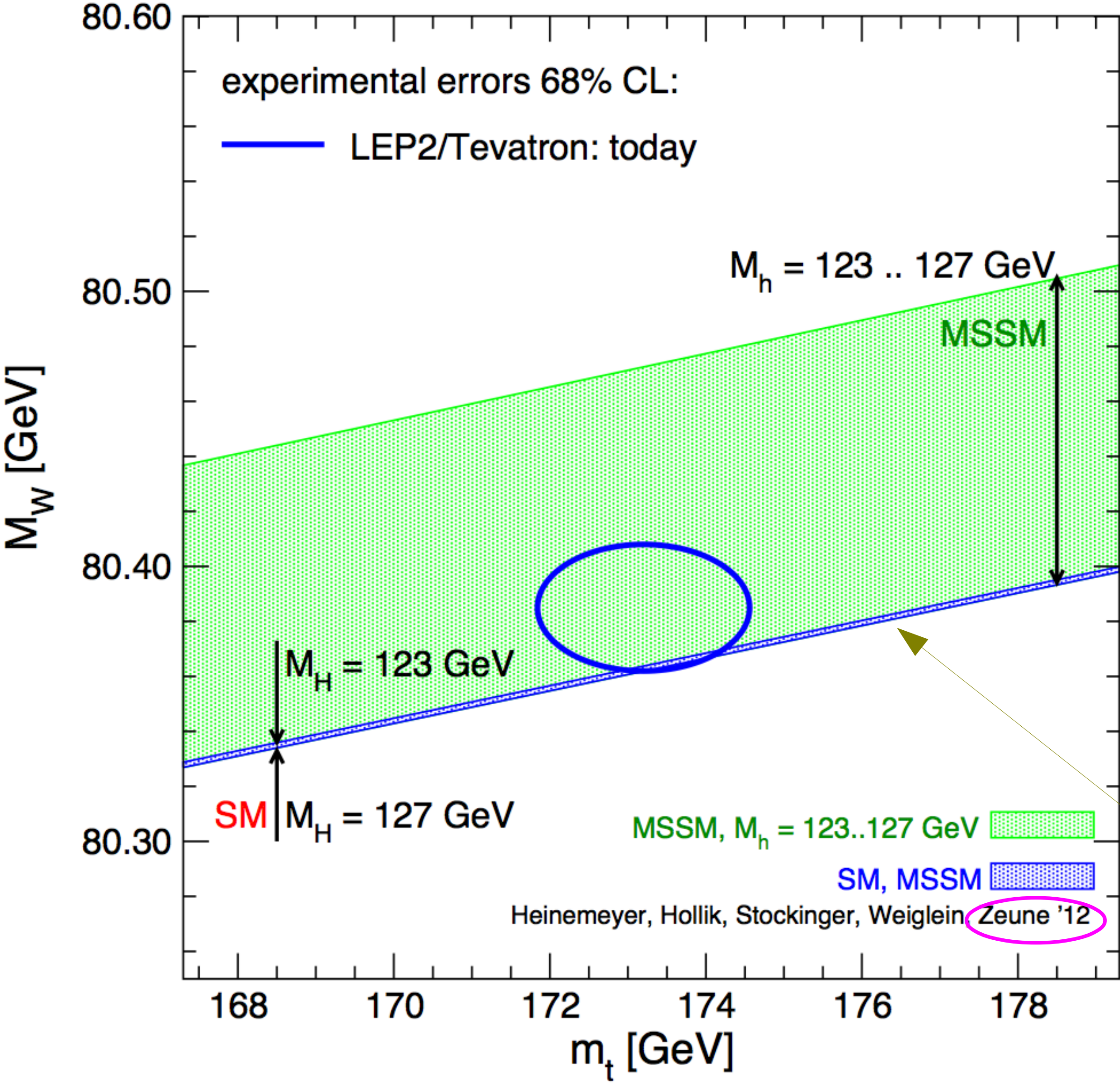

For equal contribution to the Higgs mass uncertainty need:

$\Delta m_W \approx 0.006\ \Delta m_t$.

Current (2013) Tevatron average:

$\Delta m_t = 0.87$ GeV

⇒ would need: Δm_W = 5 MeV

⇒ we have: Δm_W = 15 MeV

Before Run II had: Δm_W = 30 MeV

At this point, *i.e.* after all the precise top mass measurements from the Tevatron, the limiting factor here is Δm_W, not Δm_t .

In the context of the Standard Model (SM), the mass of the new boson discovered at CERN is inside this blue band.

W mass: measurement method

W → e ν signal

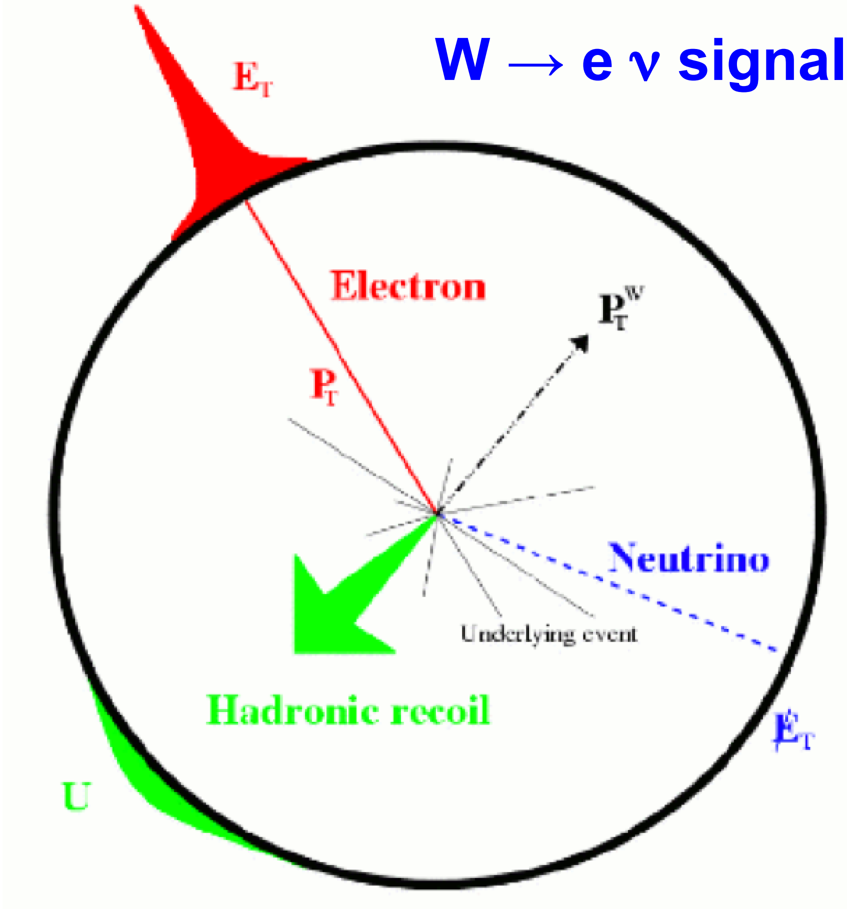

Z → e e events provide critical control sample

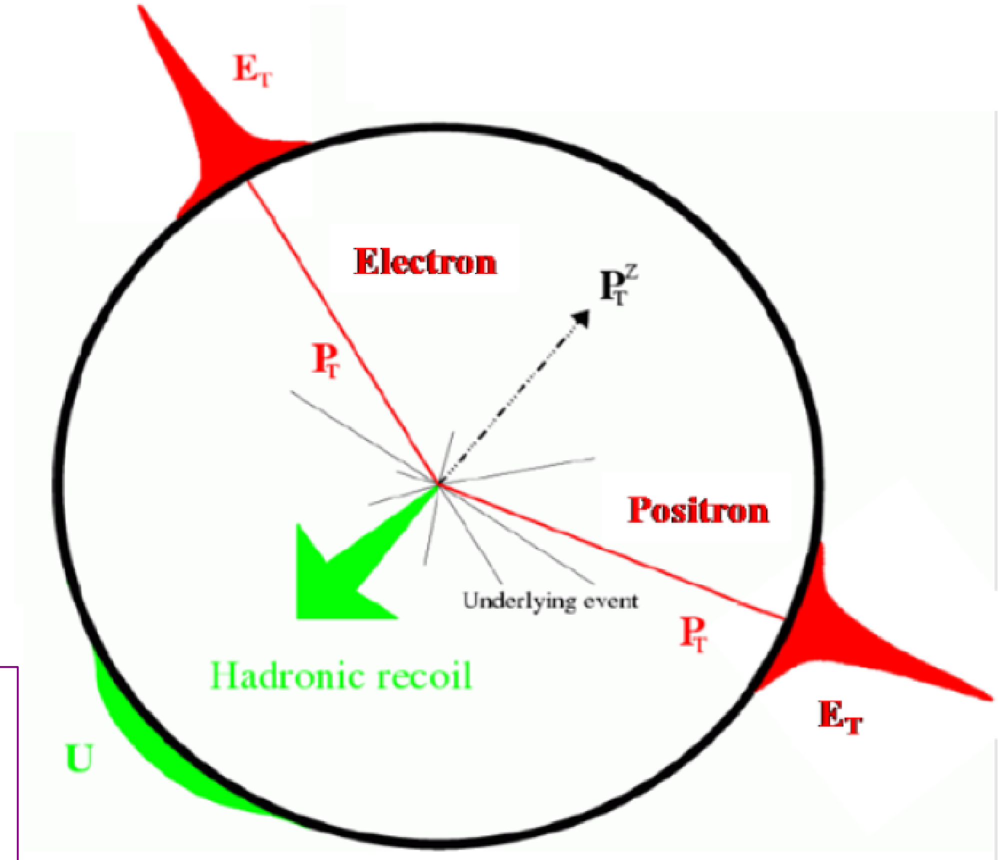

In a nutshell: measure two objects in the detector:
- Lepton (in our case an electron), need energy measurement with 0.1 per-mil precision (!!)
- Hadronic recoil, need ~1 % precision

Top mass: lepton + jets channel

The most precise measurements of the top quark mass use the "lepton + jets" channel.

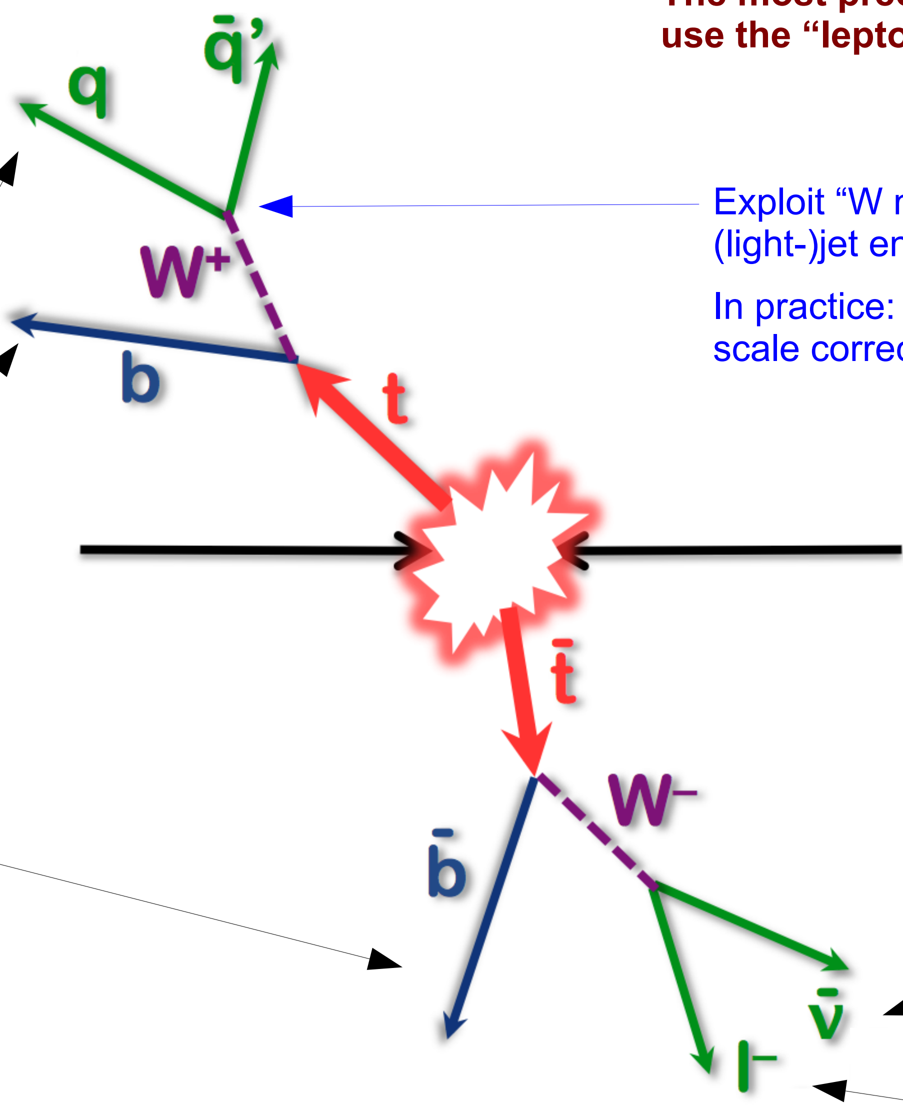

Exploit "W mass constraint" to calibrate the (light-)jet energy scale *in situ*, i.e. in the $t\bar{t}$ events themselves.

In practice: correction on top of the nominal jet energy scale corrections.

several jets of different flavours

Missing transverse energy

One isolated high-p_T lepton (in practice: electron or muon)

The upgraded DØ detector

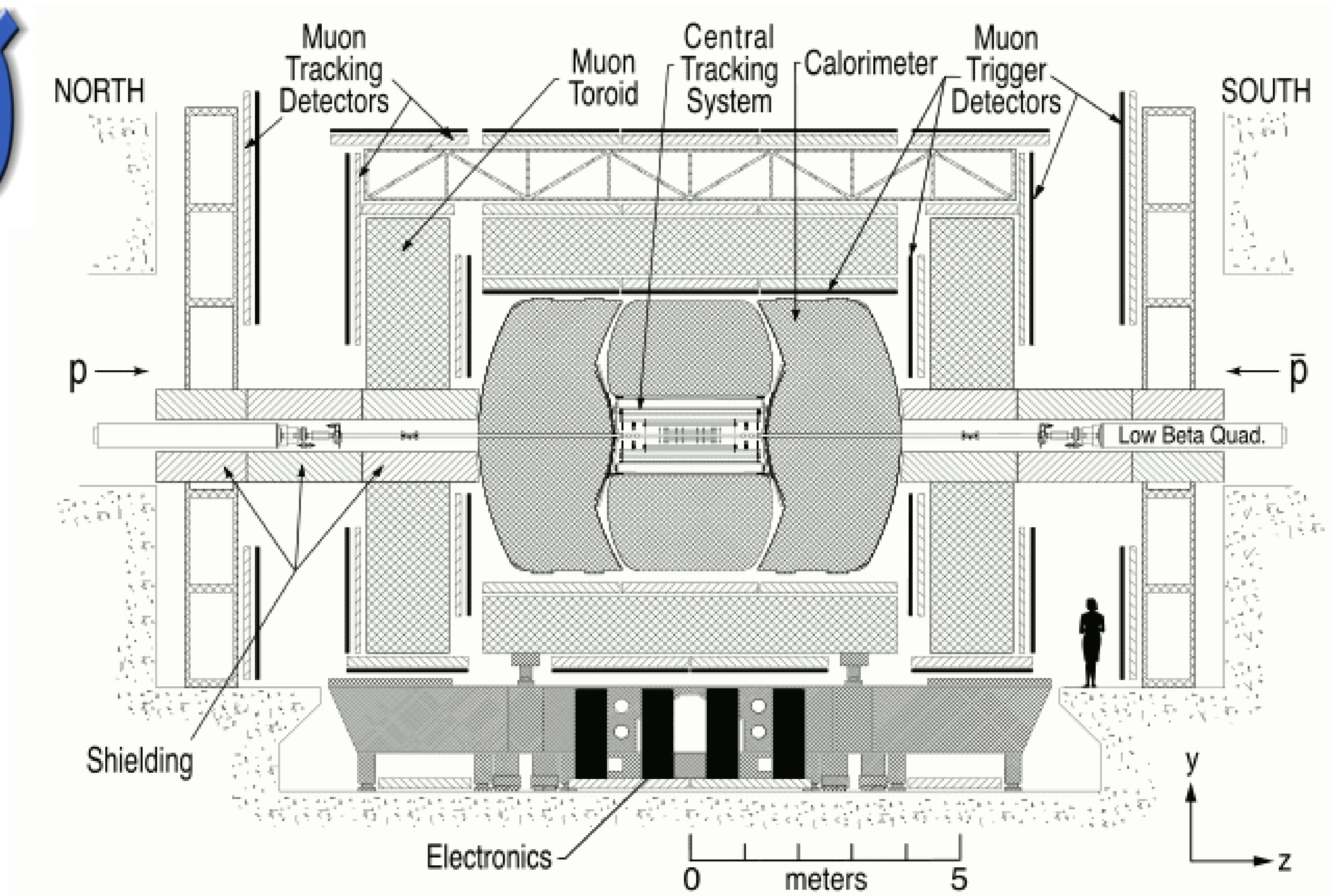

Overview of the calorimeter

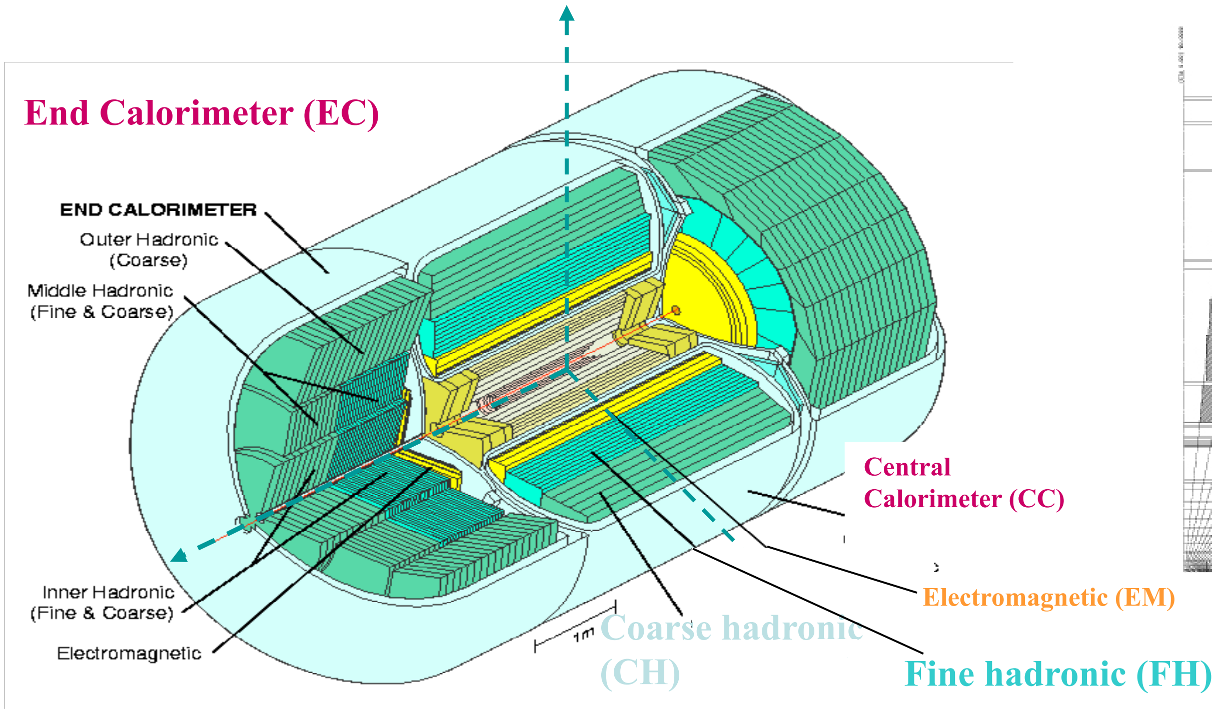

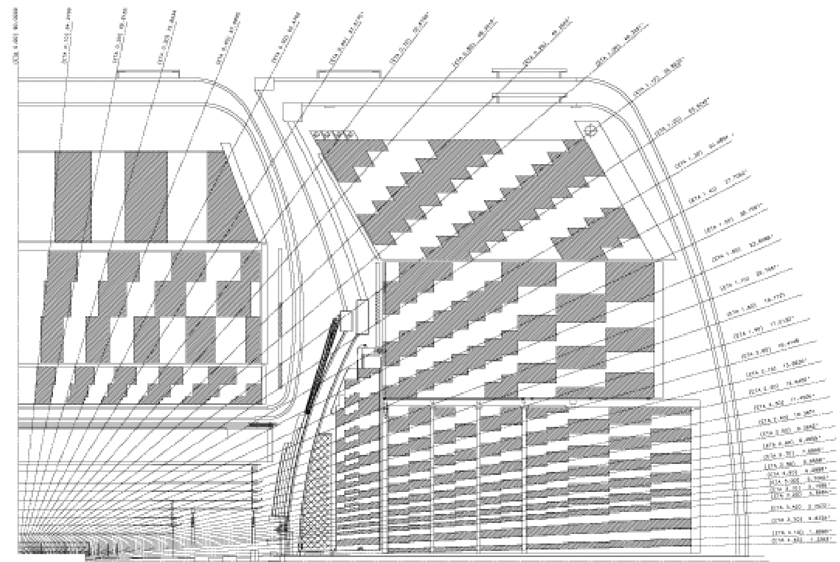

46000 cells

50 dead channels

- Liquid argon active medium and (mostly) uranium absorber
- Hermetic with full coverage : $|\eta| < 4$
- Segmentation (towers): $\Delta\eta \times \Delta\phi = 0.1 \times 0.1$

  (0.05x0.05 in third EM layer, near shower maximum)

Gain calibration: strategy

Factorise into two parts:

- calibration of the calorimeter electronics,
- calibration of the device itself.

Electronics calibrated using pulsers.

Calibration of the device itself:

Determine energy scale (i.e. multiplicative correction factor), ideally per cell.

Use phi intercalibration to "beat down the number of degrees of freedom" as much as possible.

Use $Z \rightarrow e^+ e^-$ to get access to the remaining degrees of freedom, as well as the absolute scale.

Phi intercalibration

Qiang Zhu, "*Measurement of the W boson mass in $p\bar{p}$ collisions at sqrt(s) = 1.8 TeV*", PhD thesis, April 1994, available from the D0 web server, and references therein.

$p\bar{p}$ beams in the Tevatron are not polarised.

→ Energy flow in the direction transverse to the beams should not have any azimuthal dependence. Any Φ dependence must be the result of instrumental effects.

Energy flow method:

Consider a given η bin of the calorimeter. Measure the density of calorimeter objects above a given E_T threshold as a function of Φ. With a perfect detector, this density would be flat in Φ.

Assuming that any Φ-non-uniformities are due to energy scale variations, the uniformity of the detector can be improved by applying multiplicative calibration factors to the energies of calorimeter objects in each Φ region in such a way that the candidate density becomes flat in Φ ("Φ intercalibration").

Dedicated trigger (Run II):

Level 1:
one trigger tower with total (EM+HAD) E_T > 5 GeV

↓ Level 2: require 6 GeV in EM section
↓ Level 3: precision tower with EM E_T > 8 GeV matched to above

↓ Level 2: require 5 GeV in HAD section
↓ Level 3: precision tower with HAD E_T > 7 GeV matched to above

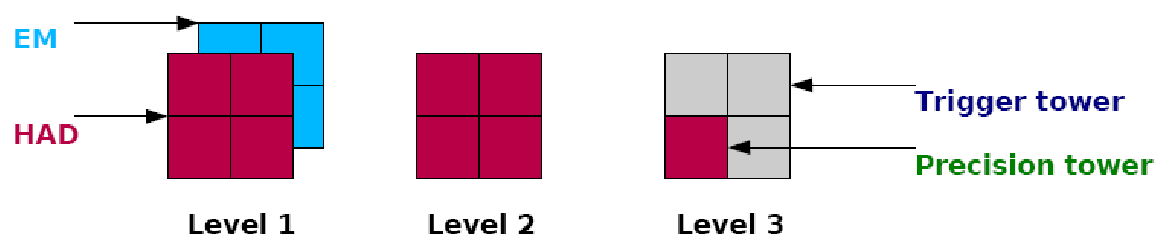

Phi intercalibration

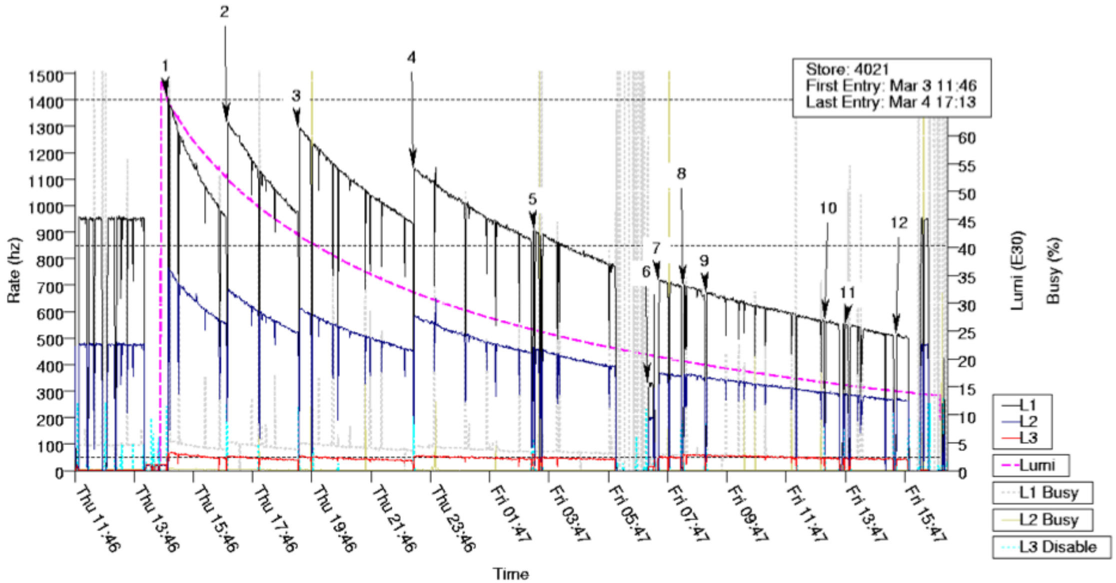

A typical Tevatron "fill" as seen by the DØ Trigger/DAQ system.

Black curve: L1 accept rate.
We observe:

- effect of prescale changes,
- lots of unused bandwidth during second half of the store.

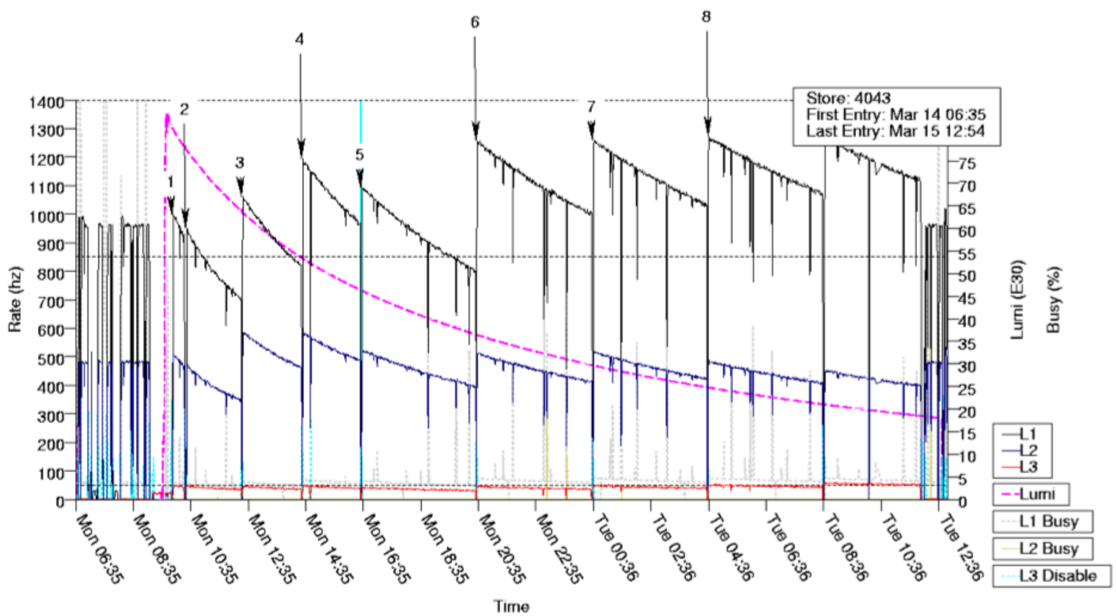

Another Tevatron "fill" where data taking for phi intercalibration is activated.

Can easily write to tape 0.5M – 1M events for phi intercalibration per "fill".

This allowed us to repeat the complete phi intercalibration of the calorimeter in a few weeks whenever it was necessary.

Gain calibration: results and impact

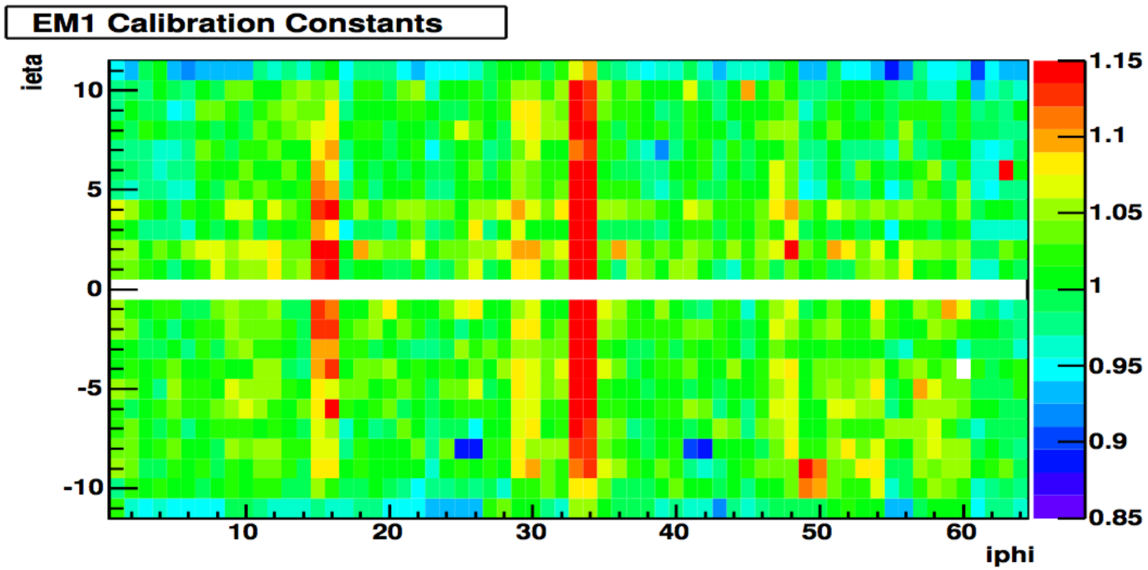

Example of results:

intercalibration constants in first layer of CC-EM.

Same Z → e e before and after calibration.

See improvement in mass resolution !

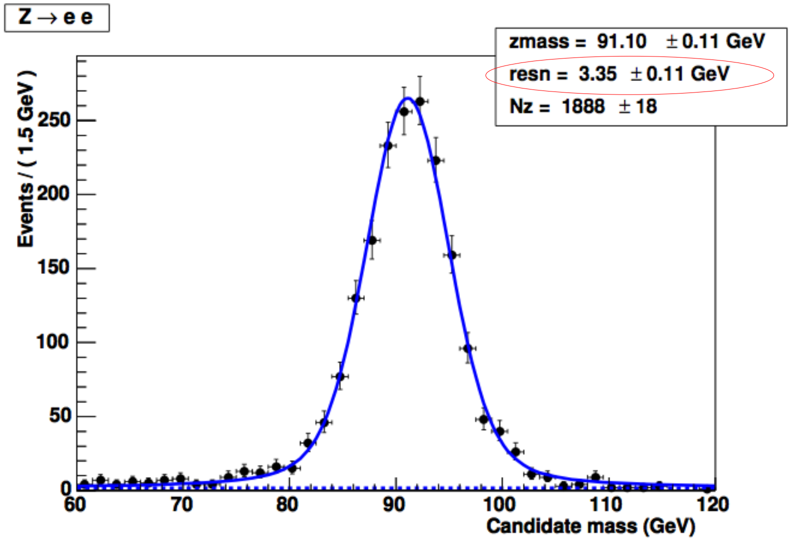

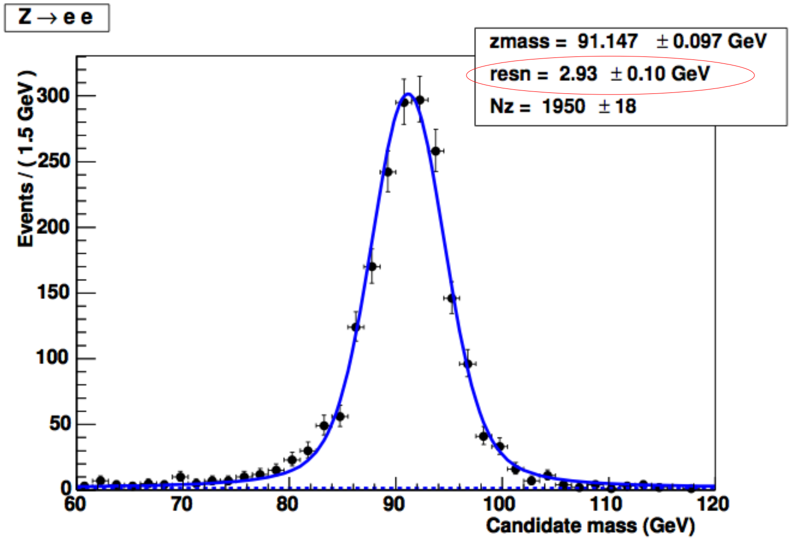

η-dependent absolute EM energy scale

After phi intercalibration, need to determine the absolute energy scale, separately for each phi ring (at fixed eta).

In EM calorimeter, this is done using $Z \to e^+ e^-$ events and the known mass (LEP).

In HAD calorimeter, this is done using di-jet balance and the requirement that the width of the imbalance distribution be minimal.

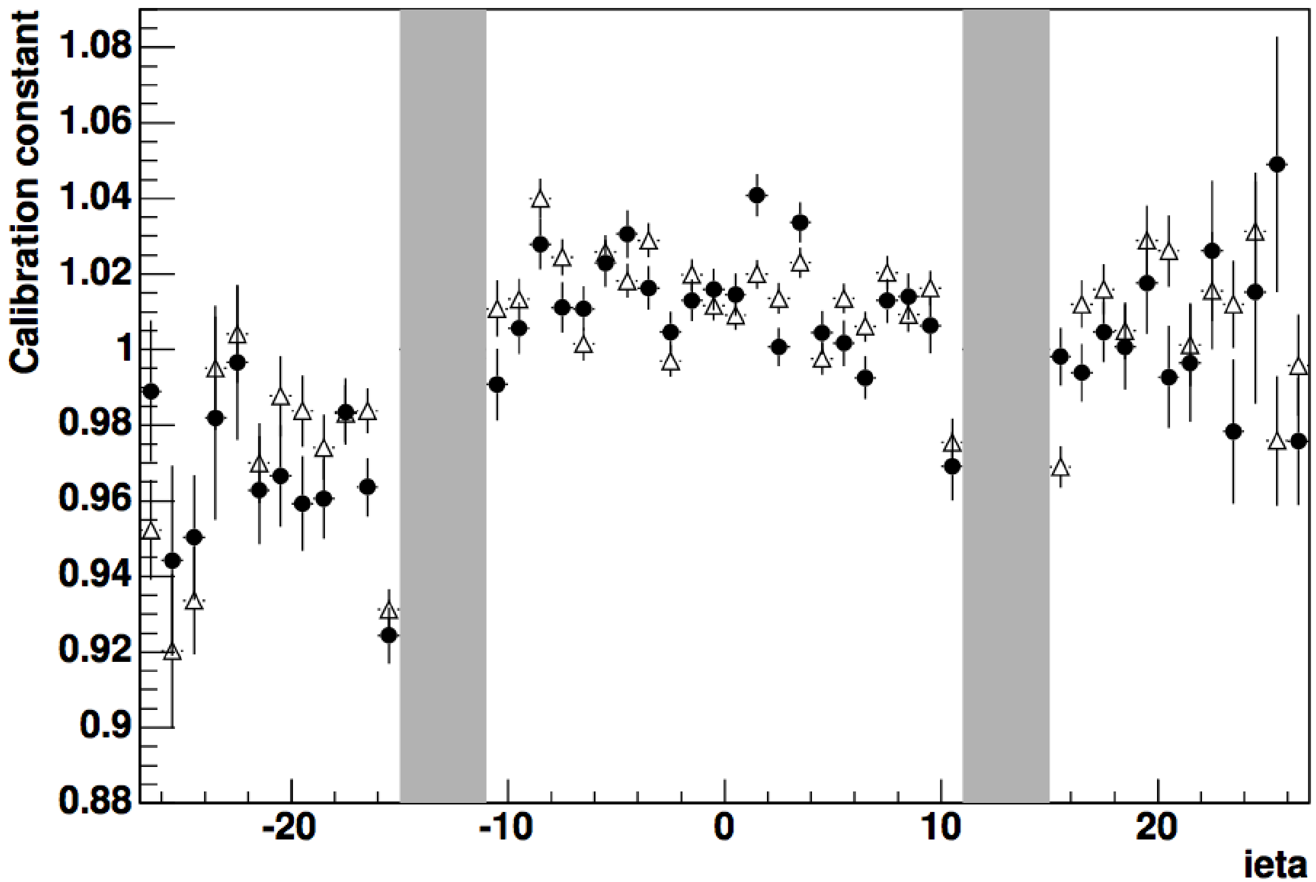

Plot: examples of multiplicative calibration constants, separately for each phi ring (at constant eta) in the EM calorimeter.

The two series of points represent two separate data taking periods (a few 100 pb^{-1} per period).

Origin of large mis-calibrations

Unit cell of the calorimeter readout:

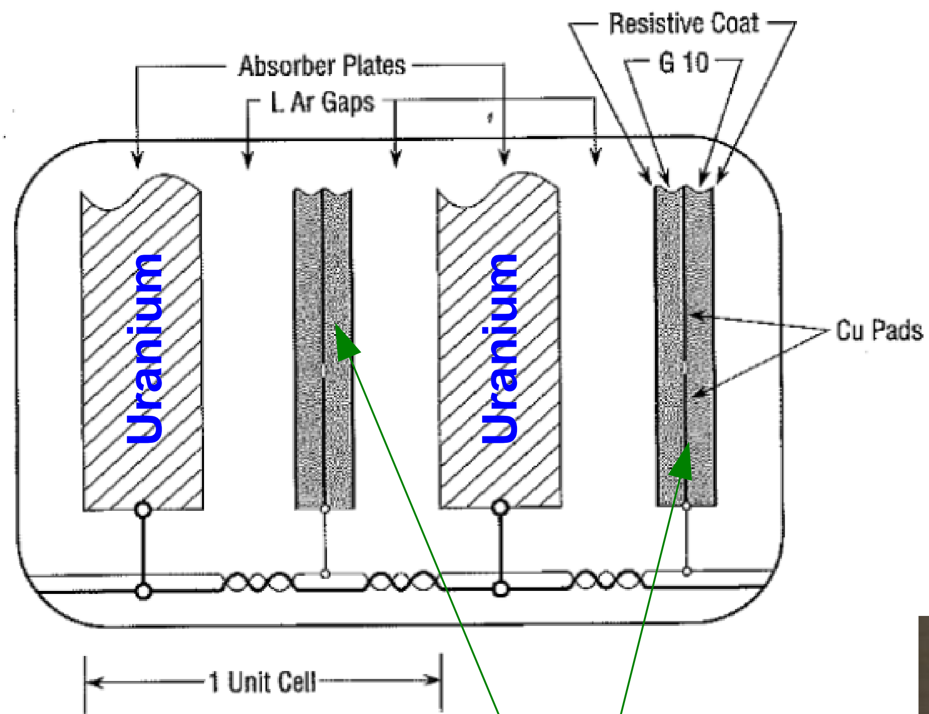

Signal board

Origin of large "outliers"

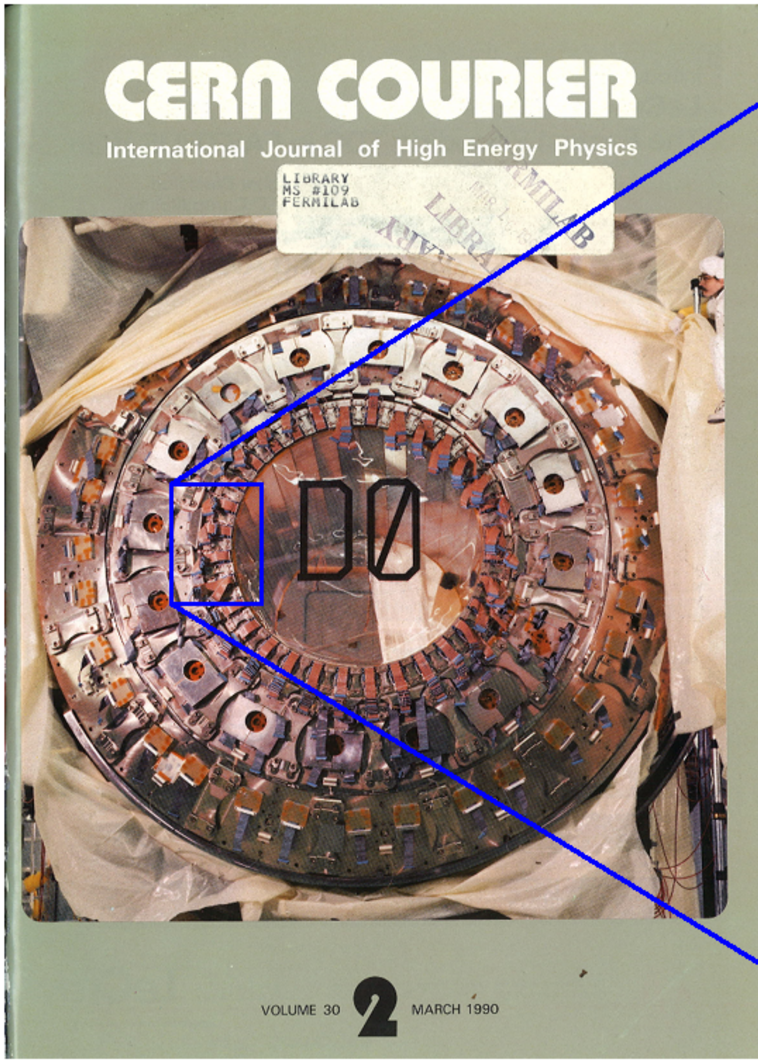

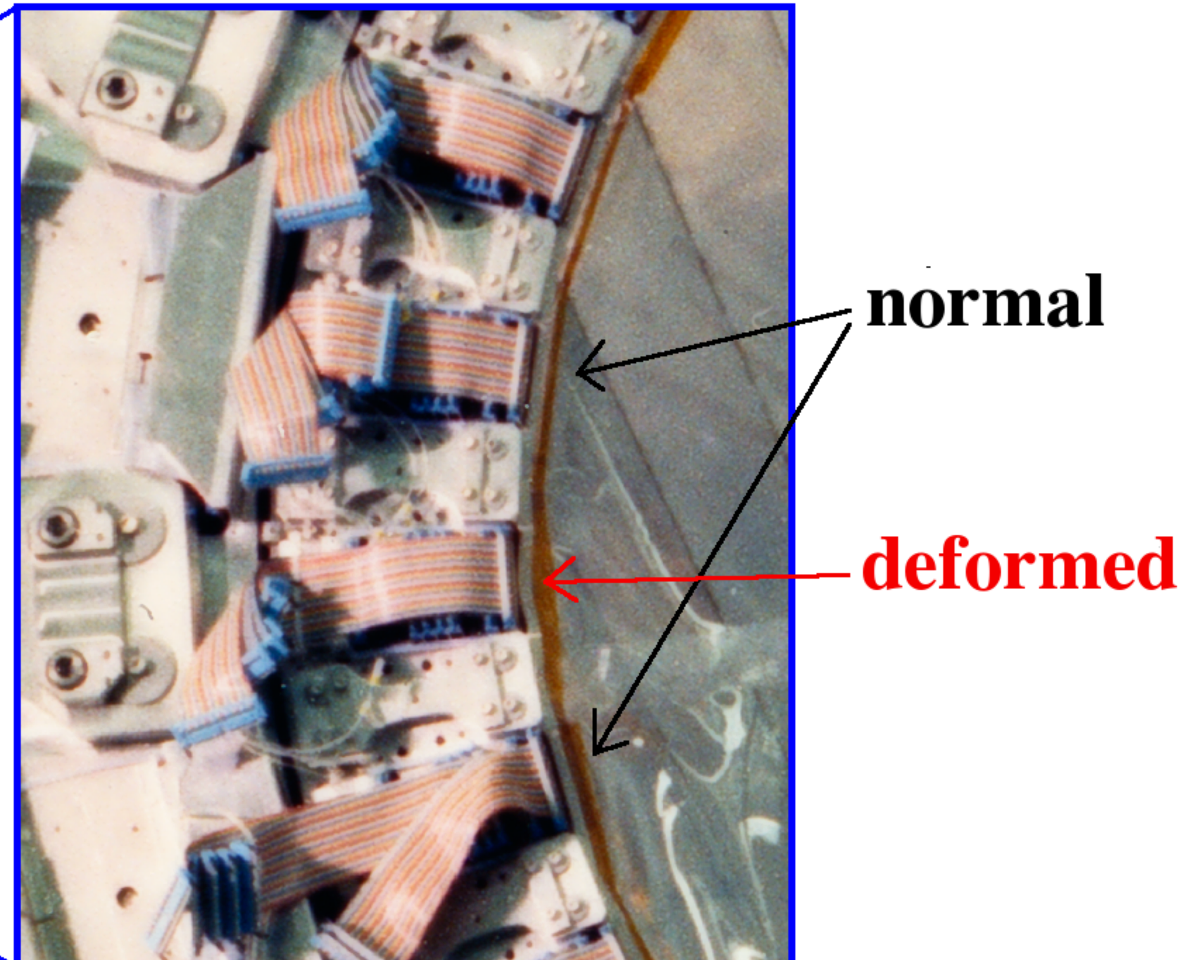

Electrons and photons: cone algorithm

For example in the W mass measurement, we use loose requirements:

fraction of core energy in the EM layers > 90 %

calorimetric isolation:

$$I = \frac{E_{tot}(R = 0.4) - E_{EM}(R = 0.2)}{E_{EM}(R = 0.2)} < 0.15$$

To define the electron four-vector:

- direction from track associated to cluster

- energy from "cone core energy" plus correction for energy lost in the uninstrumented material in front of the calorimeter (from precise first-principles simulations)

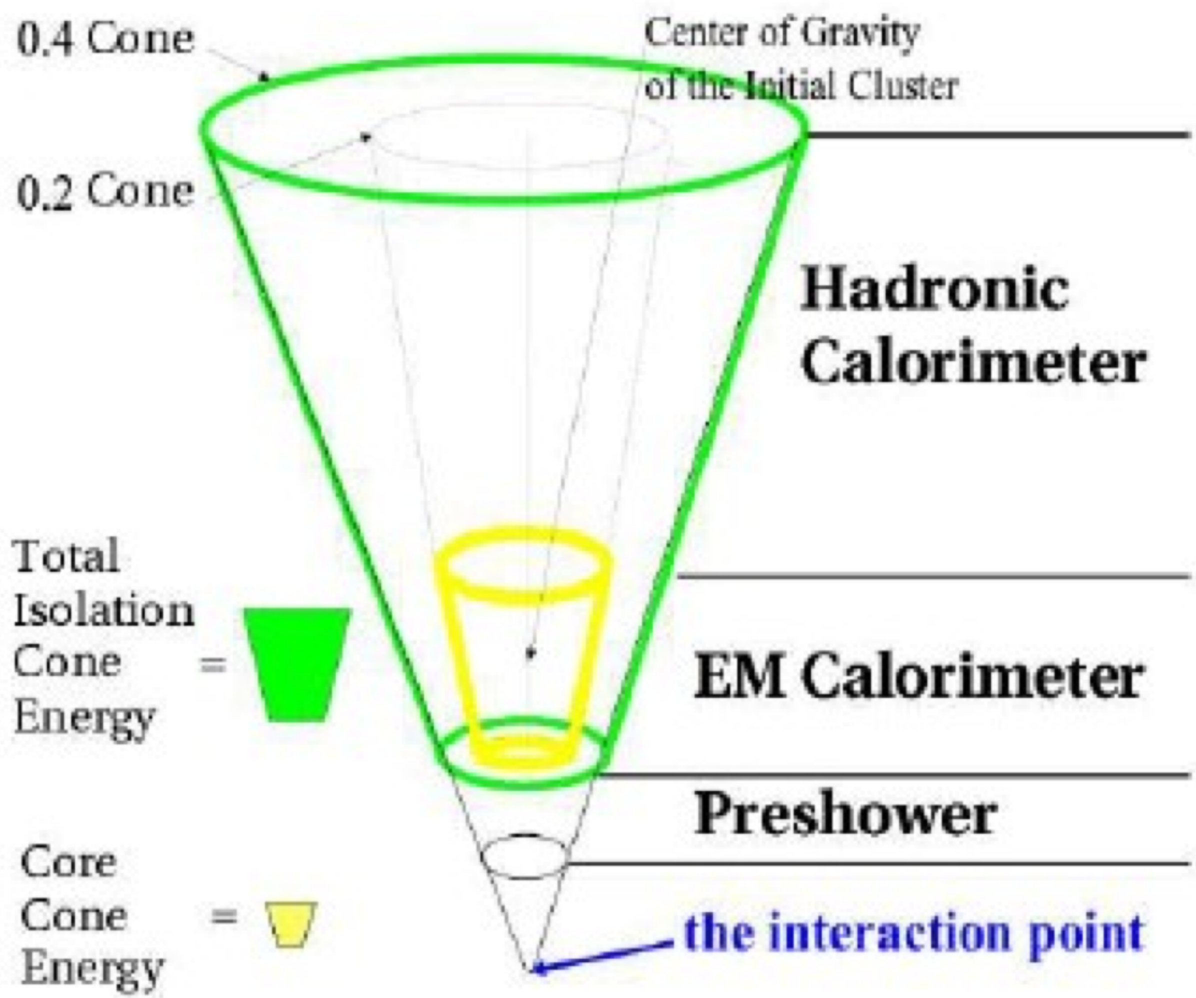

Electrons and photons: track match and “track veto”

In electron reconstruction/identification, typically require a reconstructed track matched in η/ϕ to the electron cluster.

- Residual misalignments between tracking and calorimetry are studied in detail and corrected using a clean sample of electrons from $Z \rightarrow e^+ e^-$.

- A variant of the matching algorithm also uses E/p.

For photon reconstruction, typically veto on track match.

Alternative approach: “Hits on Road”
is less sensitive to track reconstruction inefficiencies at high instantaneous luminosities.

In a nutshell: “count hits in the tracking devices inside 'roads' that represent the expected path for an electron or a positron”.

Hits on Road:

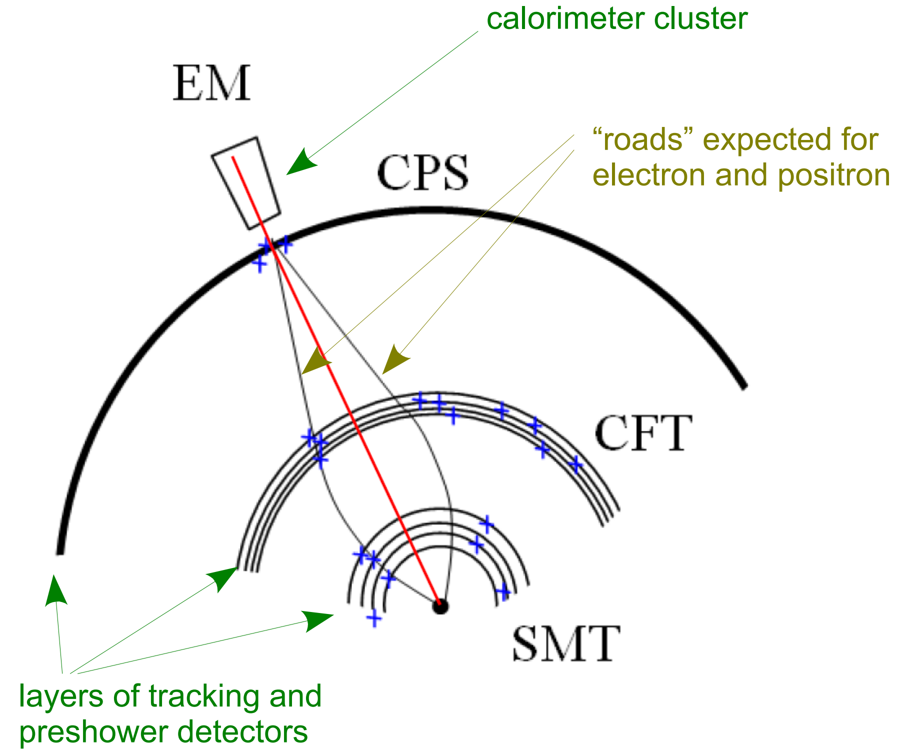

Electrons and photons: jet rejection

Heavily rely on robust variable for electron/photon identification: "HMatrix"

In a nutshell: a simple χ^2 that quantifies how electron/photon-like a given cluster is.

The following observables are input to this χ^2:

- Fractional energy deposits in the four readout layers of EM calorimeter.
- Width in $r*\phi$ of the cluster.
- The dependence of these observables on electron/photon energy and η is taken into account.

Also have more powerful (and more complex) tools for electron/photon identification that include a much larger number of discriminating variables.
E.g. artificial neutral network (ANN) that is trained to discriminate photons against jets.
Two of the extra variables in this ANN are shown below.

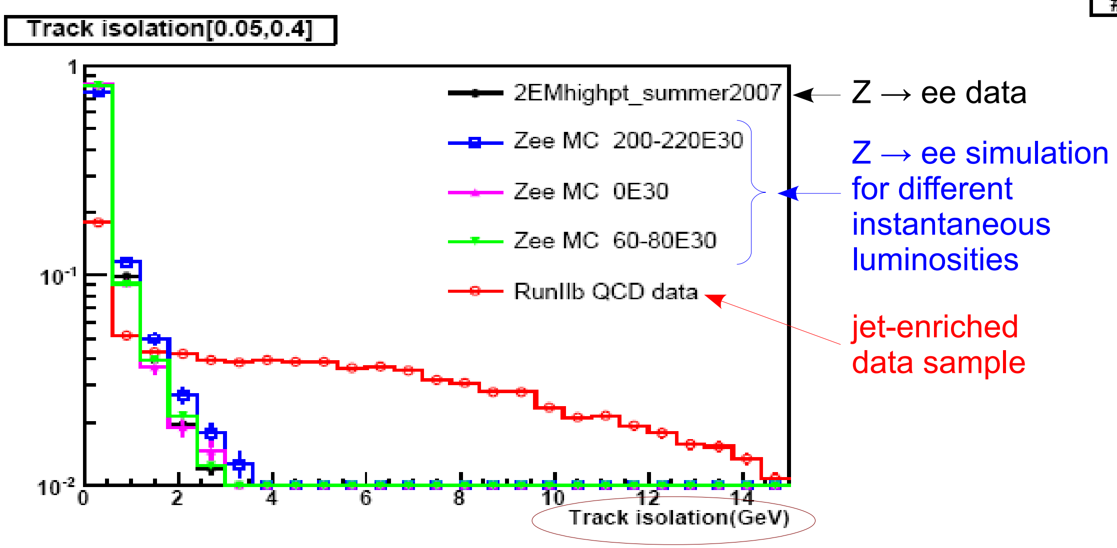

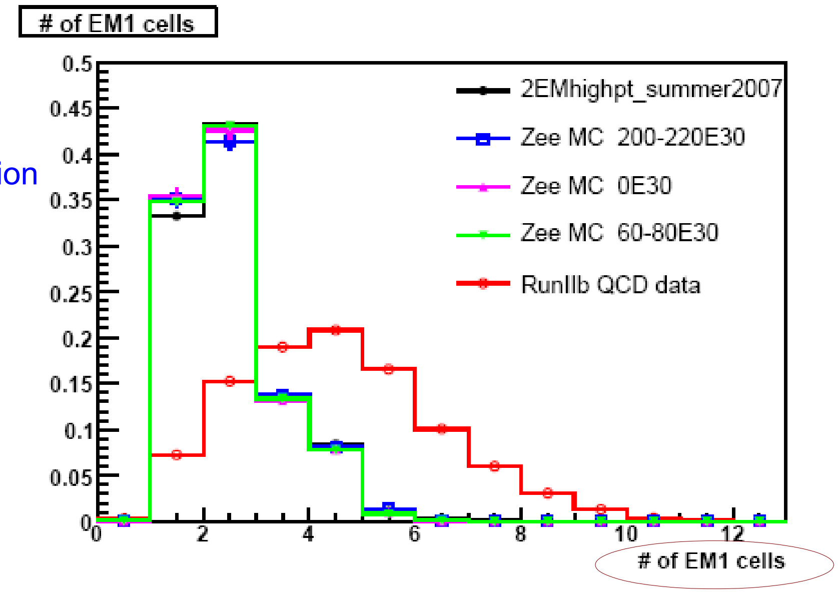

New readout electronics

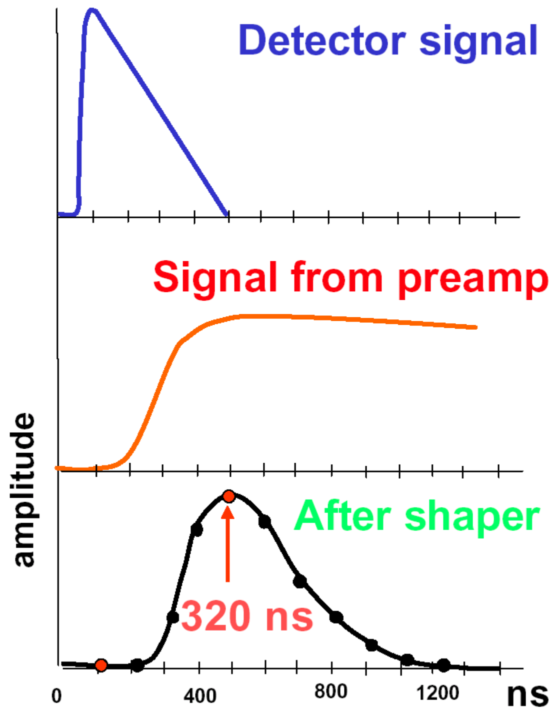

Have ability to sample and record the shaped signal also at (320 ± 120) ns to make sure we are on the peak.

- Detector signal ~ 450 ns long
  (bunch crossing time: 396 ns)
- Charge preamplifiers
- BLS (baseline subtraction) boards
  - short shaping of ~2/3 of integrated signal
  - signal sampled and stored every 132 ns in analog buffers (SCA) waiting for L1 trigger
  - samples retrieved on L1 accept, then baseline subtraction to remove pile-up and low frequency noise
  - signal retrieved after L2 accept
- Digitisation

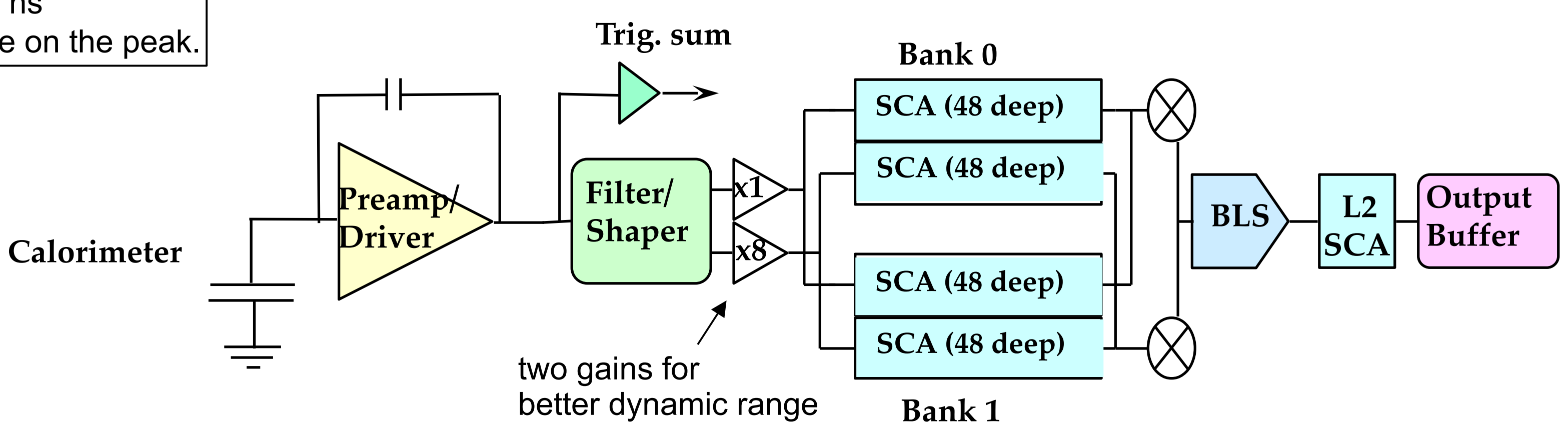

Zero suppression

Typical noise levels (from electronics, uranium decay) per readout cell, as measured from "pedestal runs" (read out detector in the absence of beam):

Layer	σ [ADC counts]	σ [MeV]
CC-EM1	3.1	48
EC-EM1	3.2	50
CC-EM3	2.0	25
CC-FH1	6.6	80
CC-CH	6.4	297

In the offline reconstruction software, we run (before object reconstruction), the "T42.5 algorithm":

Cells with energy below 2.5σ are discarded.

An isolated cell is considered "noise" and thus discarded if it is not "signal-like" and if it has no "signal-like" 3D neighbour, or if it has a negative energy. A cell is considered "signal-like" if its energy is above a relatively high threshold: 4σ .

This tight zero-suppression does have a non-trivial impact on, e.g., low-energy cells in the periphery of electron clusters and on soft hadronic activity (low-E_T jets).

To properly model this effect in detailed simulations, need
- accurate modelling of the showers electrons, low-E_T jets,
- accurate modelling of energy from additional $p\bar{p}$ interactions ("pile-up").

“Pile-up” and “ZB overlay”

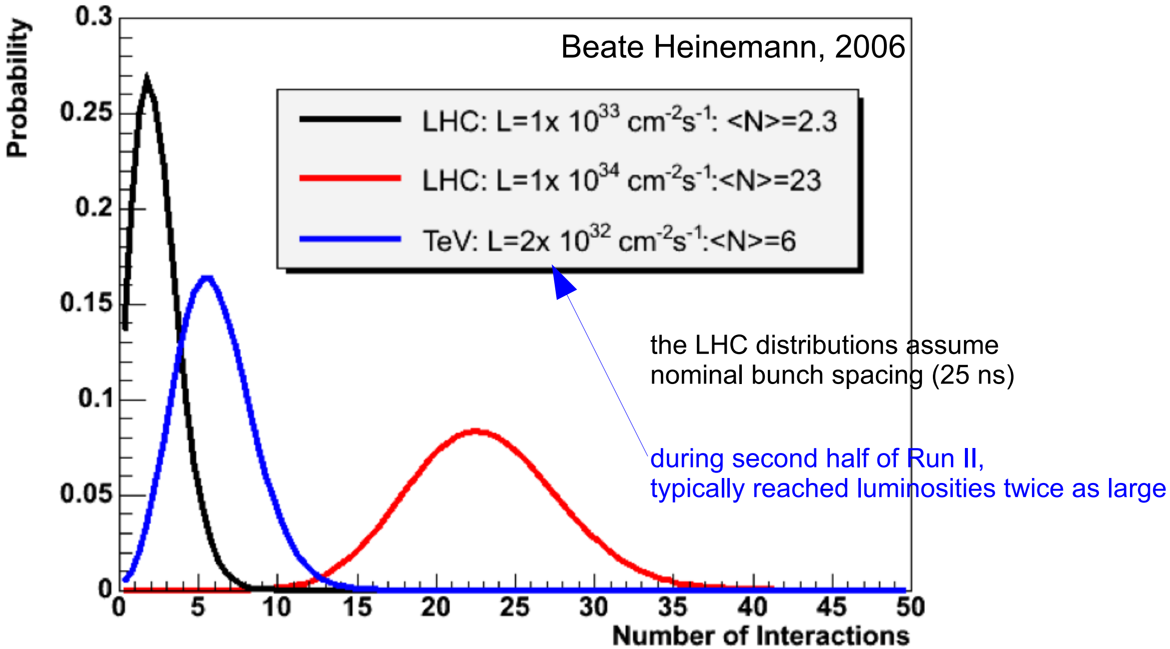

The instantaneous luminosity at the Tevatron is significantly lower than at the LHC.
But keep in mind that it is achieved with much larger bunch spacing (i.e. “few bunches filled with a lot of [anti-]protons each).

→ pile-up (both in-time and out-of-time) is also a non-negligible effect at the Tevatron.

The following technique used to model pile-up (both in-time and out-of-time) in detailed simulations has turned out to be invaluable: “Zero-bias overlay”

In a nutshell:

- do not simulate additional $p\bar{p}$ interactions from first principles
- instead: routinely collect “ZB events” (triggers on random bunch crossings) during collider operations.
  For these triggers, the online calorimeter zero suppression is turned off, i.e. all cells are read.
- … and “overlay” one of these data events on each simulated event (hard scatter) !
  (for calorimeter, “overlay” means add (cell-by-cell) energies from the ZB event and the simulated event)

Very powerful to describe contribution from pile-up to electron cone energy, effect of zero-suppression in the presence of pile-up, … will discuss the example of soft hadronic activity later in this talk.

Keep in mind: the CAL is not alone !

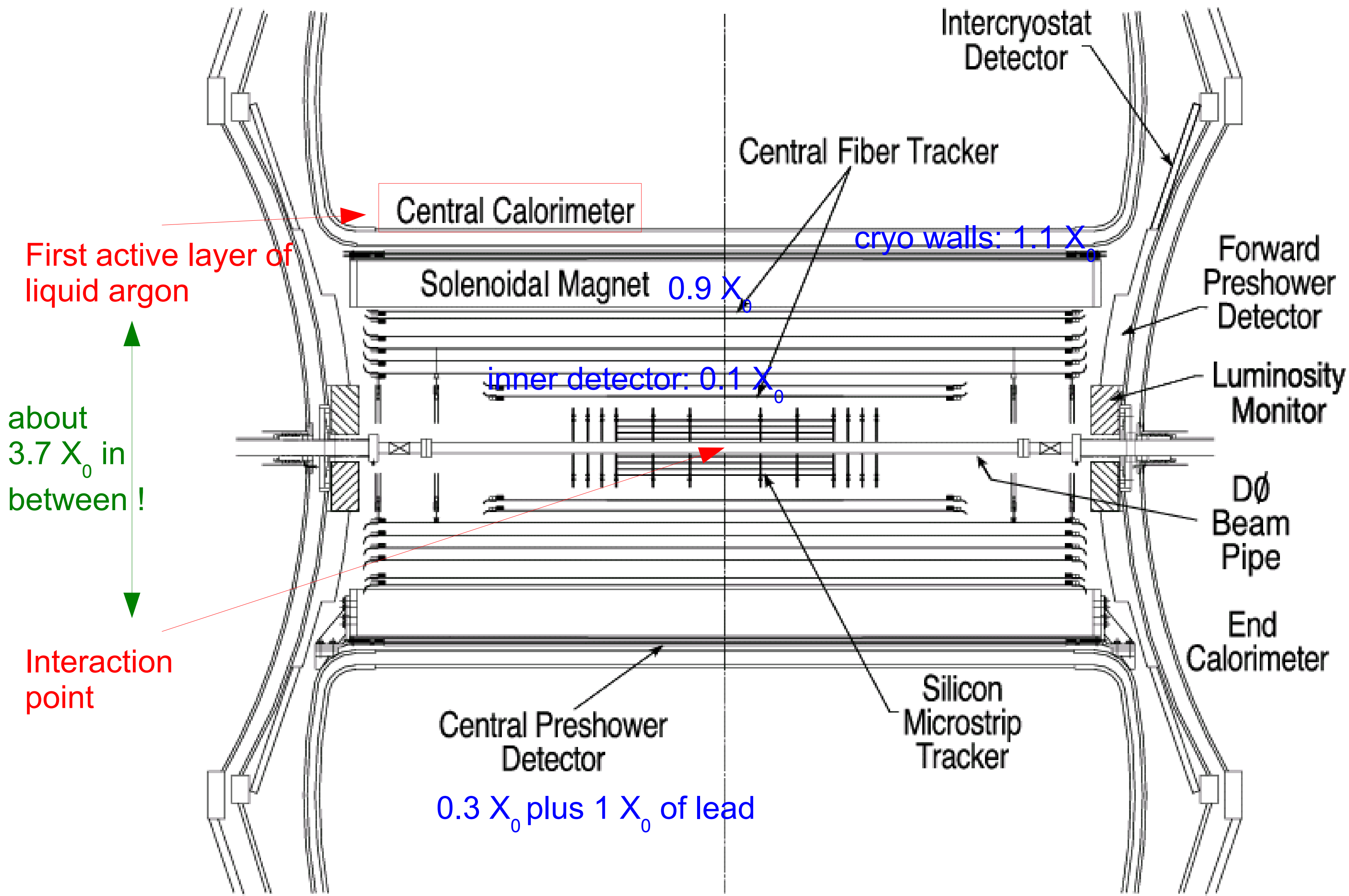

Impact of uninstrumented material

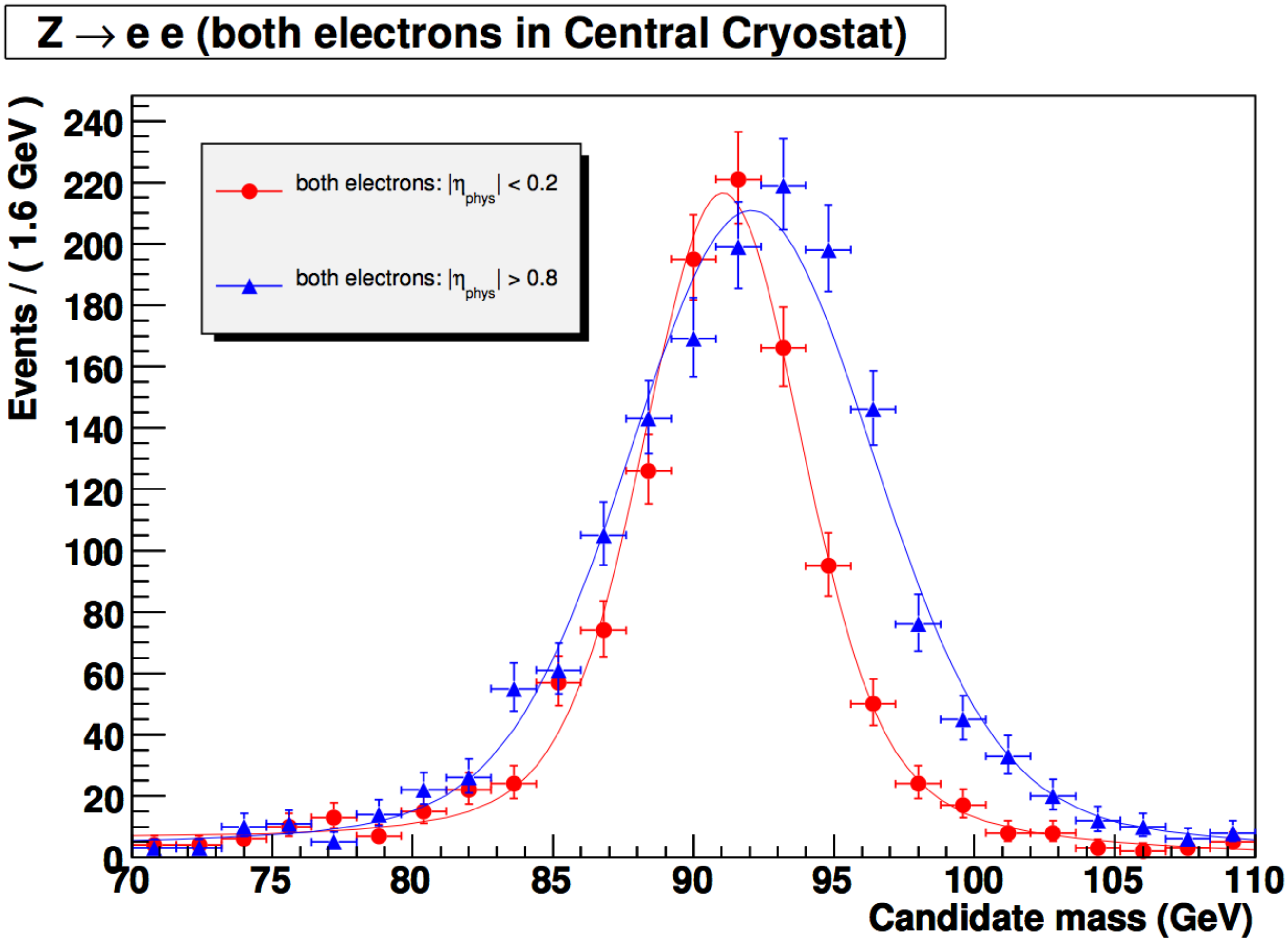

Two different subsets of CC-CC sample:

- both electrons at ~ normal incidence on dead material

- both electrons at very non-normal angle of incidence

Observations: - The width of the two peaks is very different.

- The peak positions are not in the same place.

How we sample showers in Run II

Average shower profile of an 45 GeV electron.

The positions of the readout sections of the D0 central calorimeter are indicated, for two different angles of incidence.

$\eta_{phys} = 0$

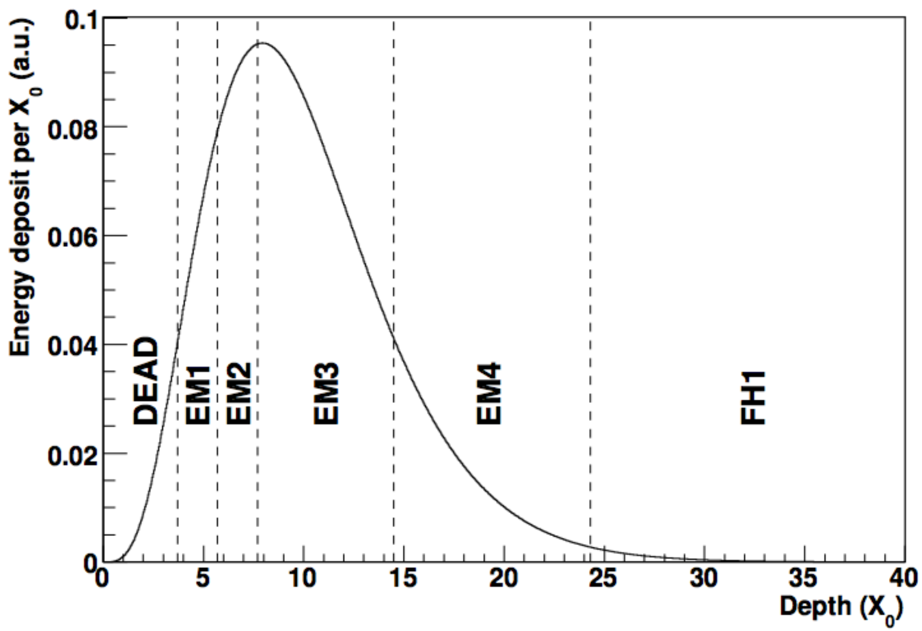

$\eta_{phys} = 1$

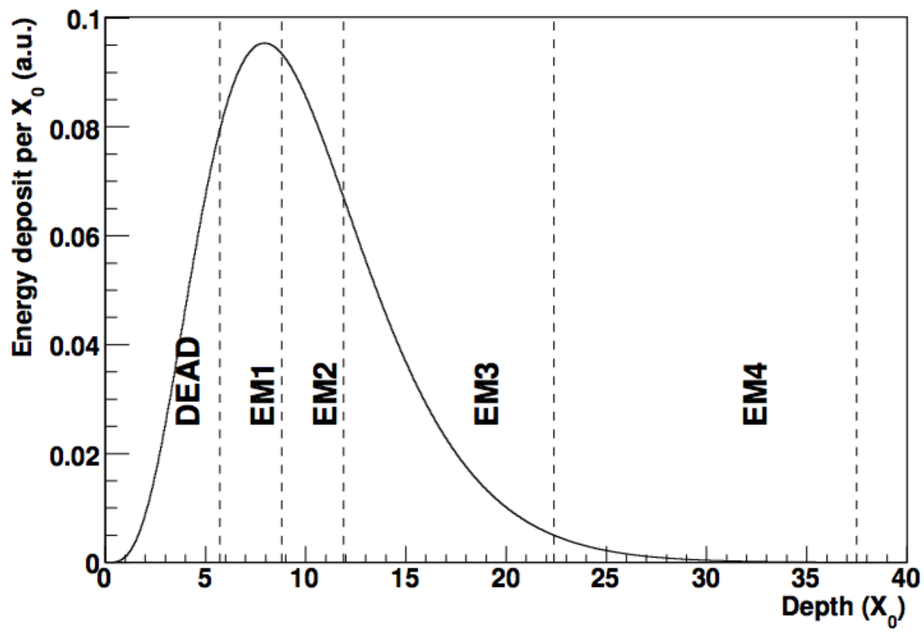

Shower fluctuations !

On the previous slide, we have discussed the average shower profile.

To illustrate the importance of fluctuations, we now show ten showers, generated using the GFlash parameterisation.

The fraction of energy lost in the dead region fluctuates from one shower to another.

Fluctuations are larger at low electron energy than at high energy.

Fluctuations are larger at non-normal incidence than at normal incidence.

E = 5 GeV $\eta_{phys} = 0$

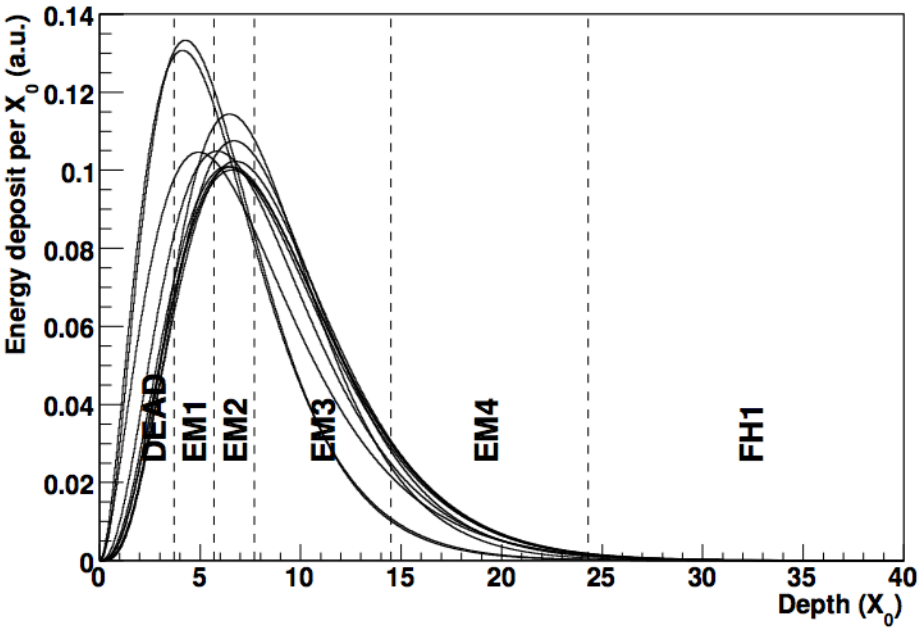

E = 45 GeV $\eta_{phys} = 0$

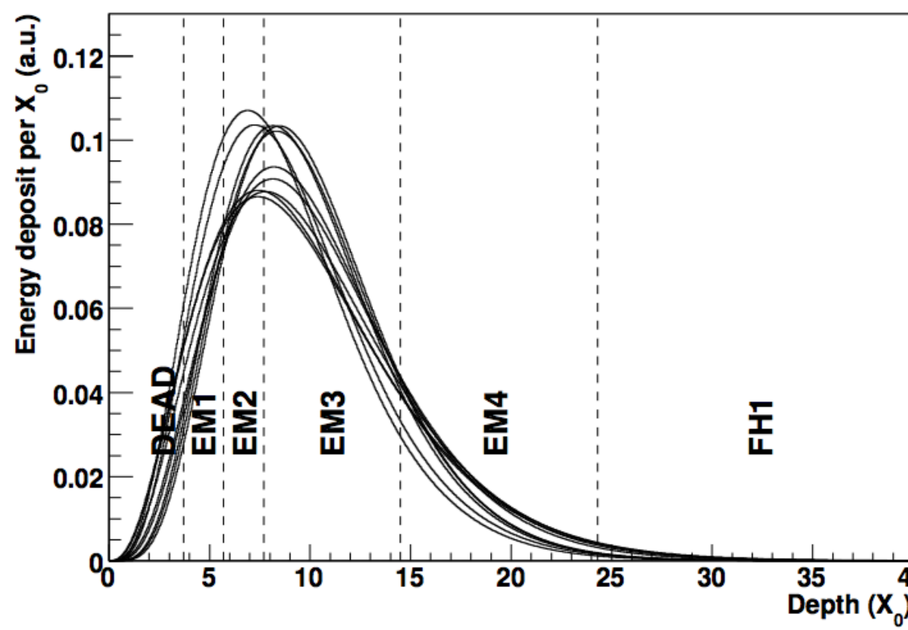

Consequences

Correction factor:

reconstructed cluster energy
→ electron energy

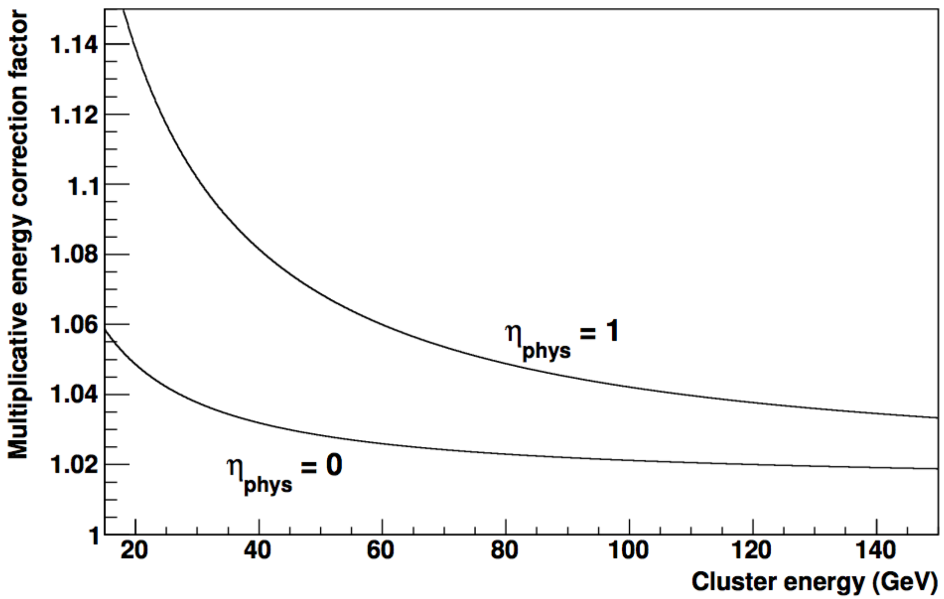

Fractional energy resolution
as a function of angle of incidence
(electrons with E = 45 GeV)

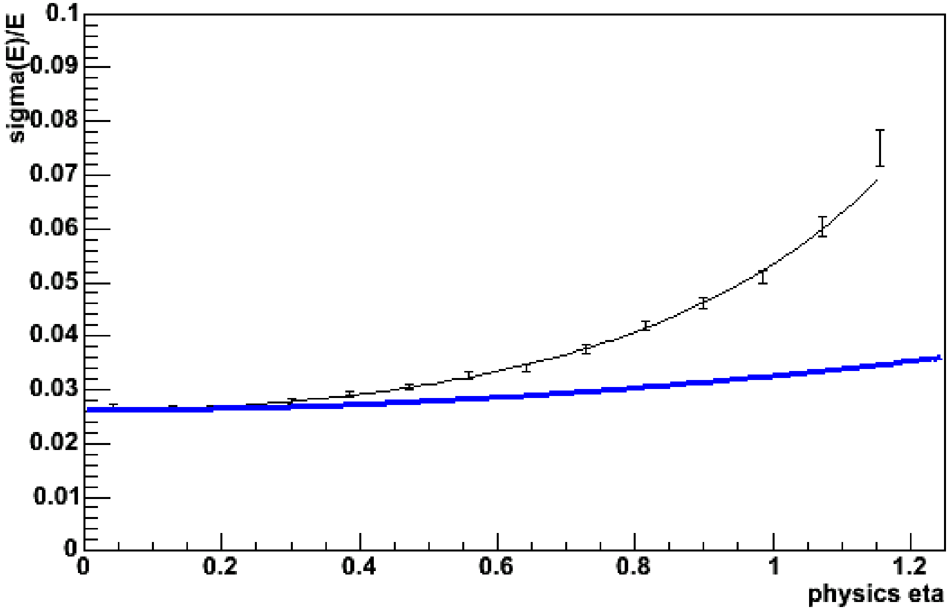

Need precise first-principles simulations to determine the energy correction factors and a model of the sampling fluctuations.

Geant 3

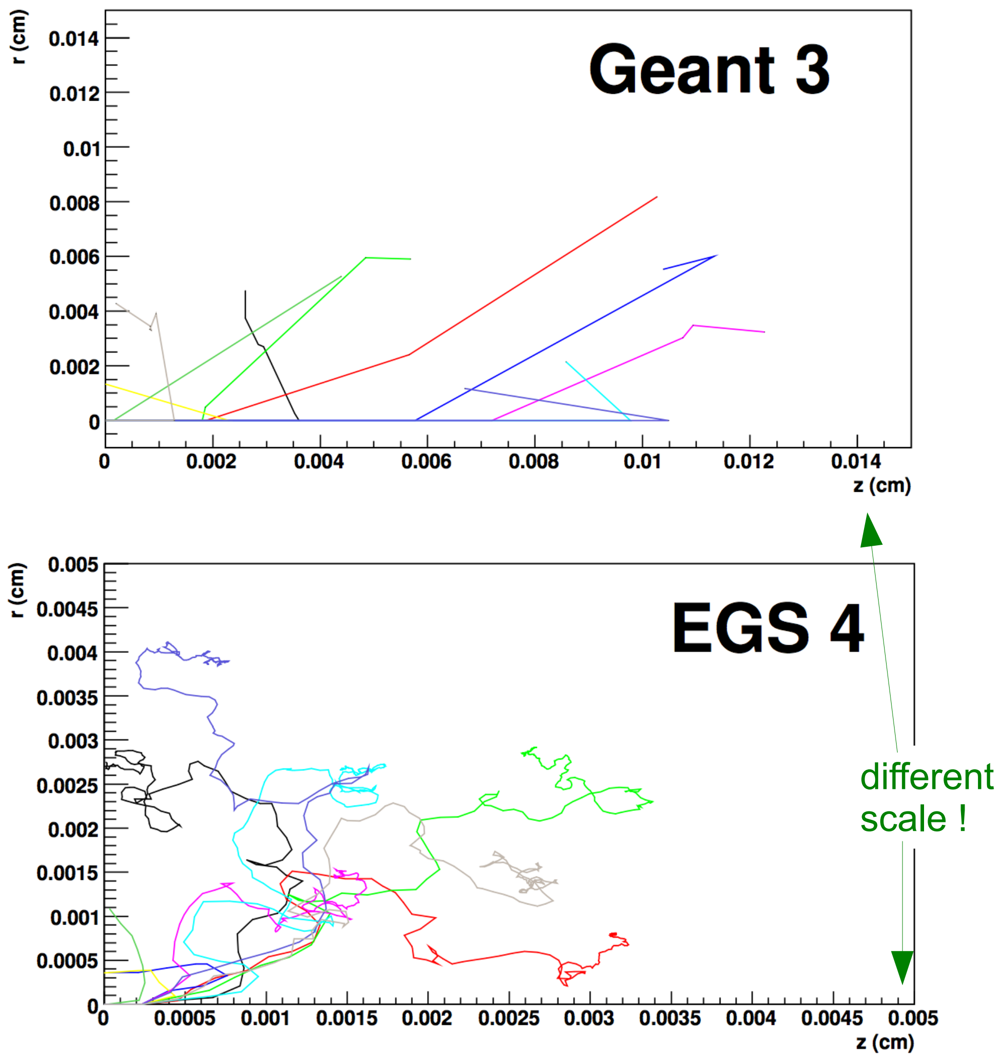

Simulated tracks of 400 keV electrons in uranium.

Identified various issues in Geant and the
in the interface between D0 software and Geant.

Key tool:
comparisons between Geant 3 and EGS 4

Bremsstrahlung cross-section for electrons in uranium:

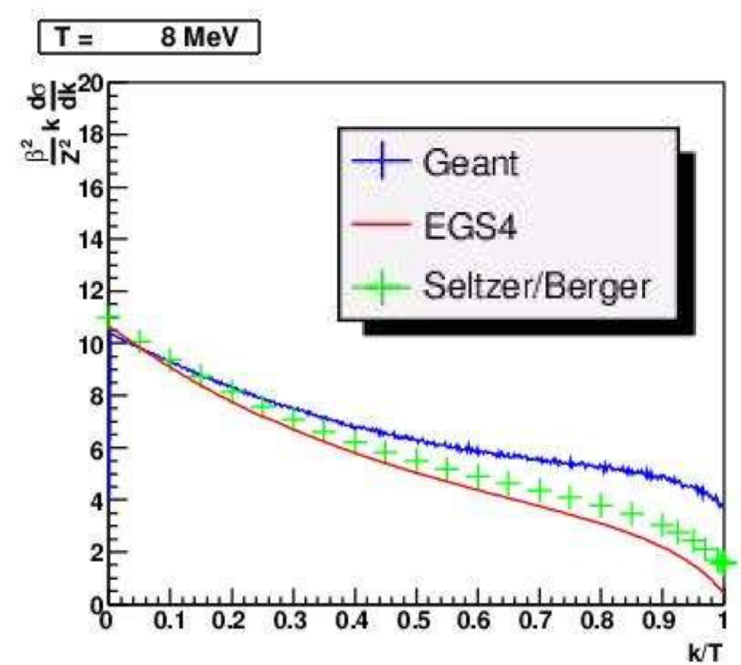

Material tune

Before adjustment of material model

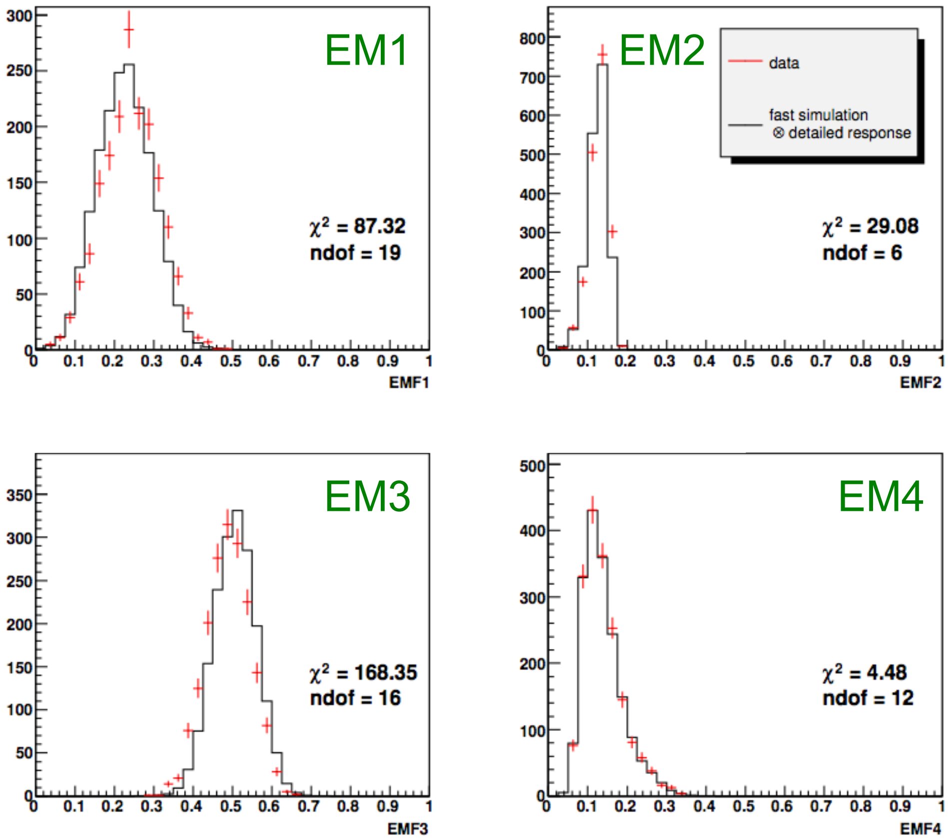

After adjustment

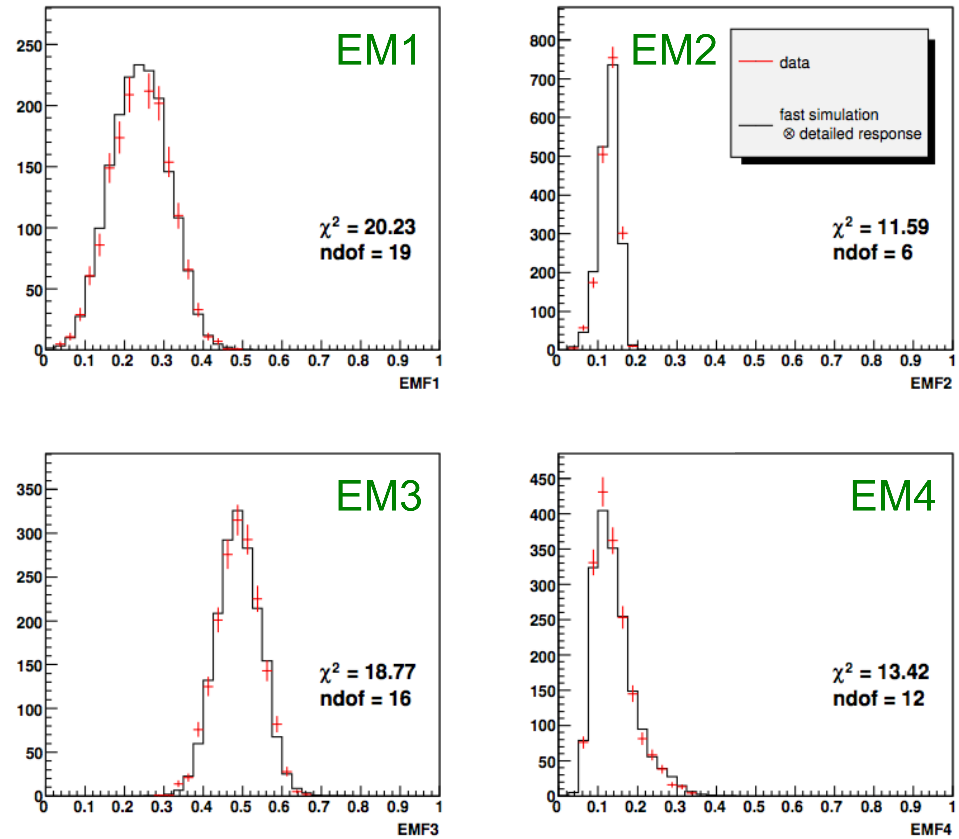

Conclusion: need to add $(0.1633 \pm 0.0095)\ X_0$ of dead material on top of the "first-principles accounting" in the detailed simulation of the DØ detector.

Jet reconstruction

Midpoint cone-based algorithm:

- Cluster objects based on their proximity in η/φ space.

- Fixed cone size (radius=0.5 for most analyses except QCD precision measurements).

- Starting from seeds (calorimeter towers above threshold), find stable cones (kinematic centroid = geometric centre).

- Seeds necessary for speed, but they are a source of infrared instability.

- To avoid infrared instability, we use the "midpoint algorithm", i.e. look for stable cones from middle points between two adjacent cones.

- Stable cones sometimes overlap
  → merge cones if p_T overlap > 75 %

Infrared instability:
soft parton emission changes jet clustering

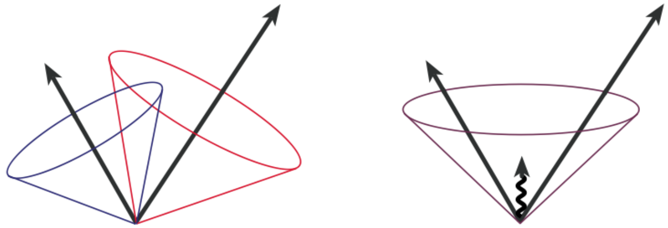

Figure 1. An illustration of infrared sensitivity in cone jet clustering. In this example, jet clustering begins around seed particles, shown here as arrows with length proportional to energy. We illustrate how the presence of soft radiation between two jets may cause a merging of the jets that would not occur in the absence of the soft radiation.

More advanced algorithms are available in our reconstruction software. But this simple algorithm works very well for the majority of measurements.

For more information: G. C. Blazey *et al.*, arXiv:hep-ex/0005012 (2000).

Jet energy scale

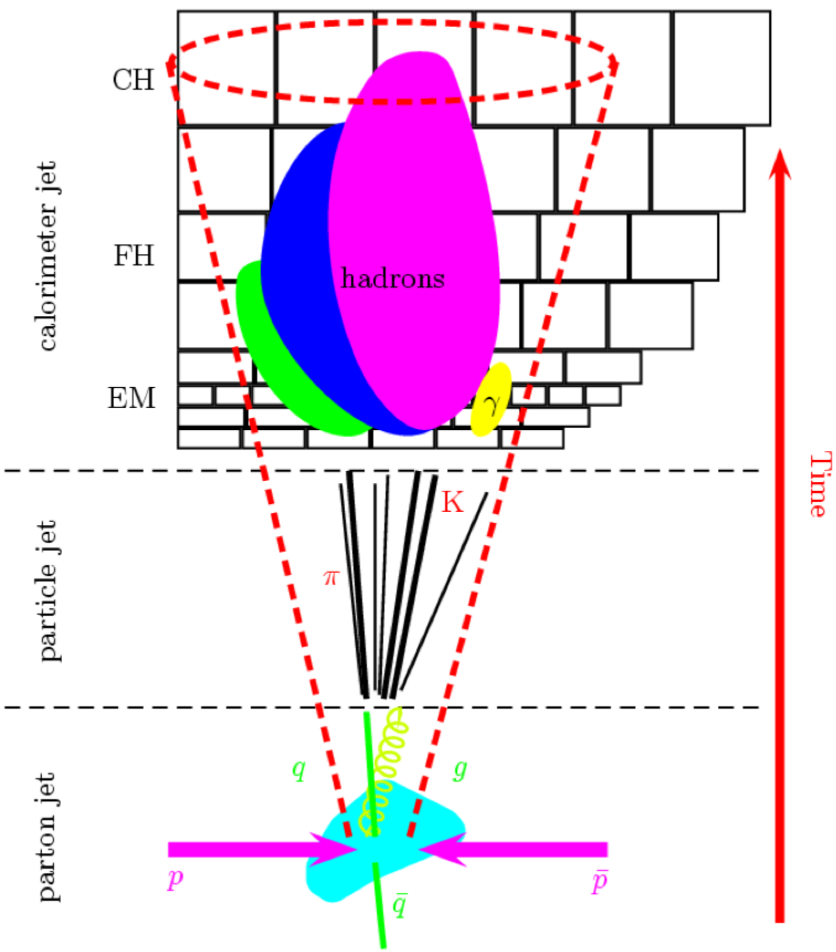

$$E_{jet}^{ptcl} = \frac{E_{jet}^{raw} - O}{F_\eta \cdot R \cdot S} \cdot k_{bias}$$

E_{jet}^{ptcl}:	corrected jet energy
E_{jet}^{raw}:	uncorrected jet energy
O:	offset energy correction
F_η:	relative response correction (η-intercalibration)
R:	absolute response correction
S:	showering correction
k_{bias}:	correction for remaining biases

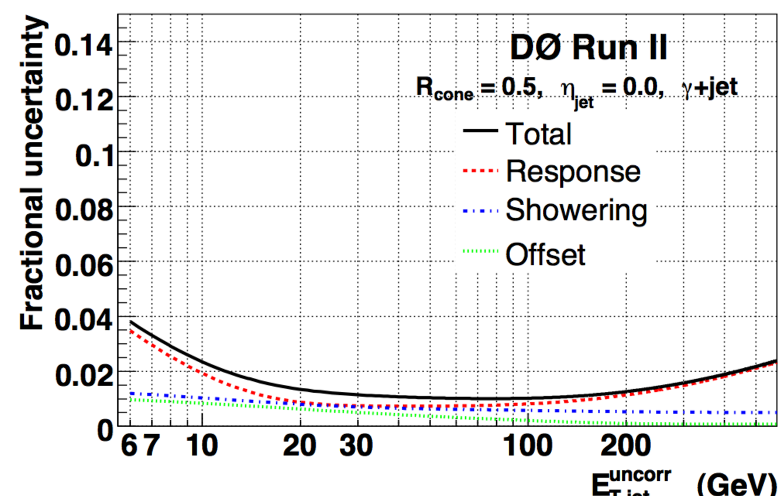

A powerful combination of measurements from data control samples (e.g. γ+jet balance) and corrections for the (relatively small) biases in measurements from data control samples. The bias corrections are derived from detailed simulation.

"Soft hadronic recoil" in vector boson events

When studying the soft hadronic system that recoils against Z or W events (essential for measurement of W mass), jet clustering is inappropriate ("the recoil is too soft for this in most events").

Instead, a very inclusive definition of the hadronic recoil vector is used:

$$\vec{u}_T = \sum_i E_i \times \sin\theta_i \times \begin{pmatrix} \cos\phi_i \\ \sin\phi_i \end{pmatrix}$$

where the sum includes all calorimeter cells that are not part of the electron cluster(s).

$\vec{u}_T$ is a 2D vector defined in the transverse plane.

Transverse momentum of Z bosons produced at the Tevatron

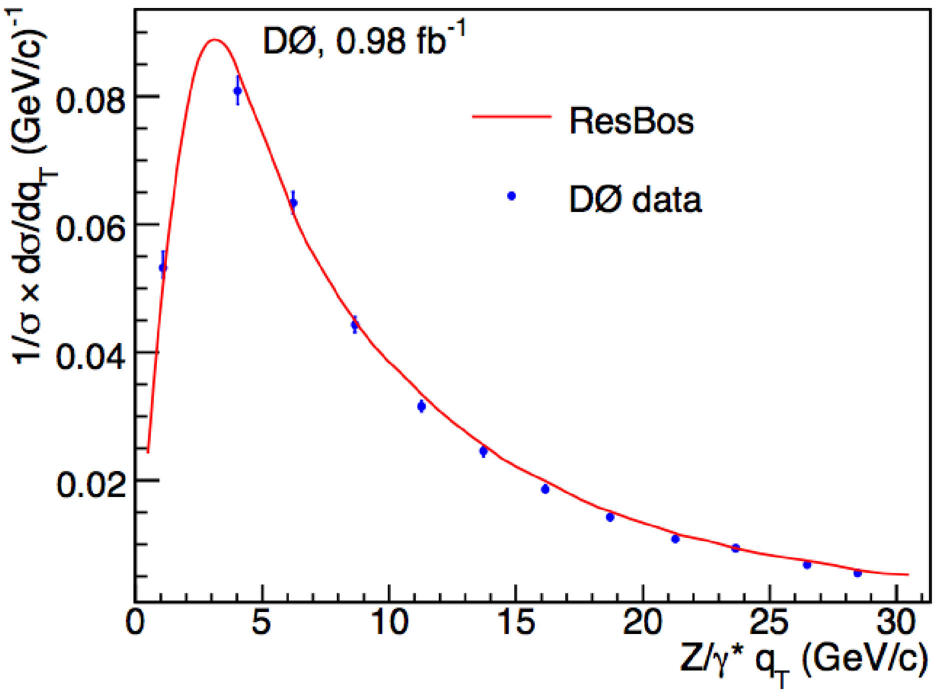

Missing E_T is the negative sum of the electron momentum vectors (in the transverse plane) and $\vec{u}_T$.

The transverse mass is defined as:

$$m_T = \sqrt{2\, p_T^e \, \not{E}_T (1 - \cos\Delta\phi)}$$

“Soft hadronic recoil”: impact of zero suppression and pileup

Pile-up has, of course, a big impact in the reconstruction of the $\vec{u}_T$ vector: pile-up adds a lot of extra energy to the event, and the net contribution to $\vec{u}_T$ is not always small compared to the contribution from the hadrons recoiling against the vector boson.

But, due to the tight zero suppression, pile-up even changes the way in which the calorimeter detects the contribution from the hadrons recoiling against the vector boson: the difference between the two simulations below is due to the fact that the presence of extra energy from pile-up “pushes more cells above the zero-suppression threshold”, thus making it easier to detect the soft contributions from the hadronic recoil.

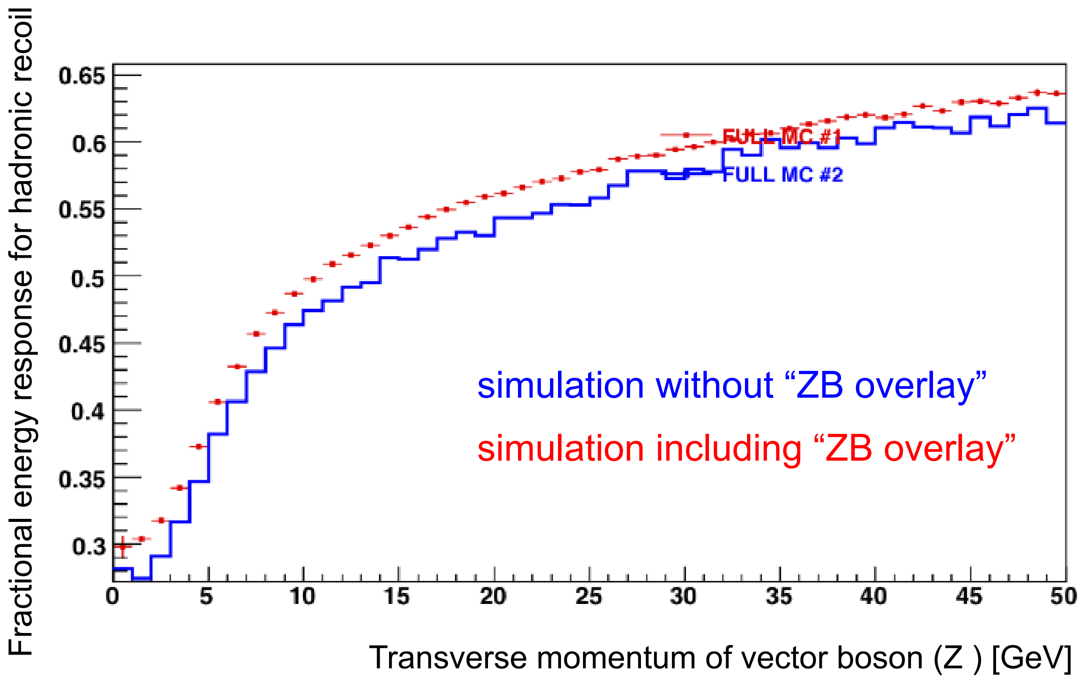

Z data

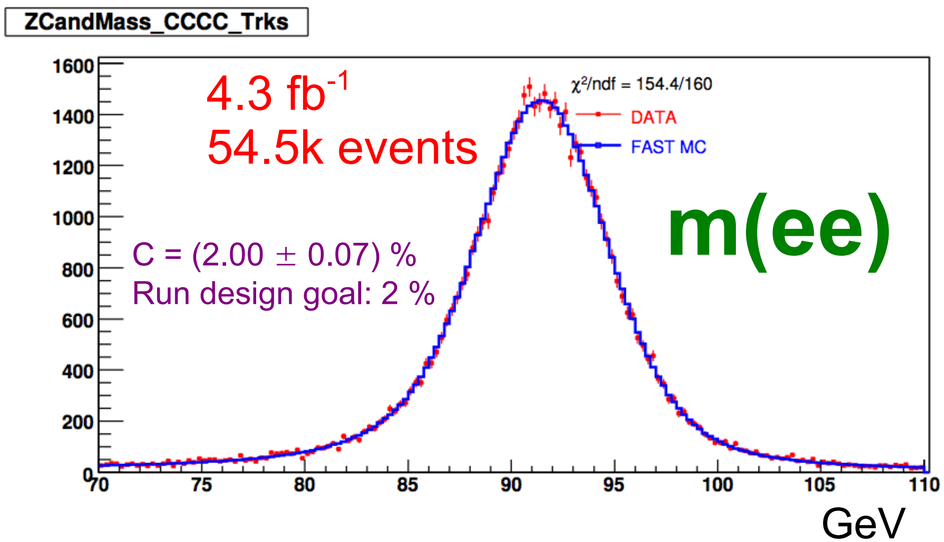

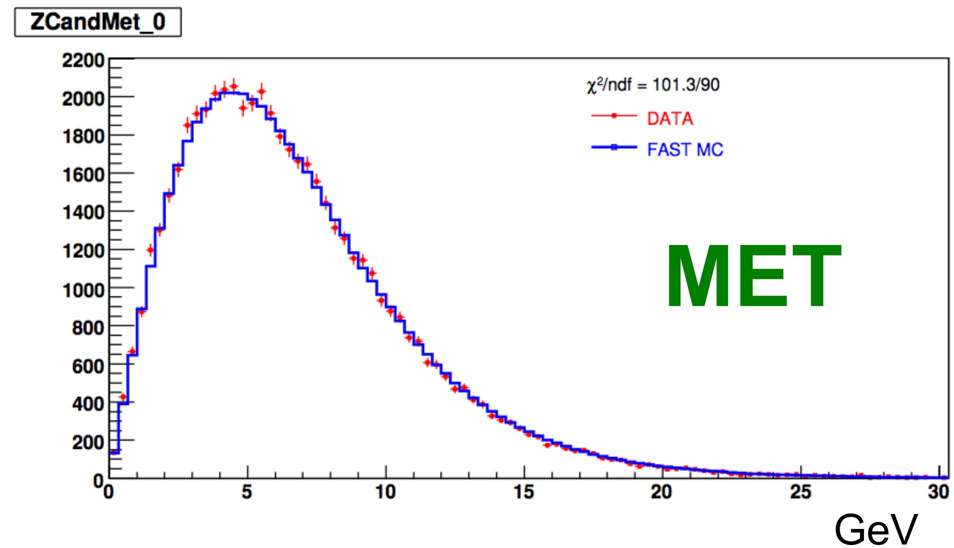

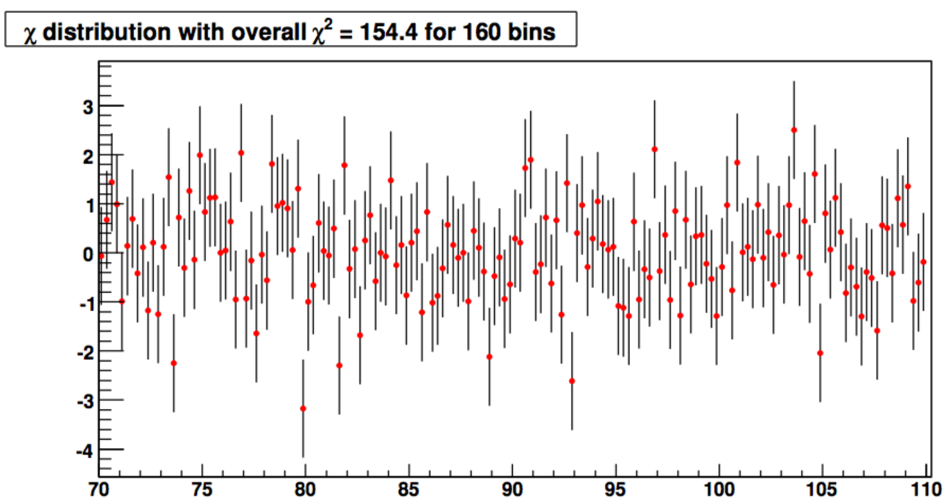

$m(Z) = 91.193 \pm 0.017$ (stat) GeV

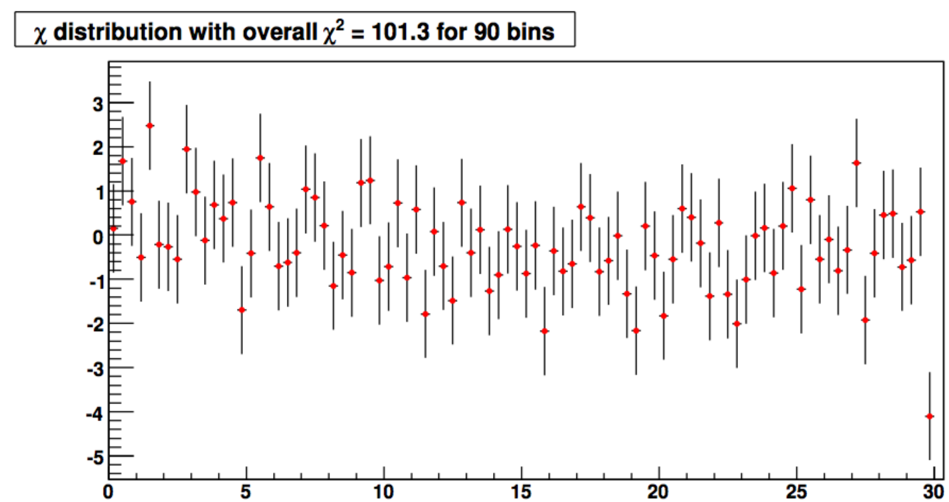

Good agreement between data and parameterised Monte Carlo.

1.68M events
central electrons ($|\eta|<1.05$)

W data

m_T

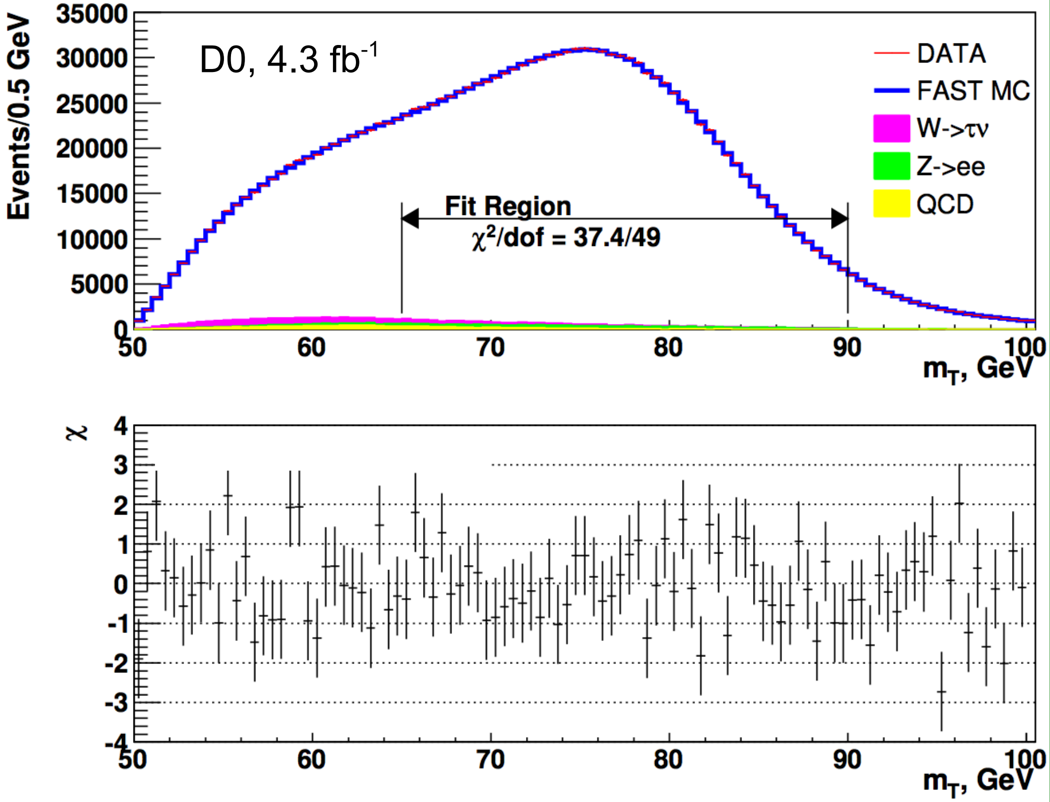

$p_T(e)$

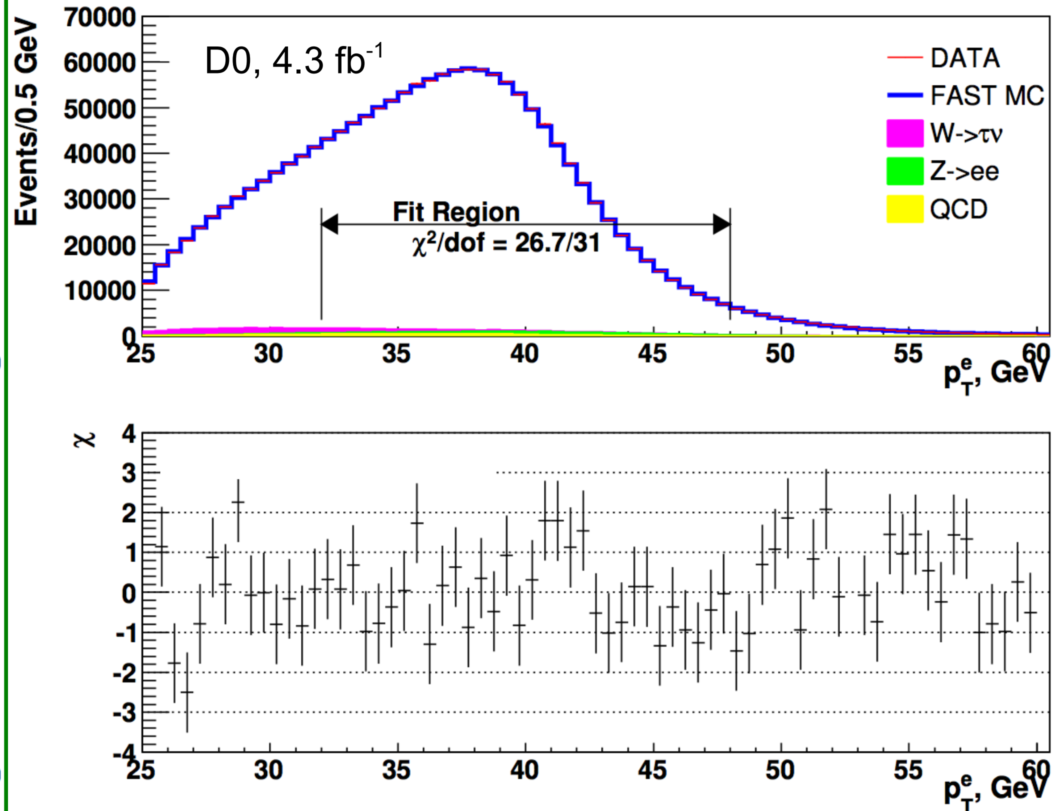

Fit results:

m(W) =
80371 ± 13 MeV (stat)

m(W) =
80343 ± 14 MeV (stat)

m(W): results and projections (DØ)

Source	Public. 2009 (1.0 fb^{-1})	Public. 2012 (4.3 fb^{-1})	Proj. 10 fb^{-1}	Proj. 10 fb^{-1} improv.	Proj. 10 fb^{-1} improv. + EC
Statistical	23	13	9	9	8
Experimental syst.					
Electron energy scale	34	16	11	11	10
Electron energy resolution	2	2	2	2	2
EM shower model	4	4	4	2	2
Electron energy loss	4	4	4	2	2
Hadronic recoil	6	5	3	3	2
Electron ID efficiency	5	1	1	1	1
Backgrounds	2	2	2	2	2
Subtotal experimental syst.	35	18	13	12	11
***W* production and decay model**					
PDF	9	11	11	11	5
QED	7	7	7	3	3
boson p_T	2	2	2	2	2
Subtotal W model	12	13	13	12	6
Total systematic uncert.	37	22	19	17	13
Total	**44**	**26**	**21**	**19**	**15**

combination: 23

m(top): results

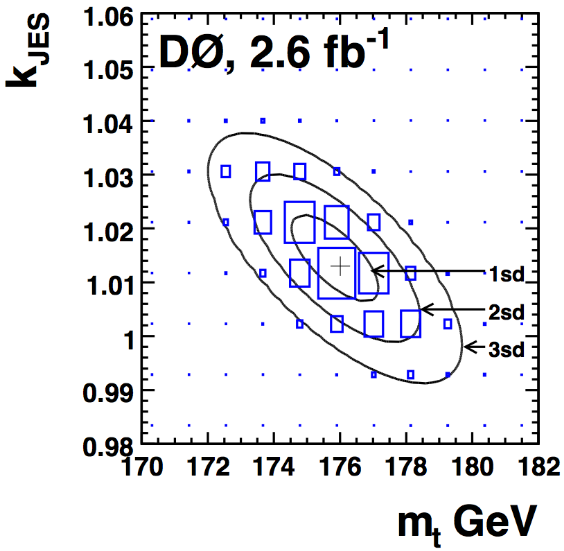

Table IV. Summary of systematic uncertainties.

Source	Uncertainty (GeV)
Modeling of production:	
Modeling of signal:	
Higher-order effects	±0.25
ISR/FSR	±0.26
Hadronization and UE	±0.58
Color reconnection	±0.28
Multiple $p\bar{p}$ interactions	±0.07
Modeling of background	±0.16
W+jets heavy-flavor scale factor	±0.07
Modeling of b jets	±0.09
Choice of PDF	±0.24
Modeling of detector:	
Residual jet energy scale	±0.21
Data-MC jet response difference	±0.28
b-tagging efficiency	±0.08
Trigger efficiency	±0.01
Lepton momentum scale	±0.17
Jet energy resolution	±0.32
Jet ID efficiency	±0.26
Method:	
Multijet contamination	±0.14
Signal fraction	±0.10
MC calibration	±0.20
Total	±1.02

Phys. Rev. **D84**, 032004 (2011)

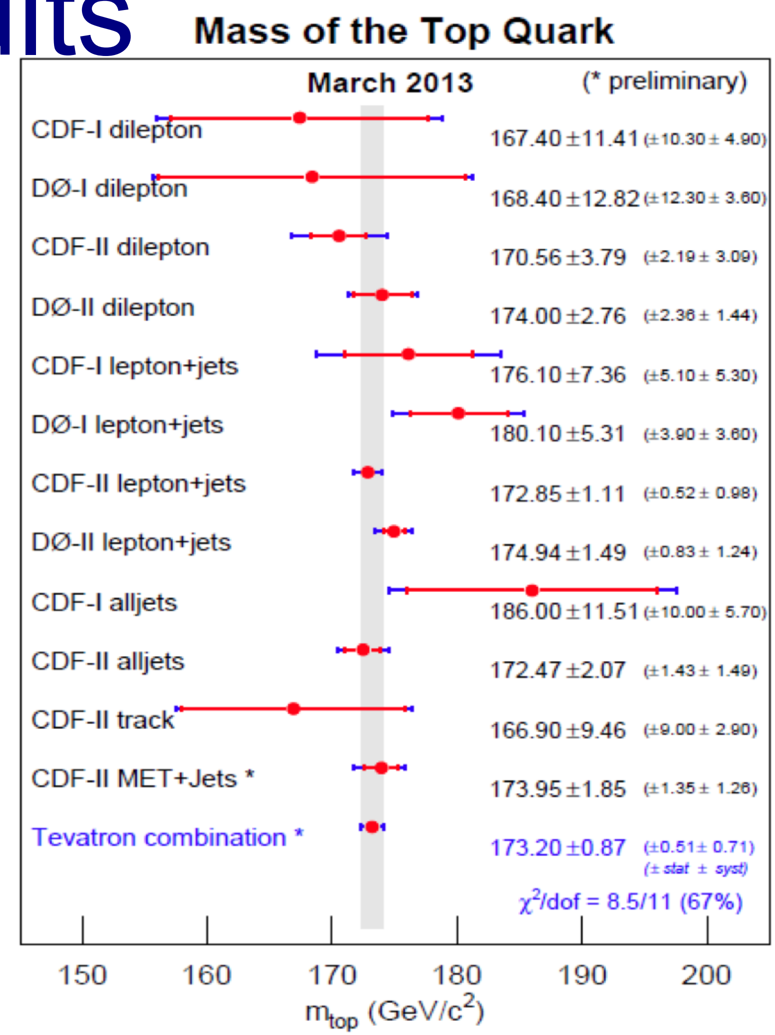

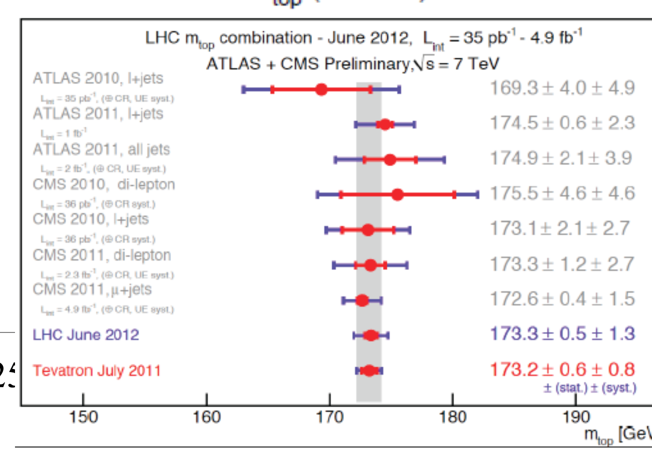

Results !

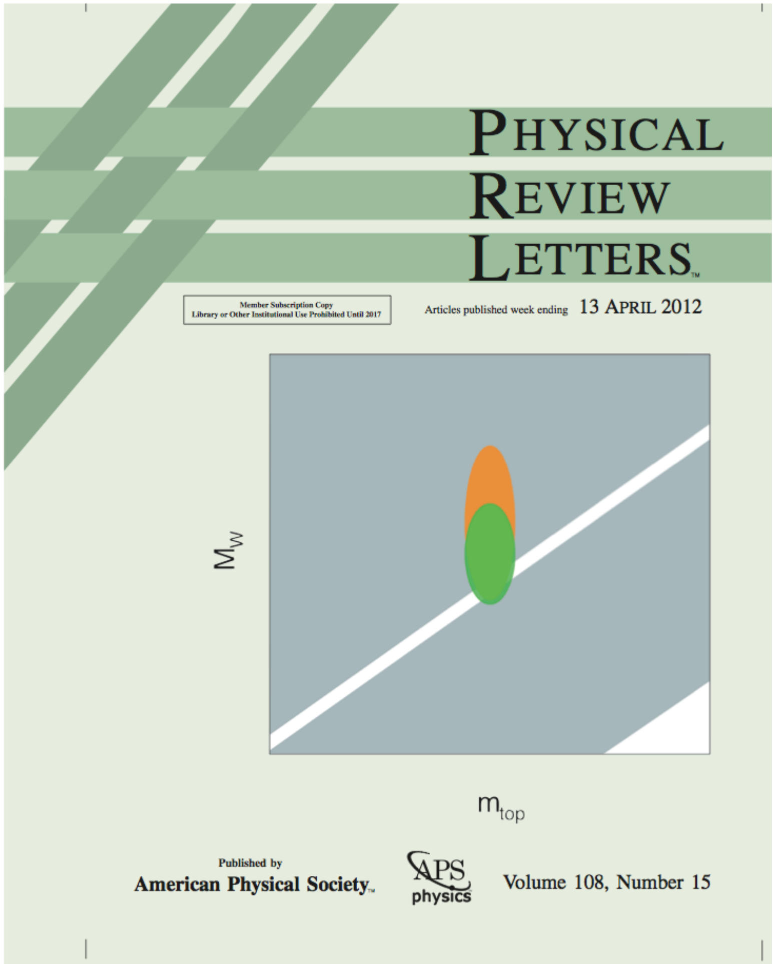
PHYSICAL
REVIEW
LETTERS
Member Subscription Copy
Library or Other Institutional Use Prohibited Until 2017
Articles published week ending 13 APRIL 2012
M_W
m_{top}
Published by
American Physical Society
APS physics
Volume 108, Number 15

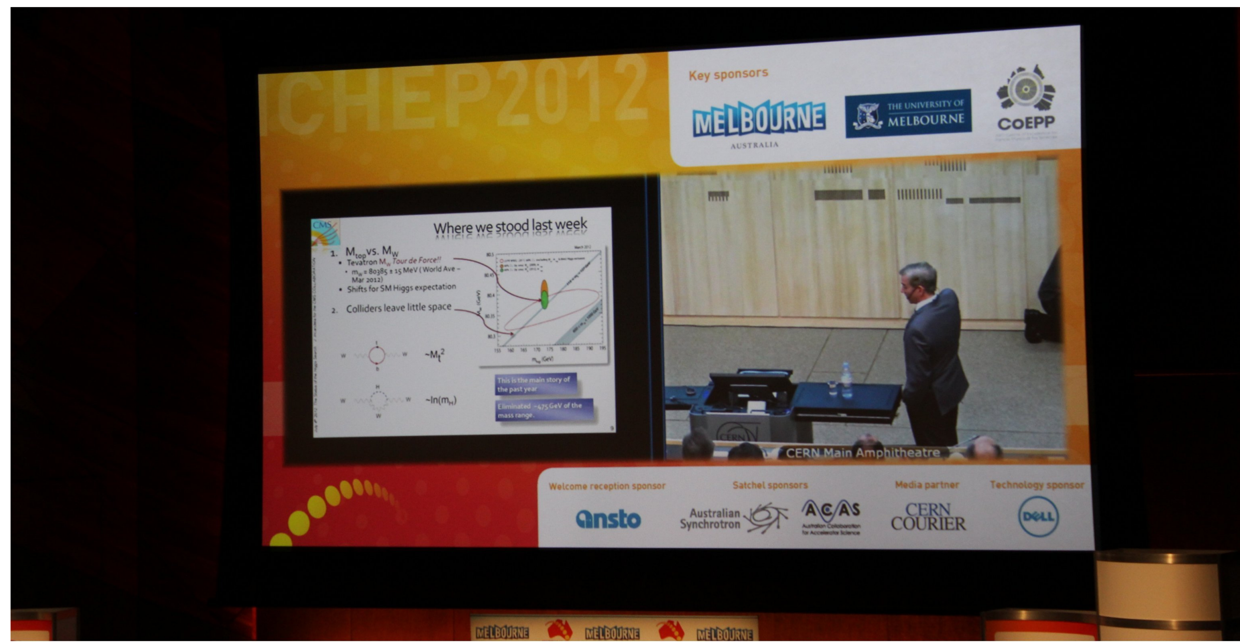
ICHEP2012
Key sponsors
MELBOURNE
THE UNIVERSITY OF MELBOURNE
CoEPP
Where we stood last week
Colliders leave little space
CERN Main Amphitheatre
Welcome reception sponsor
ansto
Satchel sponsors
Australian Synchrotron
Media partner
CERN COURIER
Technology sponsor
DELL

Conclusions

Simple object reconstruction techniques work very well (cone algorithms, track match, ….).

Major efforts went into energy calibrations:

- gain calibration, separately for each cell
- object-level calibrations:
    - electron/photon energy scale, jet energy scale
    - powerful combination of measurements based on data control samples and of corrections from first-principles simulation.

Detailed simulations are a major ingredient for precision measurements:

- detailed simulation of EM showers,
- precise tuning of material model,
- "ZB overlay" to model the effect of "pile-up",
- ….

This detailed work on calorimetry is a cornerstone of the success of the rich physics programme at DØ.
In this talk, insisted on only two measurements:

- Together with our friends across the ring,
  we have measured the top quark mass to better than 1 GeV,
  we have reduced the uncertainty in the W boson mass from 33 MeV (LEP) to 15 MeV.
- These measurements became available just at the right time, because it is a key ingredient that is needed to check if the new boson discovered at CERN has the properties of the standard model Higgs boson.

But these are just two examples of the wealth of relevant physics results from the Tevatron.

Backup Slides

Fermilab

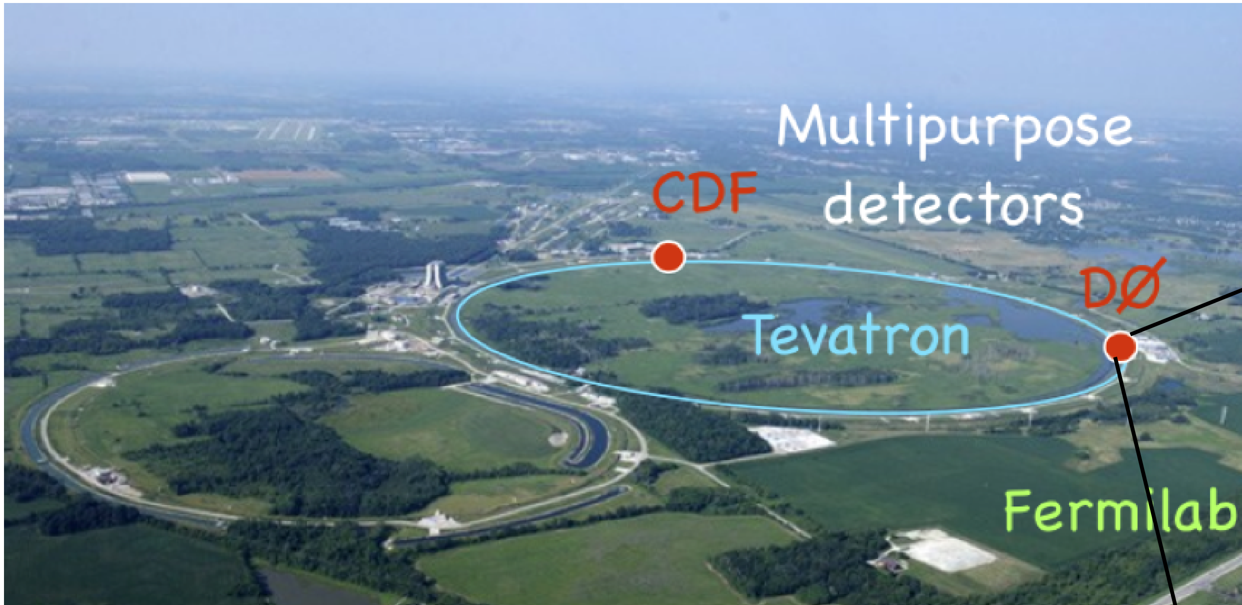

Tevatron collider at Fermilab near Chicago:
proton-antiproton collisions at 2 TeV.

Data taking periods

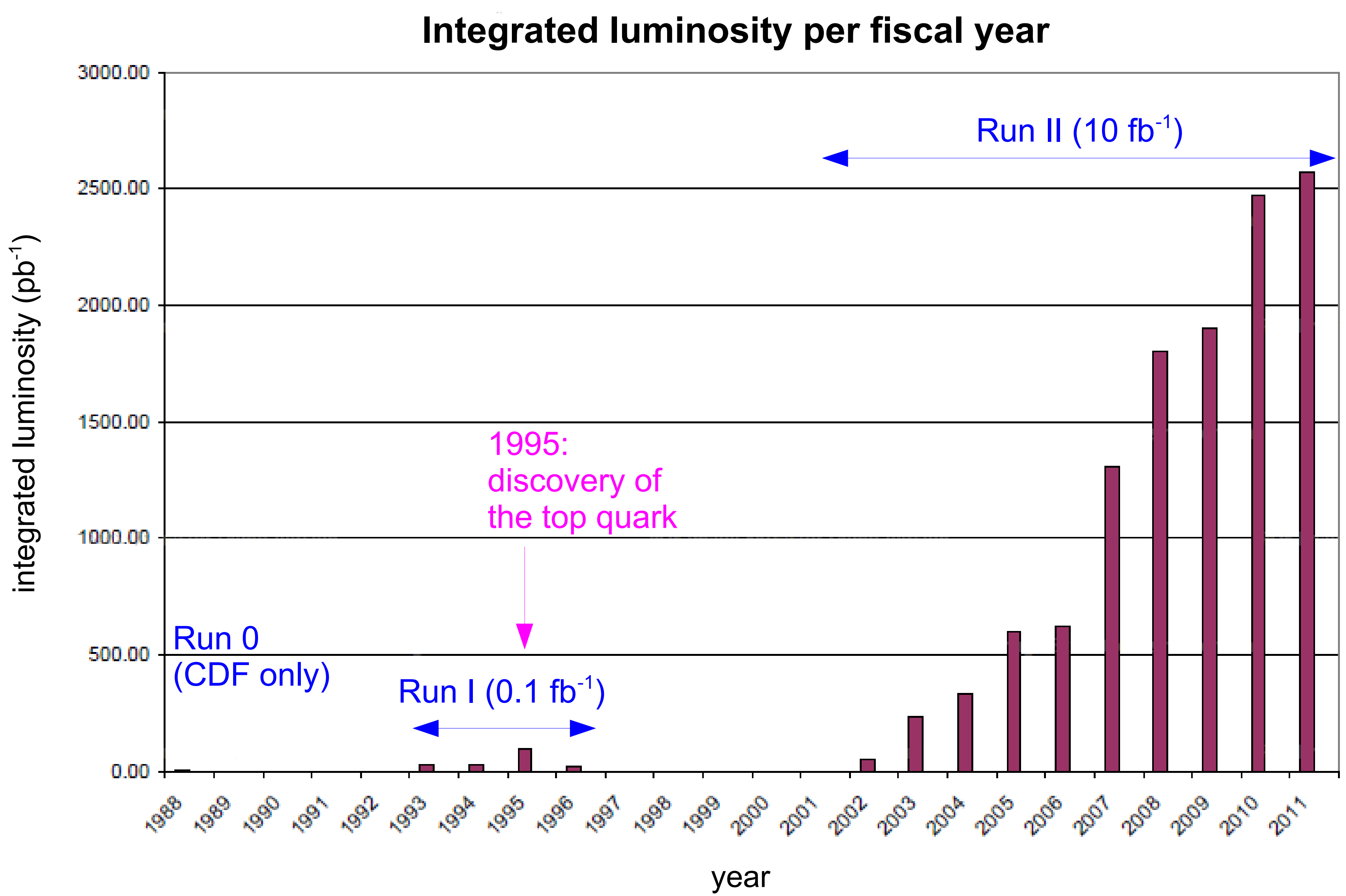

Segmentation of the calorimeter

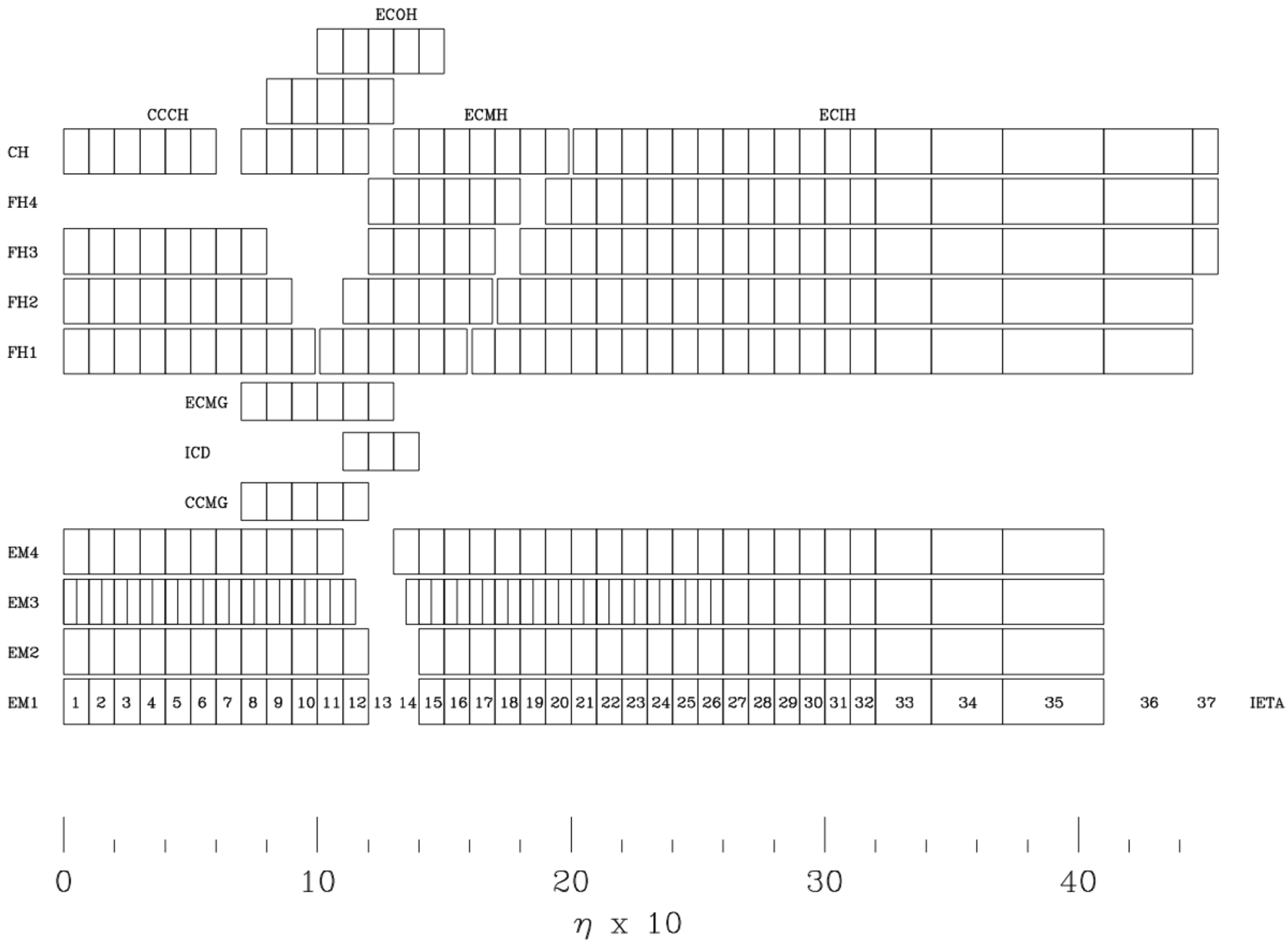

Unit cell of the calorimeter readout

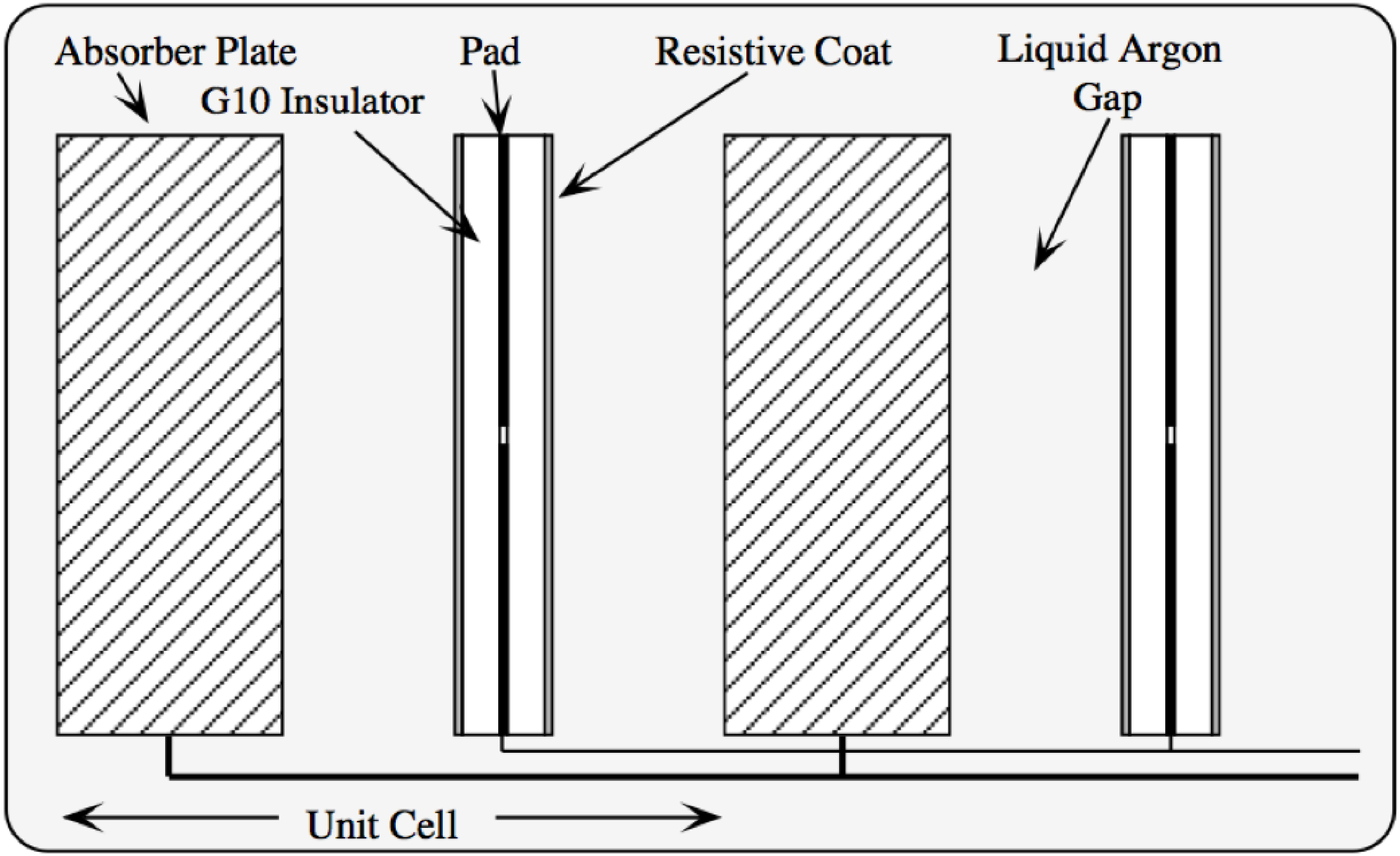

Electronics calibration

Aim: correct for channel-by-channel differences in electronics response.

Principle:
inject known signal into preamplifier and see what the electronics measures.

Do this separately for gains x8 and x1, possibly also separately for the two L1 SCAs per channel.

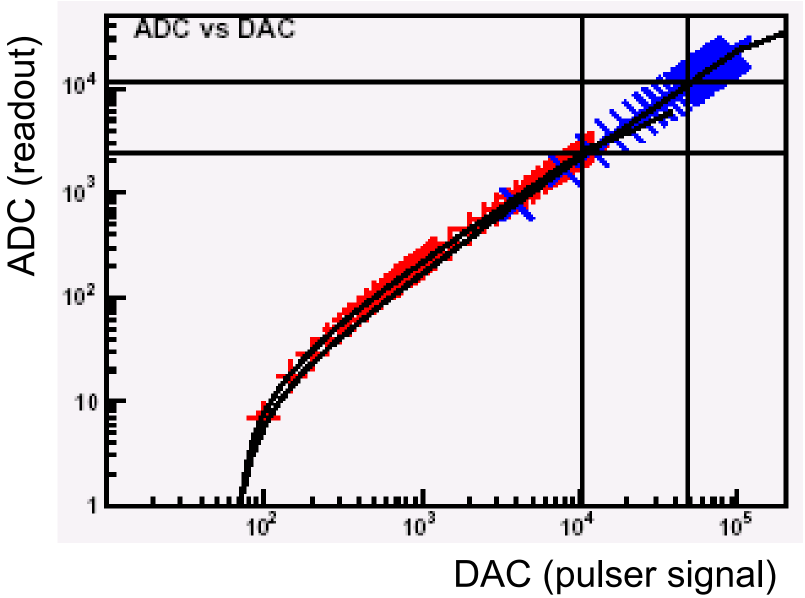

Major improvements to electronics calibration in d0reco p17:

- use database for up-to-date calibration constants (pedestals, gains, non-linearities)
- smarter pulser patterns, improved parameterisation of measured response
- improved timing corrections
- improved corrections for pulser/physics response differences

Phi intercalibration

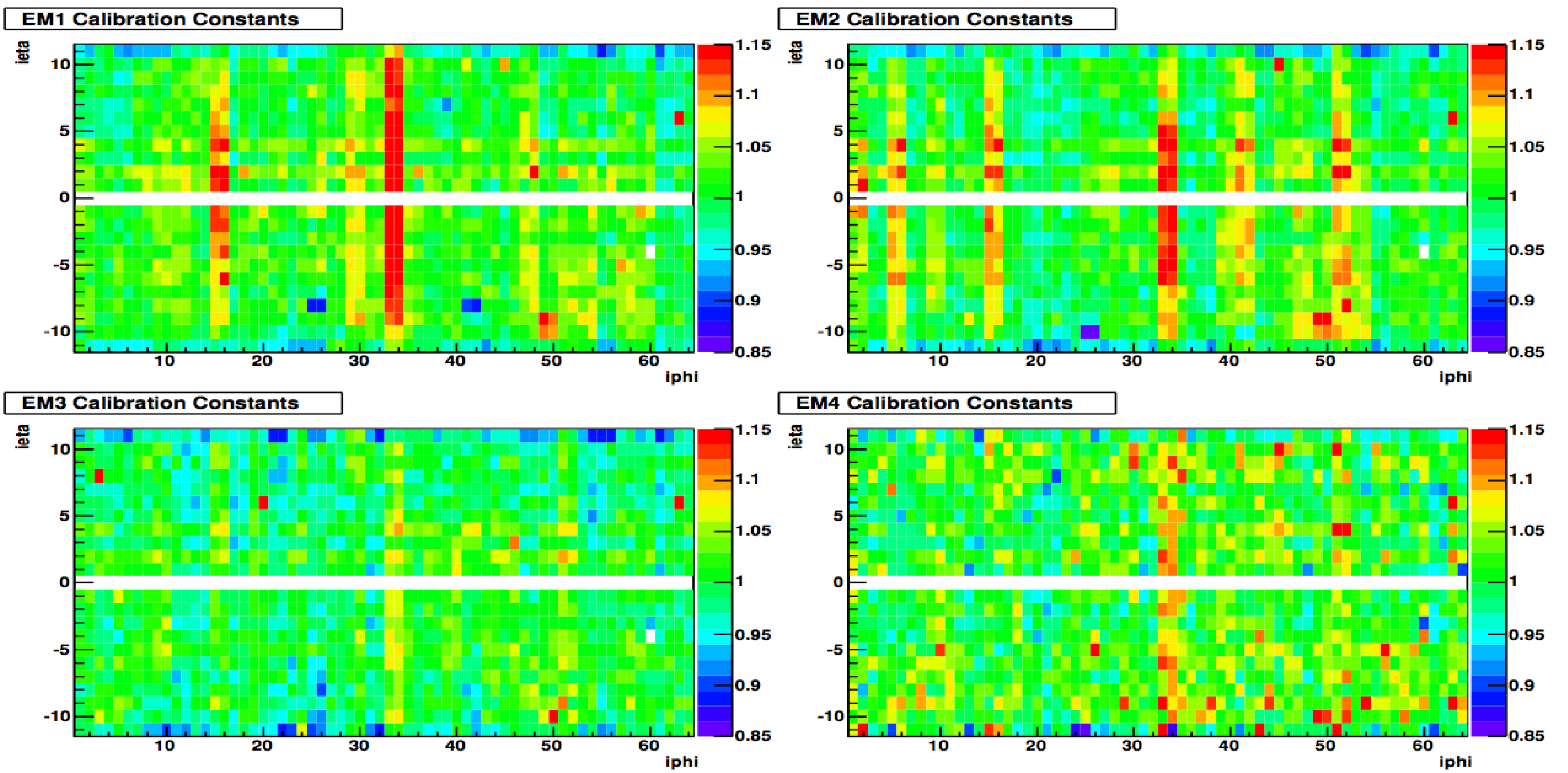

Eta equalisation and absolute scale

Write reconstructed Z mass as: $m = \sqrt{2 \cdot E_1 \cdot E_2 \cdot (1 - \cos\theta)}$,

E_1 and E_2 are the electron energies and θ is the opening angle from tracking.

The electron energies are evaluated as: $E_i = E_i^{\text{raw}} + K\left(E_i^{\text{raw}}, \vec{\alpha}\right)$.

raw energy measurement from the calorimeter

parameterised energy-loss correction from detailed detector simulation

With the raw cluster energy: $$E_i^{\text{raw}} = \sum_{j=(\text{all cells})} c_{\text{ieta}(j)} \cdot E'_j \,.$$

one (unknown) calibration constant per ring in eta

cell energy after electronics calibration, phi intercalibration and layer weights

Then determine the set of calibration constants c_{ieta} that minimise the experimental resolution on the Z mass and that give the correct (LEP) measured value for the Z mass.

Eta-dependent absolute scale

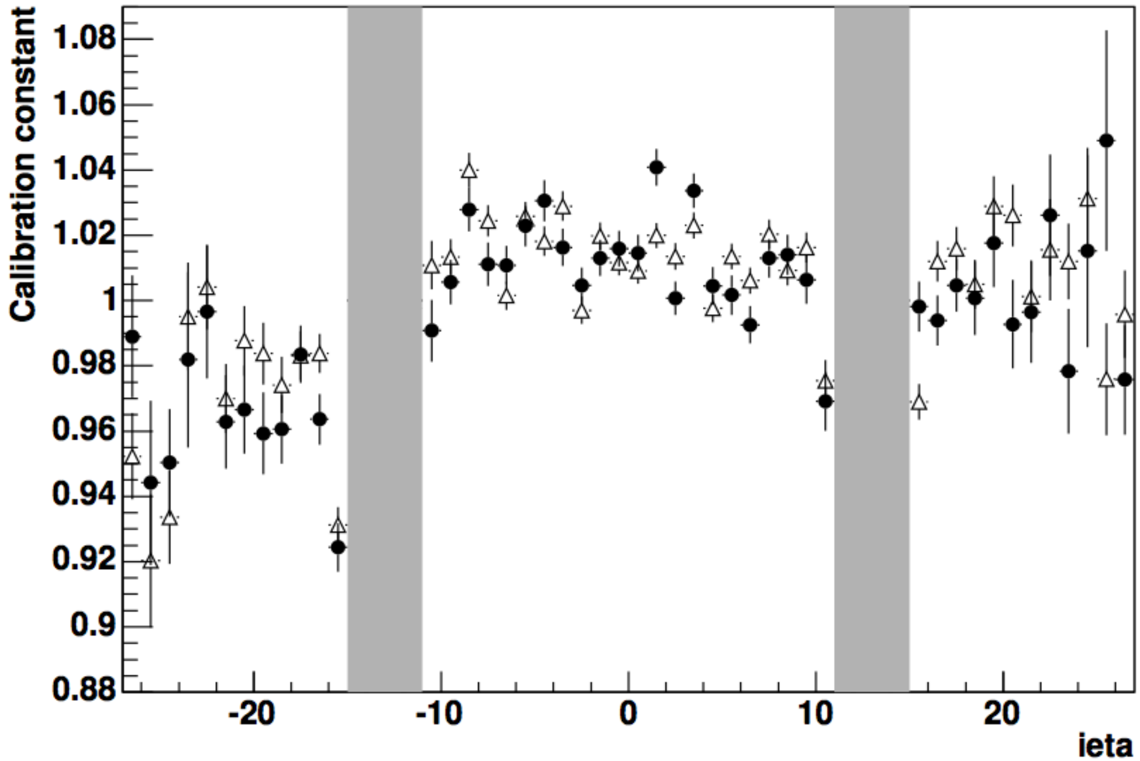

FIGURE 4.7 – Résultat de la détermination de l'échelle absolue en énergie, séparément pour chaque anneau à η (ieta) donné. Les zones grises indiquent les zones de transition entre les cryostats (elles ne sont pas prises en compte dans l'ajustement des constantes de calibration à l'aide de l'échantillon $Z \rightarrow ee$). Le point à ieta $= -27$ représente la constante commune qui est définie pour les anneaux à $-37 \leq$ ieta ≤ -27, *idem* pour ieta $= +27$. Les triangles représentent les résultats obtenus pour les données enregistrées avant la période d'arrêt en sept/nov 2003, les points représentent ceux pour les données prises juste après cette période d'arrêt.

Finite integration time

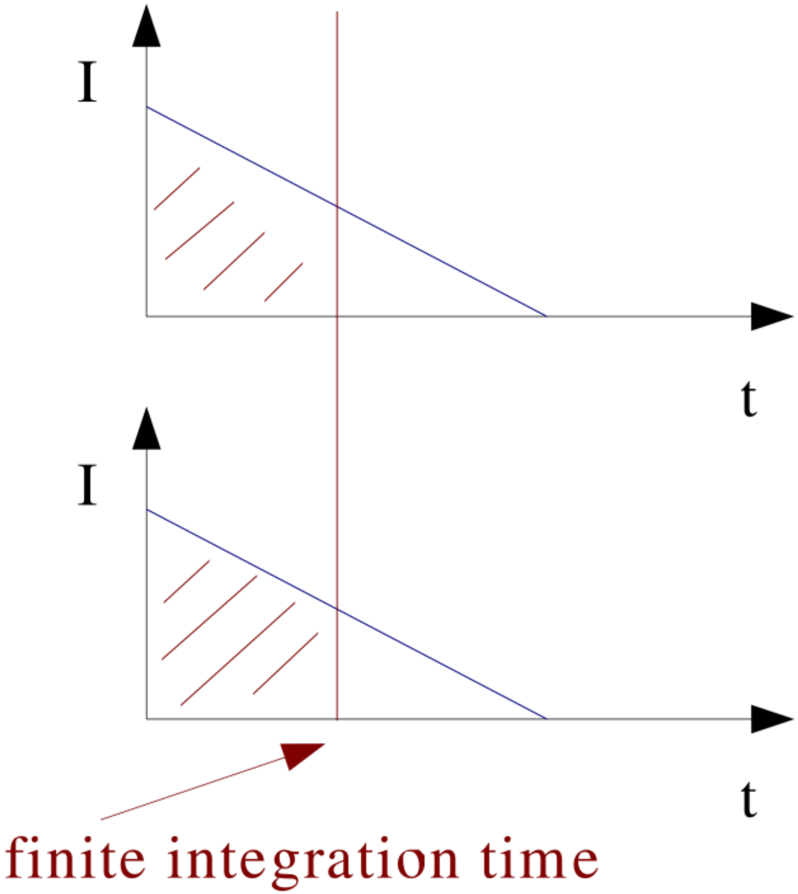

(a) géométrie parfaite du ≪ *di-gap* ≫

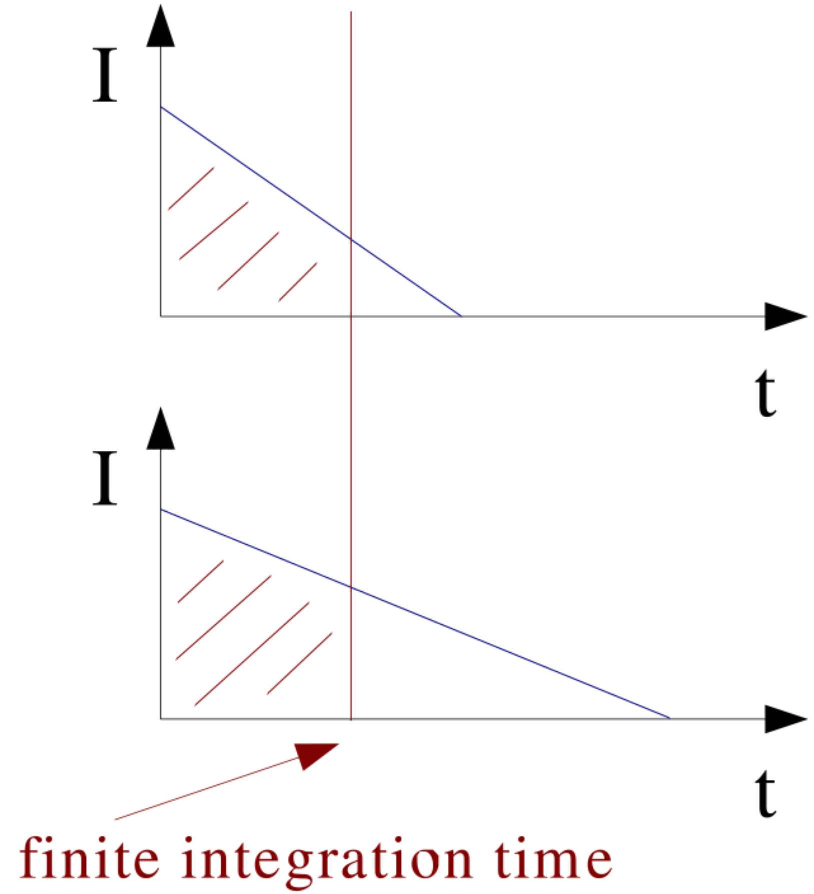

(b) la carte de lecture ne se trouve pas exactement au centre du ≪ *di-gap* ≫

Calorimeter: stability of effective HV

Unit cell of the calorimeter readout:

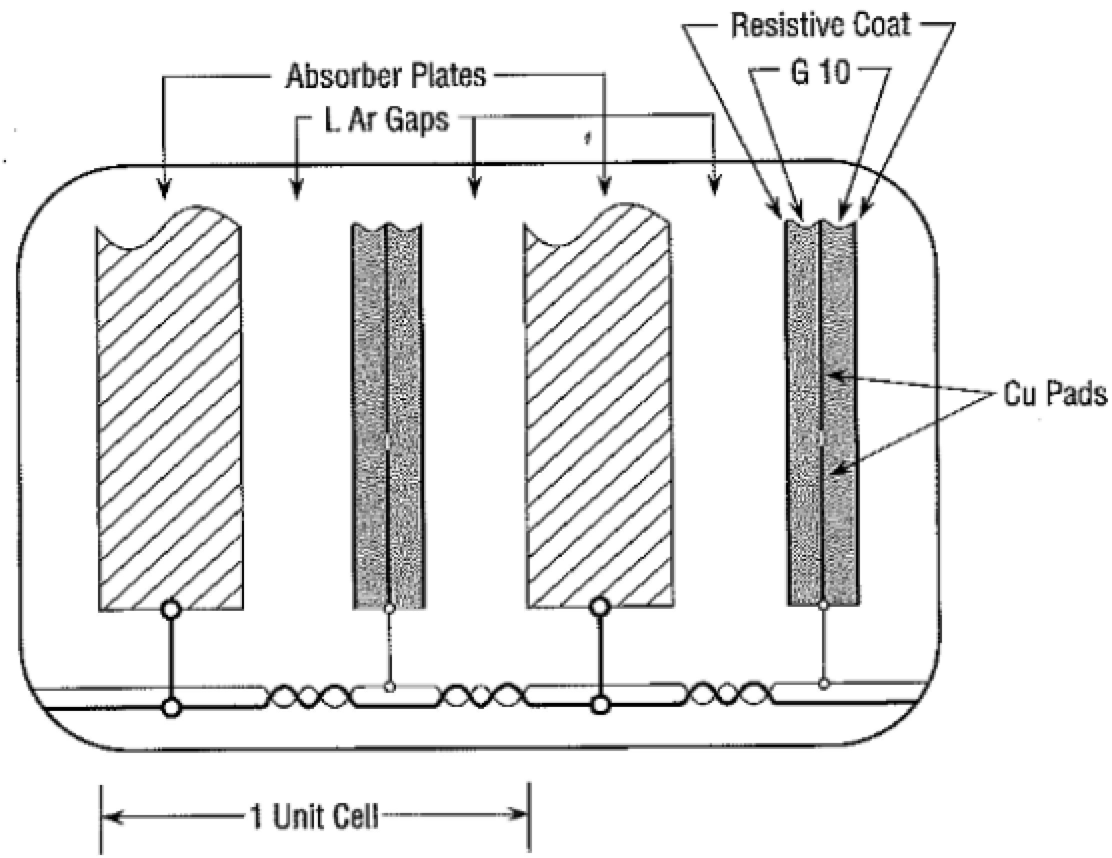

Fig. 27. Schematic view of the liquid argon gap and signal board unit cell.

Liquid Argon calorimeter:

- no intrinsic amplification
- very stable device
  - argon is pure
  - geometry is stable
  - readout electronics is monitored regularly

One caveat:

The resistive coat has very high surface resistivity:

~ 200 MΩ/☐

Any significant current will lead to a voltage drop across the resistive coat

=> reduced electric field

=> reduced drift velocity

=> (slightly) reduced energy response

Calorimeter: currents

This example channel is connected to di-gaps in CC-EM4 readout sections.

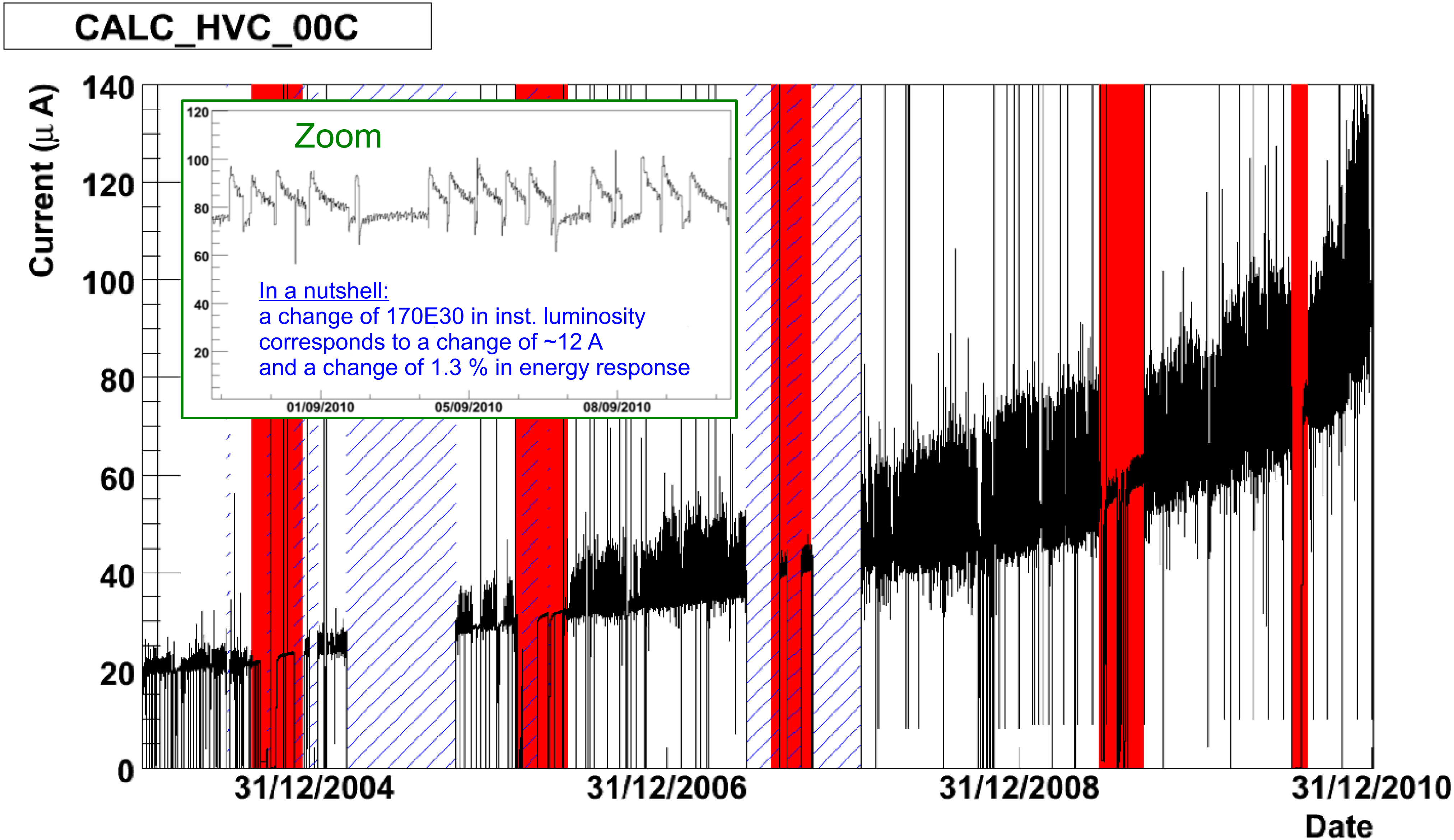

Final electron energy scale calibration

AFTER calorimeter calibration, simulation of effect of inst. luminosity, corrections for dead material, modeling of underlying energy flow:

final electron energy response calibration, using $Z \to e\, e$, the known Z mass value from LEP and the standard "f_z method":

We are effectively measuring m_W/m_Z.

$$E_{measured} = scale * (E_{true} - 43\ GeV) + offset + 43\ GeV$$

Use energy spread of electrons in Z decay (e.g. due to Z boost) to constrain scale *and* offset .

In a nutshell: the f_Z observable allows you to split your sample of electrons from $Z \to e\, e$ into subsamples of different true energy;
this way you can "scan" the electron energy response as a function of energy.

In Run IIb we do this separately for four bins of instantaneous luminosity (plot on the right).

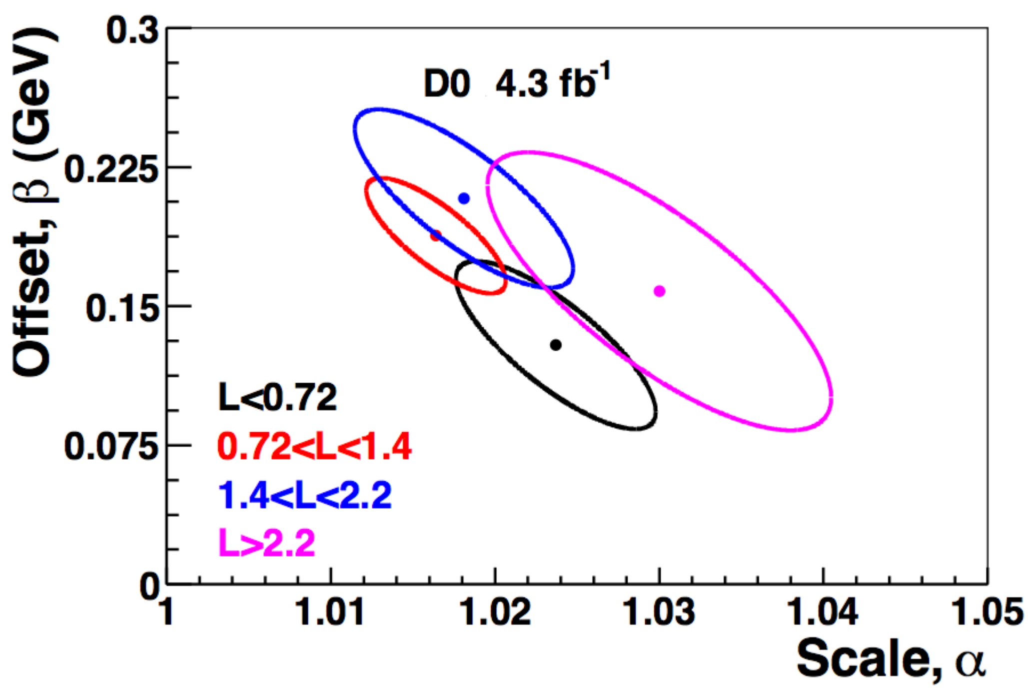

Soft electrons close to jets: "road method"

Basic idea:

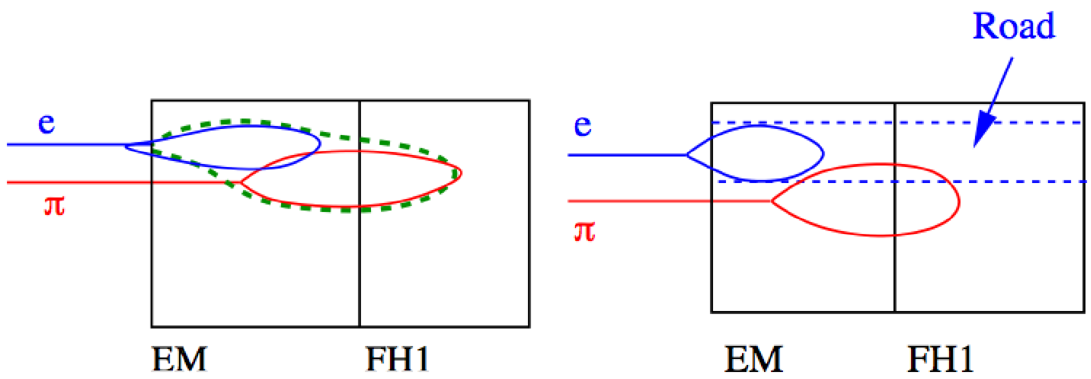

Example of a "road"
in the central calorimeter:

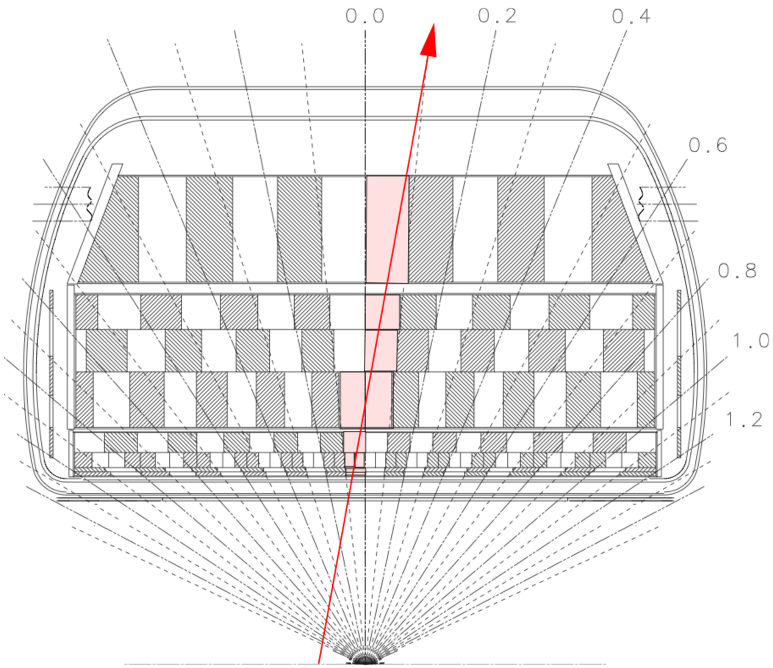

Soft electrons close to jets: “road method”

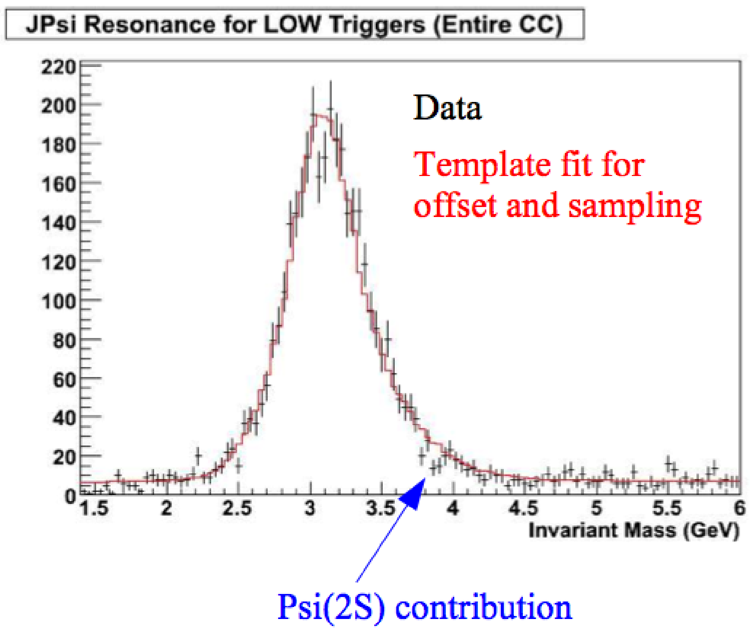

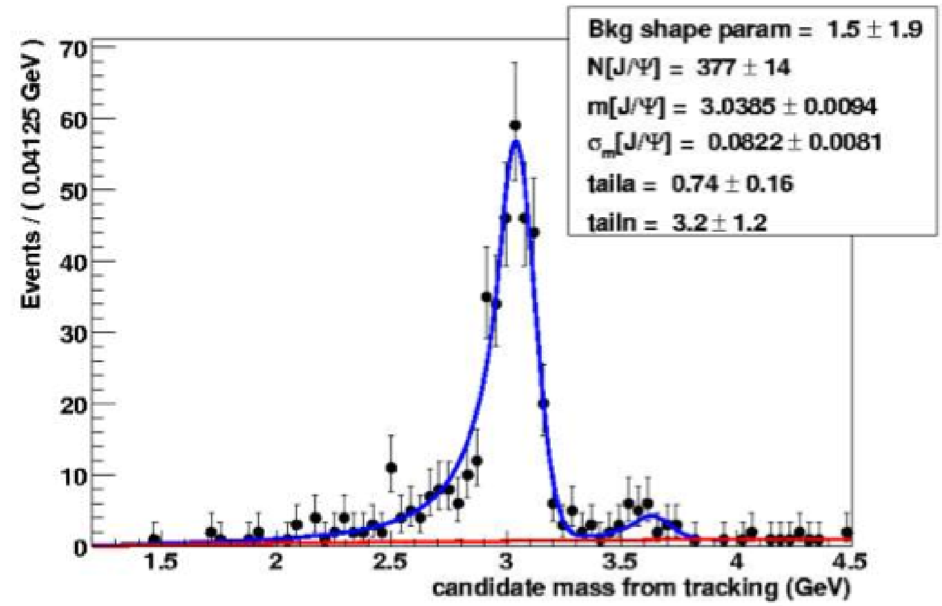

Recoil model

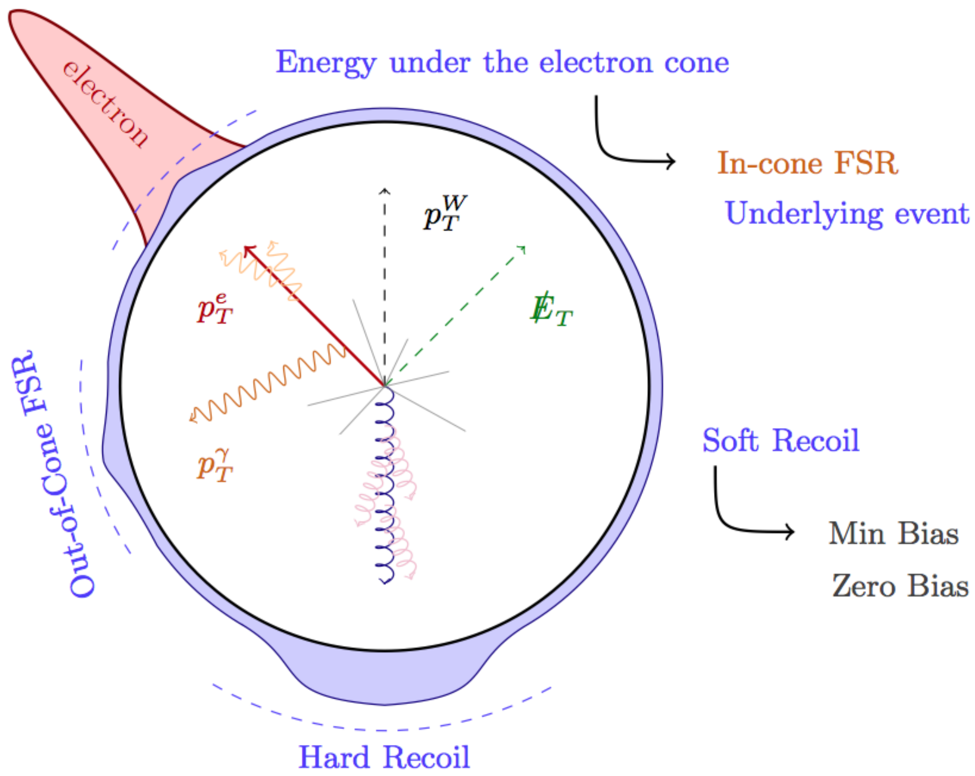

Have five tunable parameters in the recoil model that allow us to adjust the response to the hard recoil as well as the resolution (separately for hard and soft components).

$$\vec{u}_T = \vec{u}_T^{\,\mathrm{HARD}} + \vec{u}_T^{\,\mathrm{SOFT}} + \vec{u}_T^{\,\mathrm{ELEC}} + \vec{u}_T^{\,\mathrm{FSR}}$$

- $\vec{u}_T^{\,\mathrm{HARD}}$ models the hard hadronic energy from the W recoil.
- $\vec{u}_T^{\,\mathrm{SOFT}}$ models the soft hadronic activity from zero bias and minimum bias activity.
- $\vec{u}_T^{\,\mathrm{ELEC}} = -\sum_e \Delta u_{\parallel} \cdot \hat{p}_T(e) + \vec{p}_T^{\,\mathrm{LEAK}}$ models the recoil energy that was reconstructed under the electron cone, as well as any energy form the electron that leaked outside the cone.
- $\vec{u}_T^{\,\mathrm{FSR}}$ models the out–of–cone FSR that is reconstructed as hadronic recoil.

Recoil calibration

Final adjustment of free parameters in the recoil model is done *in situ* using balancing in Z → e e events and the standard UA2 observables.

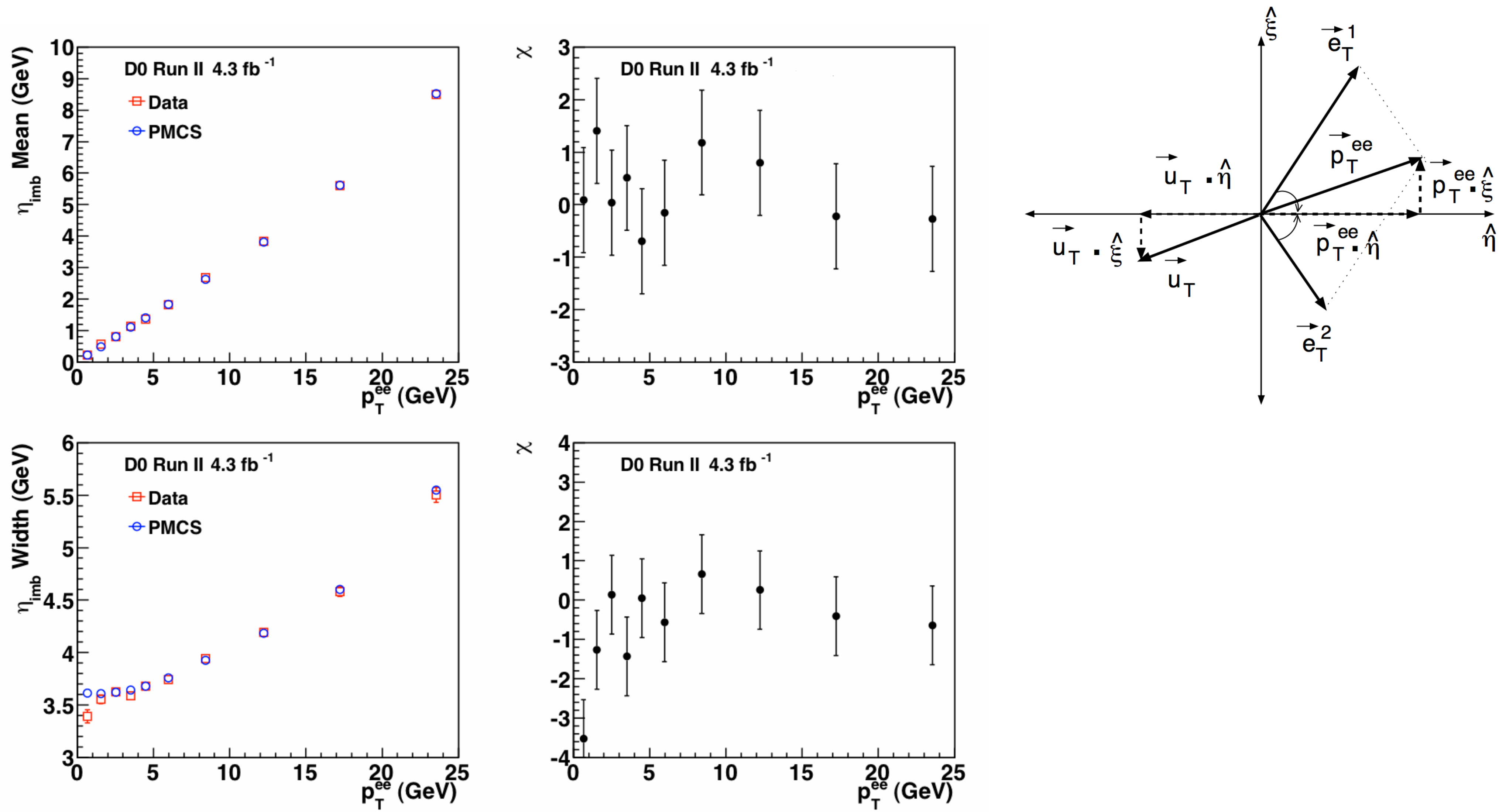

Electrons from Z → e e and W → e ν

Black: W → e ν

Red: Z → e e

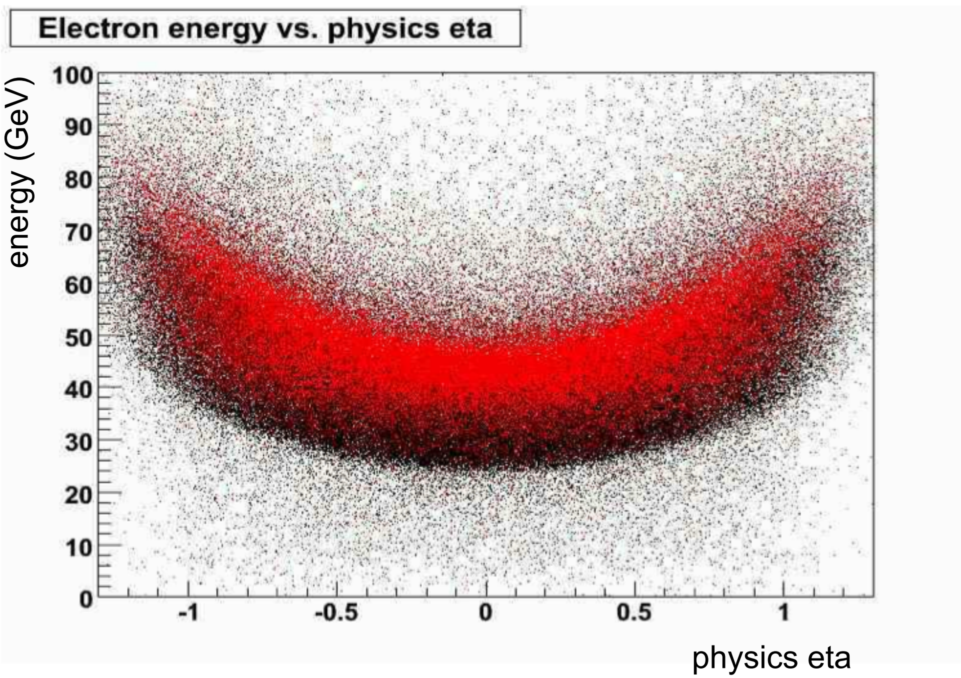

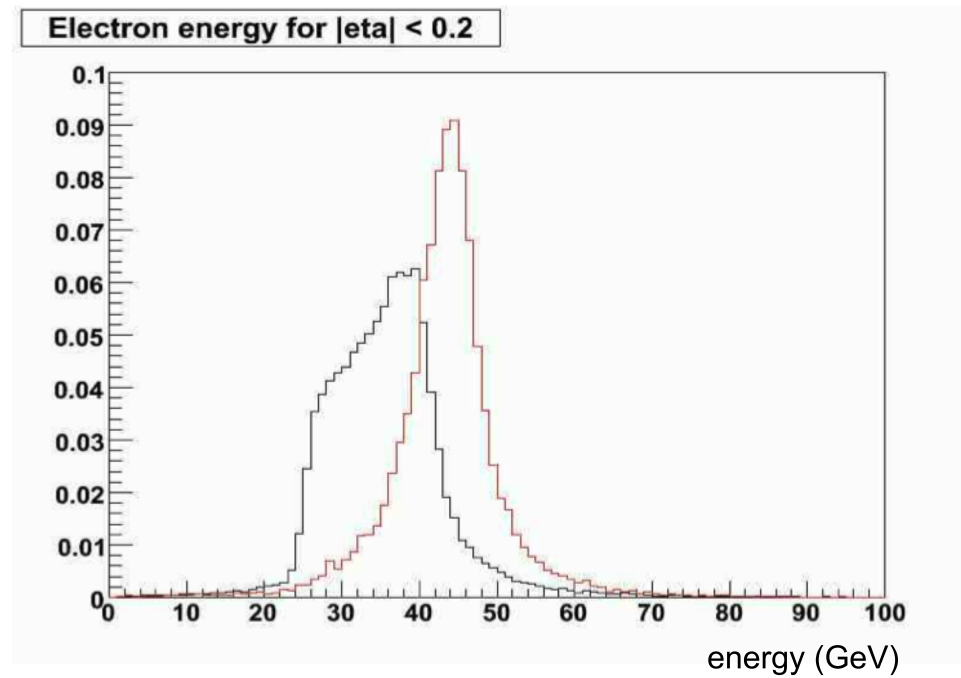

At a given physics eta, the spread in energy of electrons from Z → e e is small.
Also, the overlap with the energy spectrum of electrons from W → e ν is limited.

NB: overlap can be increased by including Z events in the CC-EC configuration (at the cost of understanding the EC).

Run IIb-specific challenges

Higher lumi, hence "way more activity in the detector":

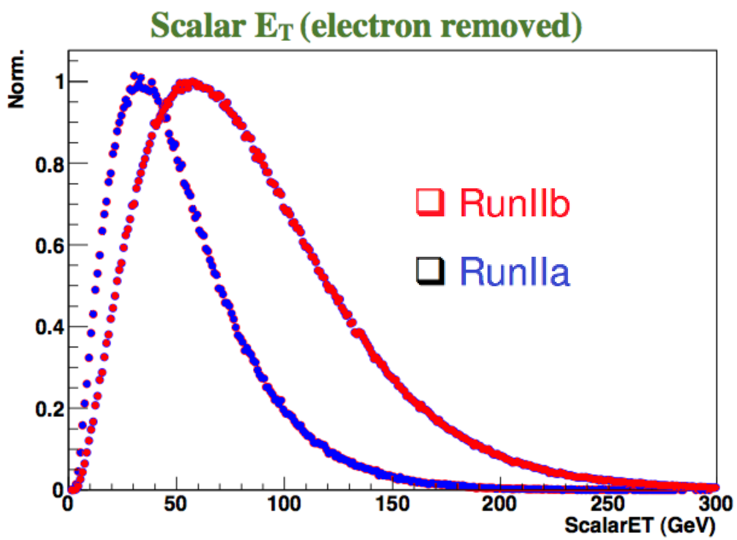

Does have quite an impact on the observables of interest (as shown on the right).

This is why we had to do significant additional R&D (w.r.t. to Run IIa analysis). No additional R&D is expected for the final 5 fb^{-1} (similar lumi spectrum as in current analysis).

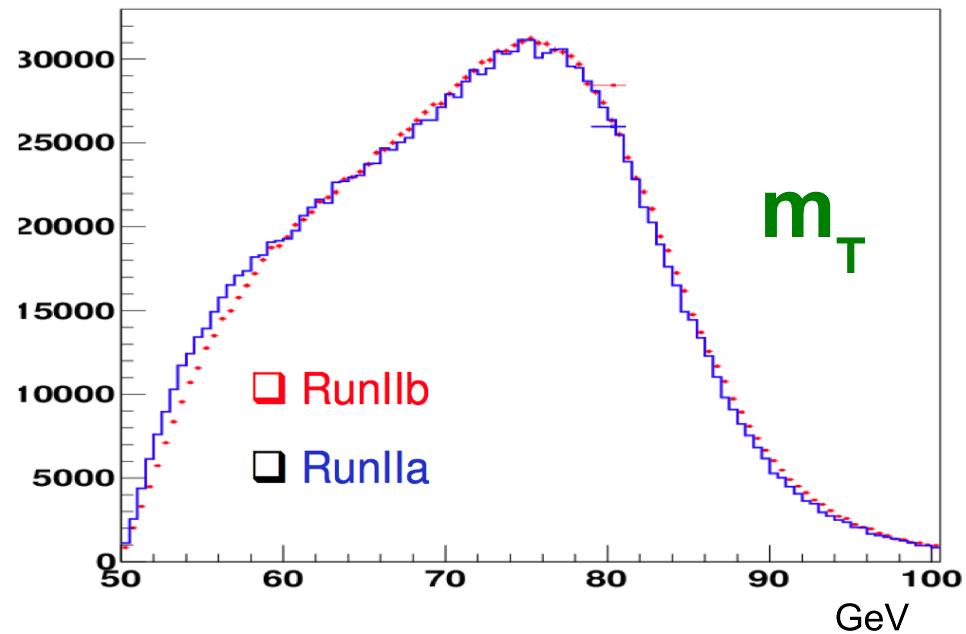

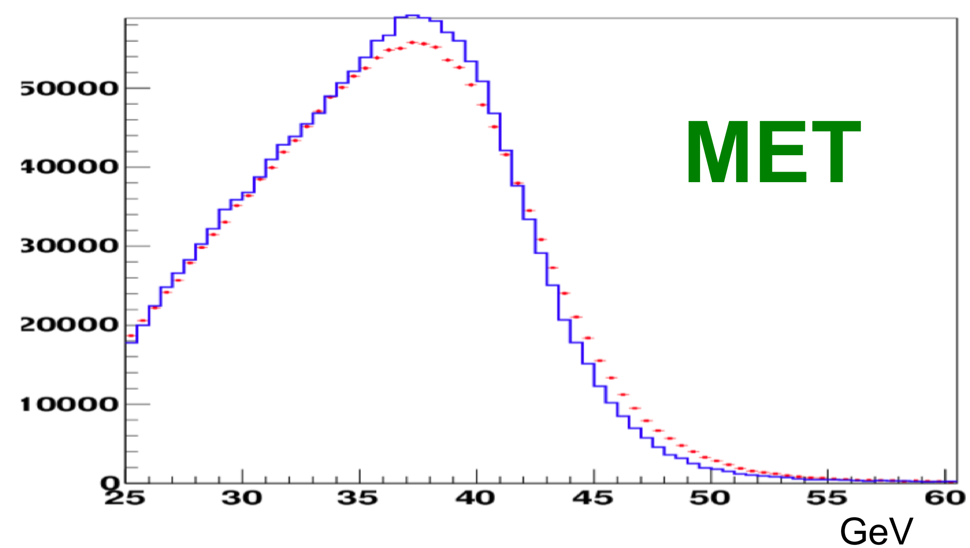

Electron efficiency model

Detailed model of electron reconstruction/identification efficiency in the busy Run IIb environment:

- dependence on electron kinematics (p_T, rapidity)
- effect of the hard recoil
- effect of pileup

Two critical control samples:

- W and Z events from detailed simulation, with “overlay” of collider data (trigger on random bunch crossing)
- $Z \rightarrow e\ e$ (can be selected with minimal electron requirements)

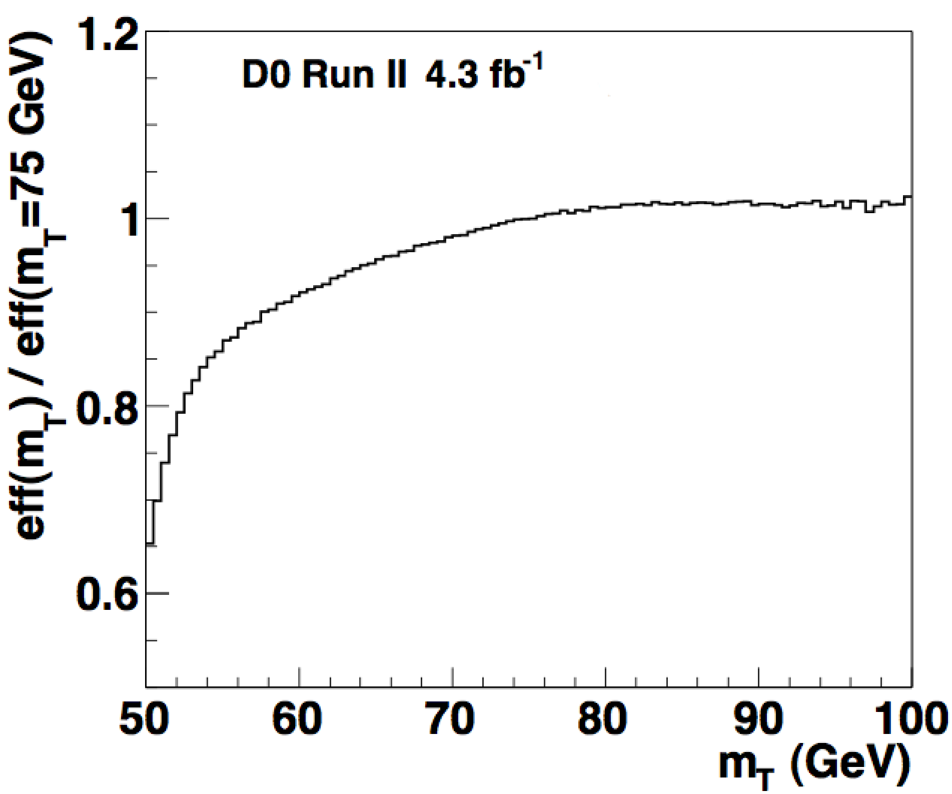

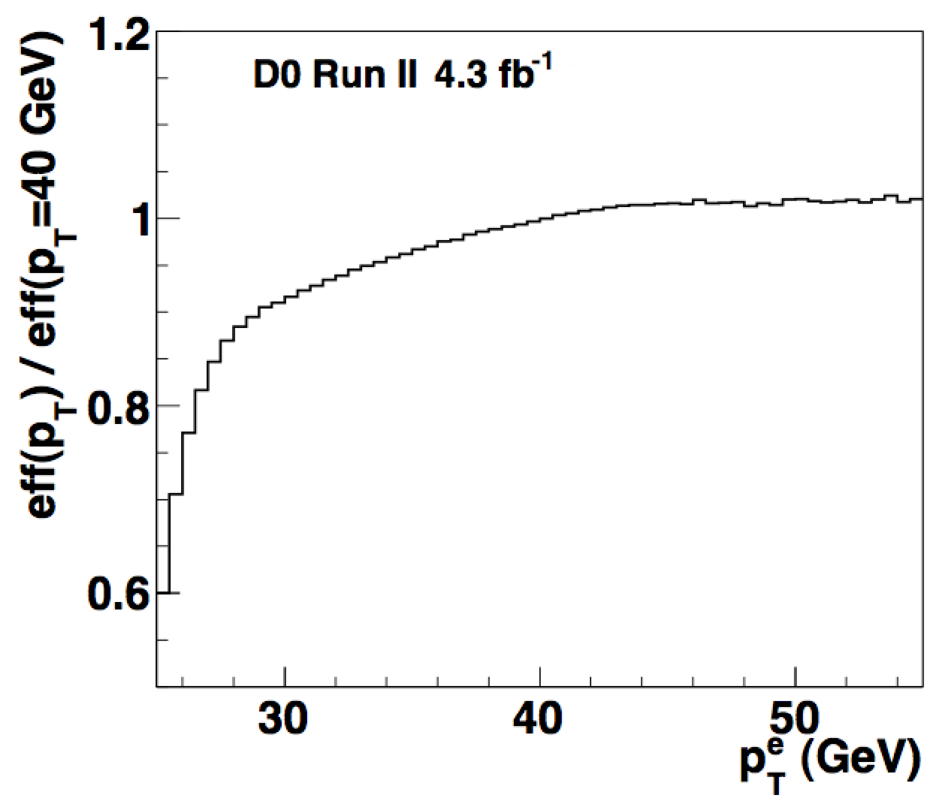

Recoil model

Have five tunable parameters in the recoil model that allow us to adjust the response to the hard recoil as well as the resolution (separately for hard and soft components):

$$\vec{u}_{T,smear}^{soft} = \sqrt{\alpha_{MB}}\vec{u}_T^{MB} + \vec{u}_T^{ZB}$$

model of spectator partons (based on soft collisions in collider data)

model of pileup/noise (from collider data, random trigger)

$$u_{T,smear}^{\|,hard} = \left(\mathrm{R}_A + \mathrm{R}_B \cdot e^{-p_T^Z/\tau_{HAD}}\right) p_T^Z \langle \frac{u_T}{p_T^Z} \rangle^{\|} + \mathrm{S}_A \left(u_T^{\|} - p_T^Z \langle \frac{u_T}{p_T^Z} \rangle^{\|} \right)$$

model of hard recoil response (from detailed first-principles simulation)

Combination of the three observables

We take the results from the three observables (with their correlations) and combine them:

m_T: 80.371± 0.013 (stat) ± 0.022 (syst)

p_T^e: 80.343± 0.014 (stat) ± 0.024 (syst)

MET: 80.355± 0.015 (stat) ± 0.029 (syst)

$$\rho = \begin{pmatrix} \rho_{m_T m_T} & \rho_{m_T p_T^e} & \rho_{m_T \not{E}_T} \\ \rho_{m_T p_T^e} & \rho_{p_T^e p_T^e} & \rho_{p_T^e \not{E}_T} \\ \rho_{m_T \not{E}_T} & \rho_{p_T^e \not{E}_T} & \rho_{\not{E}_T \not{E}_T} \end{pmatrix} = \begin{pmatrix} 1.0 & 0.89 & 0.86 \\ 0.89 & 1.0 & 0.75 \\ 0.86 & 0.75 & 1.0 \end{pmatrix}$$

When considering only the uncertainties which are allowed to decrease in the combination (i.e. *not* QED and PDF), we find that the MET measurement has negligible weight. We therefore only retain p_T^e and m_T for the combination.

The combined result is:

$$\begin{aligned} M_W &= 80.367 \pm 0.013\ (\text{stat}) \pm 0.022\ (\text{syst})\ \text{GeV} \\ &= 80.367 \pm 0.026\ \text{GeV}. \end{aligned}$$

The probability to observe a larger spread between the three measurements than in the data is 5 %.

We further combine with our earlier Run II result (1 fb^{-1}) to obtain the new D0 Run II result:

$$\begin{aligned} M_W &= 80.375 \pm 0.011\ (\text{stat}) \pm 0.020\ (\text{syst})\ \text{GeV} \\ &= 80.375 \pm 0.023\ \text{GeV}. \end{aligned}$$

Comparison with previous results; New averages

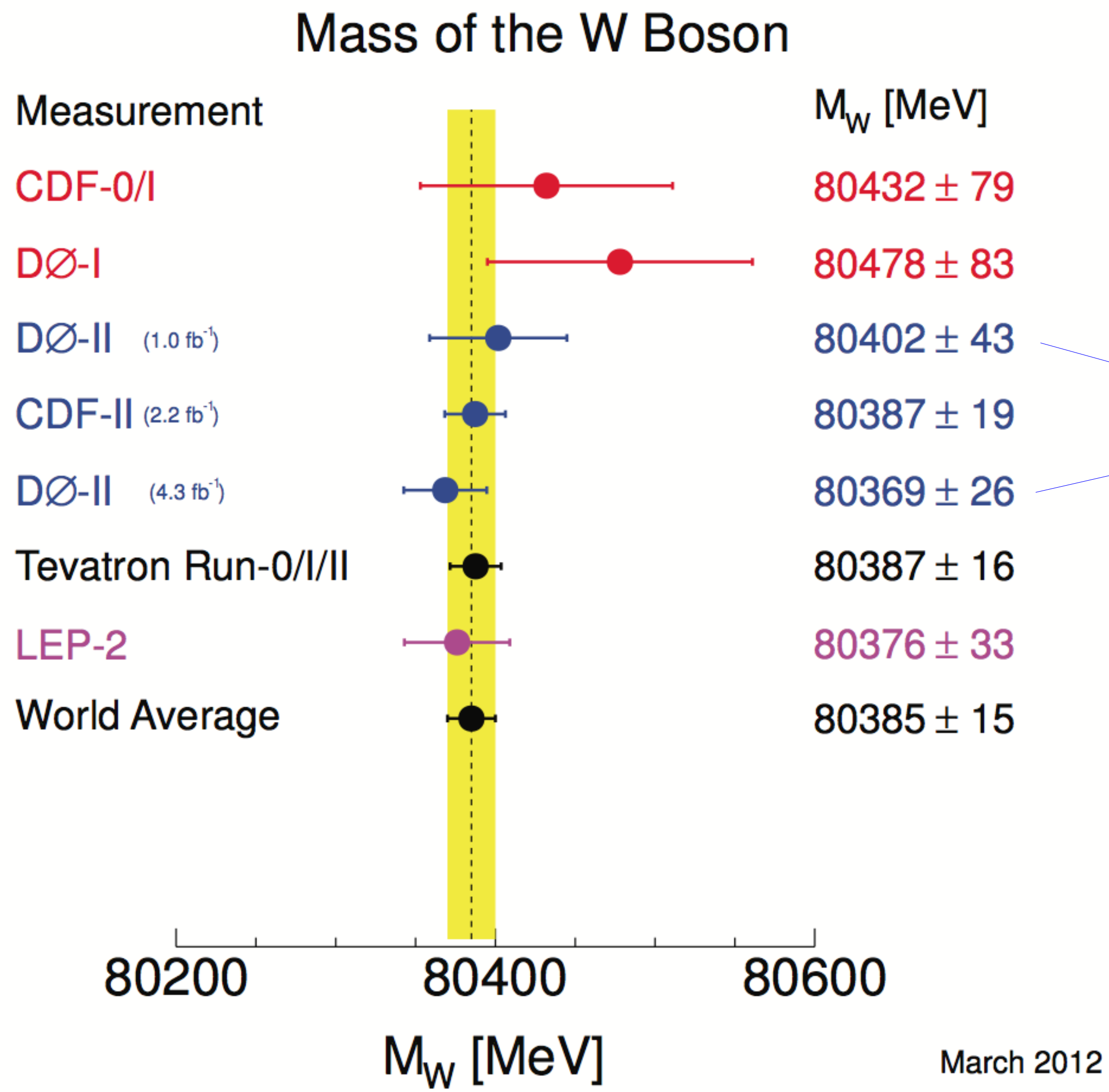

DØ Run II combination:
80375 ± 23 MeV

arXiv:1204.0042 [hep-ex]

PDF uncertainties

In principle:
transverse observables (*e.g.* m_T) are insensitive to the uncertainties in the (longitudinal) parton distribution functions (PDFs)

In practice:
the uncertainties are to some extent reintroduced via the limited η coverage of experiments,
which are not invariant under longitudinal boosts

How to reduce the impact of the PDF uncertainties in measurements of the W boson mass ?

- Reduce the uncertainties in the PDFs

  e.g. via measurements of the W charge asymmetry
  at the Tevatron and the LHC (complementarity of the two colliders)

- Reduce the impact of the PDF uncertainties on W boson mass

  by extending the η coverage as much as possible
  (challenging: understanding lepton energy scale and pile-up and backgrounds in the forward detectors)

- Possibly reduce the impact of the PDF uncertainties on W boson mass

  by exploring even more robust observables
  ("single out events with small longitudinal momentum") to replace/complement m_T

A. De Rújula, A. Galindo, JHEP 08, 023 (2011)

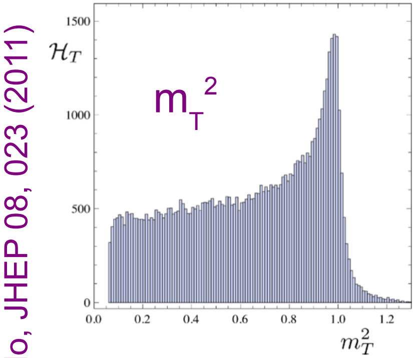

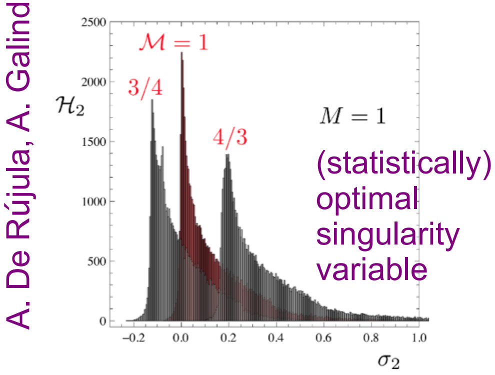

These three approaches are not mutually exclusive, *i.e.* they can be pursued at the same time and gains should "add up".

Future PDF sets

Our theory friends are also active on improvements to PDF sets.

An example:

MSUHEP-100707, SMU-HEP-10-10, arXiv:1007.2241[hep-ph]

New parton distributions for collider physics

Hung-Liang Lai,[1,2] Marco Guzzi,[3] Joey Huston,[1] Zhao Li,[1] Pavel M. Nadolsky,[3] Jon Pumplin,[1] and C.-P. Yuan[1]

[1] *Department of Physics and Astronomy, Michigan State University, East Lansing, MI 48824-1116, U.S.A.*
[2] *Taipei Municipal University of Education, Taipei, Taiwan*
[3] *Department of Physics, Southern Methodist University, Dallas, TX 75275-0175, U.S.A.*

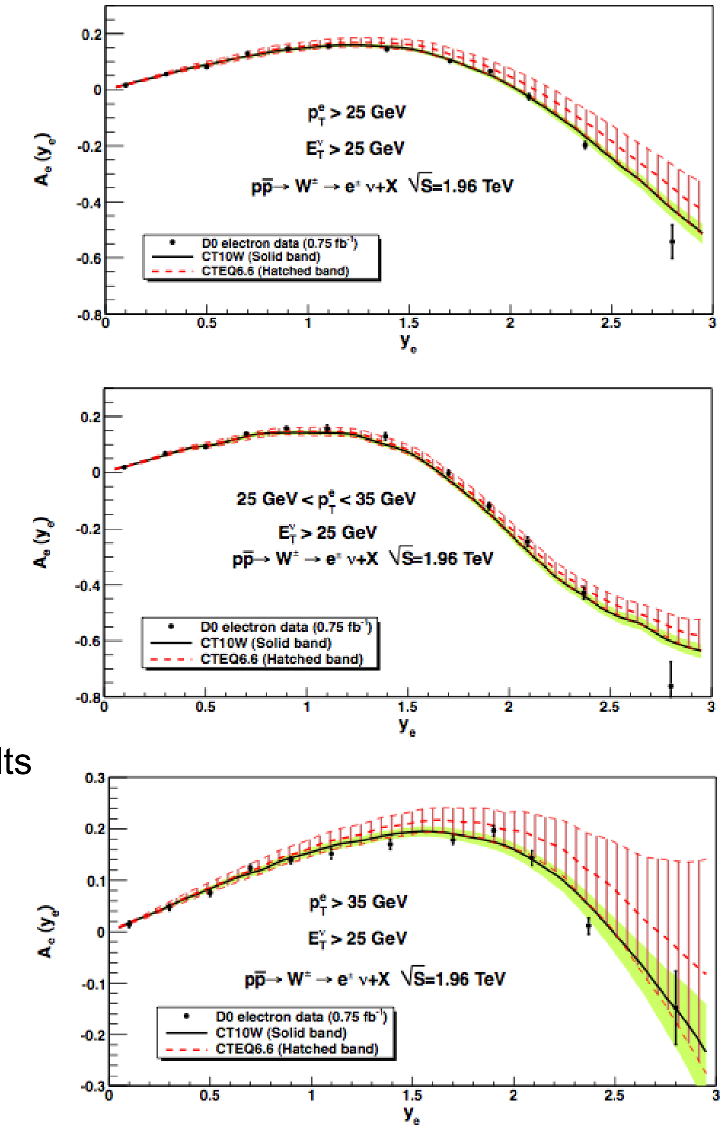

The PDF set “CT10W” is an important step towards including new results on W (lepton) charge asymmetry from the Tevatron into PDF sets. Critical to further constrain the u/d ratio !

Not quite “production quality” yet, but this is going into the right direction.

Constraints on the Higgs boson mass

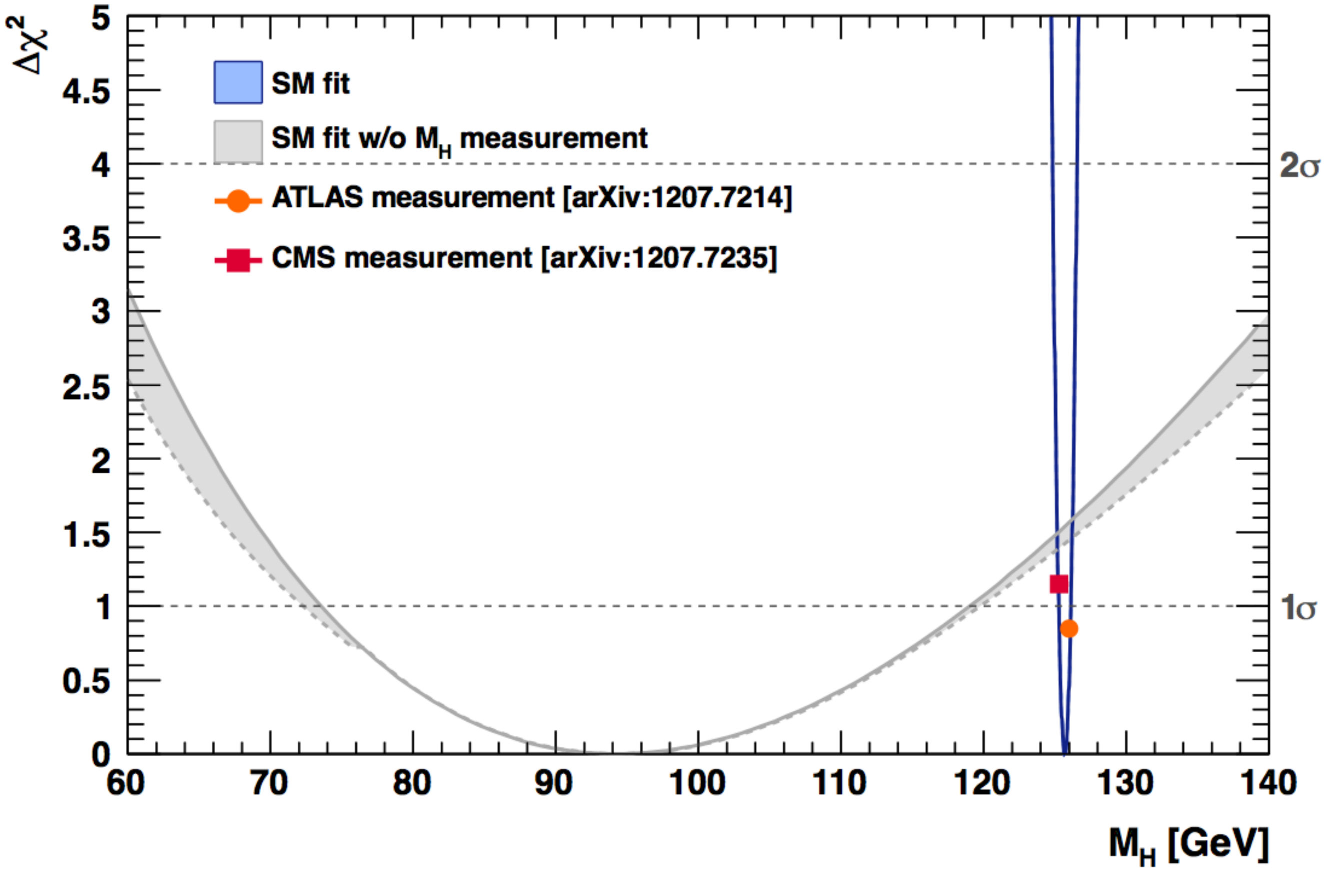

Indirect constraint on Higgs mass:

$M_H = 94^{+25}_{-22}$ GeV

Consistent (1.3 σ) with direct measurements the mass of the new boson discovered at CERN.

Gfitter group, arXiv:1209.2716 [hep-ph]

Alternatively, this test can be "turned around": use electroweak fit, including measurement of Higgs boson mass, to predict the W boson mass:

$$M_W = 80.3593 \pm 0.0056_{m_t} \pm 0.0026_{M_Z} \pm 0.0018_{\Delta\alpha_{\text{had}}} \pm 0.0017_{\alpha_S} \pm 0.0002_{M_H} \pm 0.0040_{\text{theo}}$$

$$= 80.359 \pm 0.011_{\text{tot}}$$

Direct measurement:
$M_W = 80.385 \pm 0.015$

Global electroweak fit

Sept 12 version of Gfitter standard model fit includes, in addition to the latest theory calculations, the LEP/SLD precision legacy, …, various updates:

- latest top quark combination from Tevatron,
- latest world average W boson mass,
- measurements of the "Higgs boson mass" from the LHC.

Parameter	Input value	Free in fit	Fit result incl. M_H	Fit result not incl. M_H	Fit result incl. M_H but not exp. input in row
M_H [GeV]$^{(\circ)}$	125.7 ± 0.4	yes	125.7 ± 0.4	$94\,^{+25}_{-22}$	$94\,^{+25}_{-22}$
M_W [GeV]	80.385 ± 0.015	–	80.367 ± 0.007	80.380 ± 0.012	80.359 ± 0.011
Γ_W [GeV]	2.085 ± 0.042	–	2.091 ± 0.001	2.092 ± 0.001	2.091 ± 0.001
M_Z [GeV]	91.1875 ± 0.0021	yes	91.1878 ± 0.0021	91.1874 ± 0.0021	91.1983 ± 0.0116
Γ_Z [GeV]	2.4952 ± 0.0023	–	2.4954 ± 0.0014	2.4958 ± 0.0015	2.4951 ± 0.0017
$\sigma^0_{\rm had}$ [nb]	41.540 ± 0.037	–	41.479 ± 0.014	41.478 ± 0.014	41.470 ± 0.015
R^0_ℓ	20.767 ± 0.025	–	20.740 ± 0.017	20.743 ± 0.018	20.716 ± 0.026
$A^{0,\ell}_{\rm FB}$	0.0171 ± 0.0010	–	0.01627 ± 0.0002	0.01637 ± 0.0002	0.01624 ± 0.0002
A_ℓ $^{(\star)}$	0.1499 ± 0.0018	–	$0.1473\,^{+0.0006}_{-0.0008}$	0.1477 ± 0.0009	$0.1468 \pm 0.0005^{(\dagger)}$
$\sin^2\theta^\ell_{\rm eff}(Q_{\rm FB})$	0.2324 ± 0.0012	–	$0.23148\,^{+0.00011}_{-0.00007}$	$0.23143\,^{+0.00010}_{-0.00012}$	0.23150 ± 0.00009
A_c	0.670 ± 0.027	–	$0.6680\,^{+0.00025}_{-0.00038}$	$0.6682\,^{+0.00042}_{-0.00035}$	0.6680 ± 0.00031
A_b	0.923 ± 0.020	–	$0.93464\,^{+0.00004}_{-0.00007}$	0.93468 ± 0.00008	0.93463 ± 0.00006
$A^{0,c}_{\rm FB}$	0.0707 ± 0.0035	–	$0.0739\,^{+0.0003}_{-0.0005}$	0.0740 ± 0.0005	0.0738 ± 0.0004
$A^{0,b}_{\rm FB}$	0.0992 ± 0.0016	–	$0.1032\,^{+0.0004}_{-0.0006}$	0.1036 ± 0.0007	0.1034 ± 0.0004
R^0_c	0.1721 ± 0.0030	–	0.17223 ± 0.00006	0.17223 ± 0.00006	0.17223 ± 0.00006
R^0_b	0.21629 ± 0.00066	–	0.21474 ± 0.00003	0.21475 ± 0.00003	0.21473 ± 0.00003
$\overline{m}_c$ [GeV]	$1.27\,^{+0.07}_{-0.11}$	yes	$1.27\,^{+0.07}_{-0.11}$	$1.27\,^{+0.07}_{-0.11}$	–
$\overline{m}_b$ [GeV]	$4.20\,^{+0.17}_{-0.07}$	yes	$4.20\,^{+0.17}_{-0.07}$	$4.20\,^{+0.17}_{-0.07}$	–
m_t [GeV]	173.18 ± 0.94	yes	173.52 ± 0.88	173.14 ± 0.93	$175.8\,^{+2.7}_{-2.4}$
$\Delta\alpha^{(5)}_{\rm had}(M_Z^2)$ $^{(\triangle\triangledown)}$	2757 ± 10	yes	2755 ± 11	2757 ± 11	$2716\,^{+49}_{-43}$
$\alpha_s(M_Z^2)$	–	yes	0.1191 ± 0.0028	0.1192 ± 0.0028	0.1191 ± 0.0028
$\delta_{\rm th} M_W$ [MeV]	$[-4, 4]_{\rm theo}$	yes	4	4	–
$\delta_{\rm th} \sin^2\theta^\ell_{\rm eff}$ $^{(\triangle)}$	$[-4.7, 4.7]_{\rm theo}$	yes	-1.4	4.7	–

$^{(\circ)}$Average of ATLAS ($M_H = 126.0 \pm 0.4$ (stat) ± 0.4 (sys)) and CMS ($M_H = 125.3 \pm 0.4$ (stat) ± 0.5 (sys)) measurements assuming no correlation of the systematic uncertainties (see discussion in Sect. 2). $^{(\star)}$Average of LEP ($A_\ell = 0.1465 \pm 0.0033$) and SLD ($A_\ell = 0.1513 \pm 0.0021$) measurements, used as two measurements in the fit. $^{(\dagger)}$The fit w/o the LEP (SLD) measurement gives $A_\ell = 0.1474\,^{+0.0005}_{-0.0009}$ ($A_\ell = 0.1467\,^{+0.0006}_{-0.0004}$). $^{(\triangle)}$In units of 10^{-5}. $^{(\triangledown)}$Rescaled due to α_s dependency.

Global electroweak fit

Complete fit:
χ^2_{min} = 21.8 for 14 degrees of freedom.

Pull values for the different observables are shown on the right.

- no value exceeds 3 sigma
- largest individual contribution to χ^2 from FB asymmetry of bottom quarks.

Overall good agreement between precision data and standard model.

As is well known, some tension between A_l(SLD) and $A_{FB}^{0,b}$ from LEP.

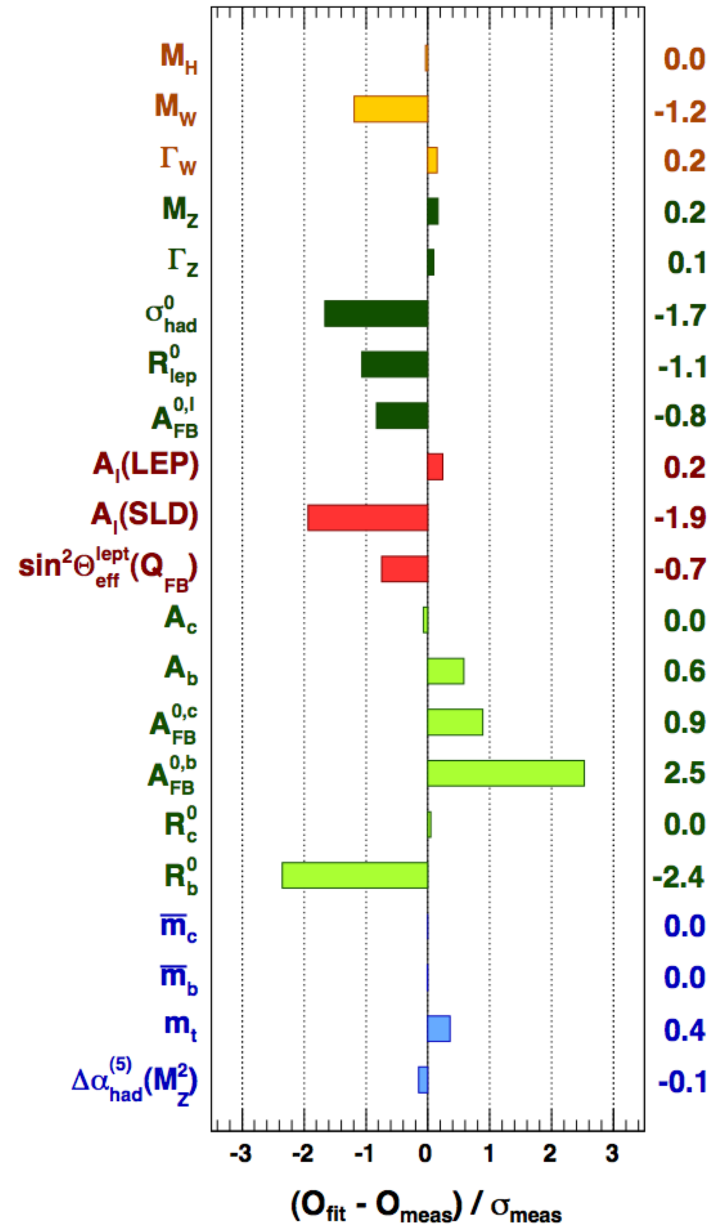

Global electroweak fit

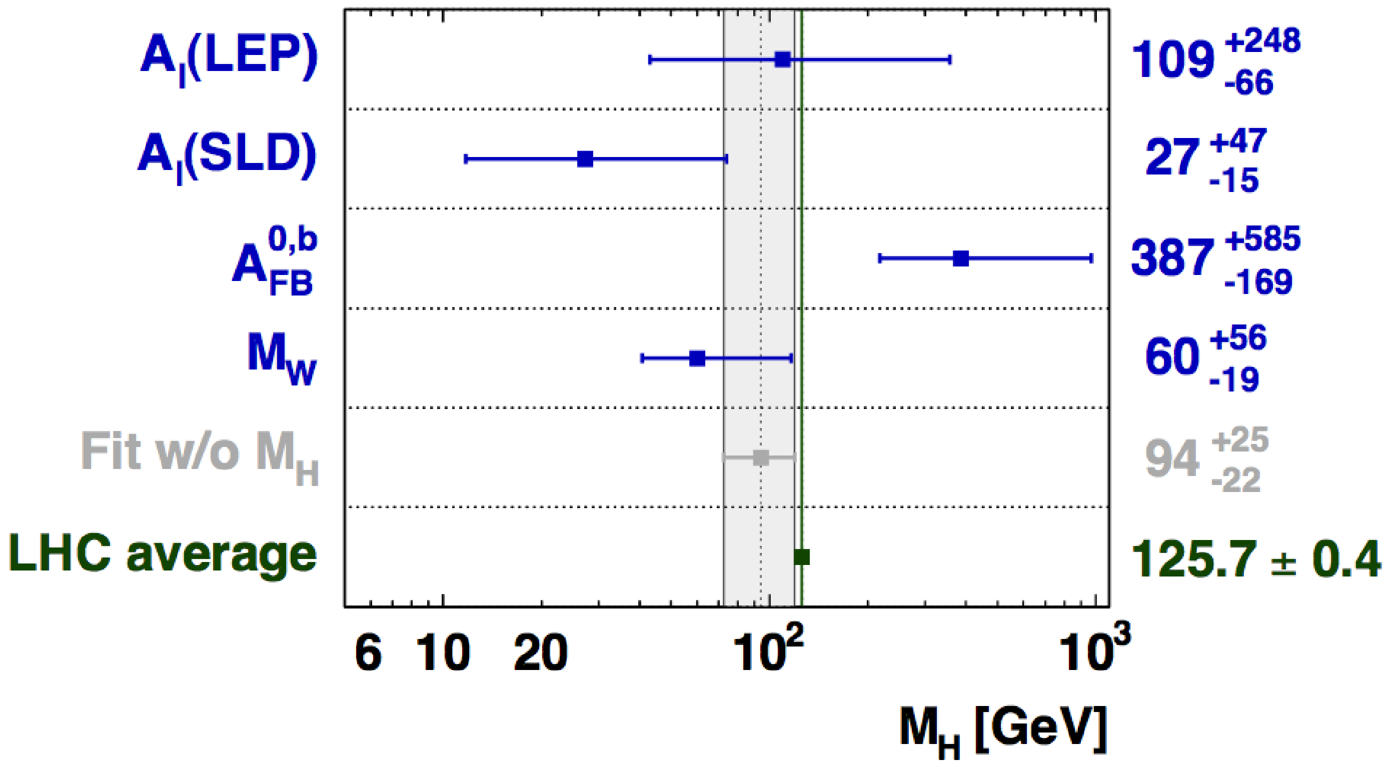

Figure 2: Left: pull comparison of the fit results with the direct measurements in units of the experimental uncertainty. Right: determination of M_H excluding the direct M_H measurements and all the sensitive observables from the fit, except the one given. Note that the fit results shown are not independent.

Hadronic contributions to $\alpha(M_Z^2)$

Electroweak fit requires the knowledge of the electromagnetic coupling strength at the Z mass scale to an accuracy of 1% or better.

Hadronic contribution for quarks with masses smaller than M_Z cannot be obtained from perturbative QCD alone (low energy scale).

Constrain photon vacuum polarisation function using measured total cross section for e^+e^- annihilation to hadrons above the two-pion threshold.

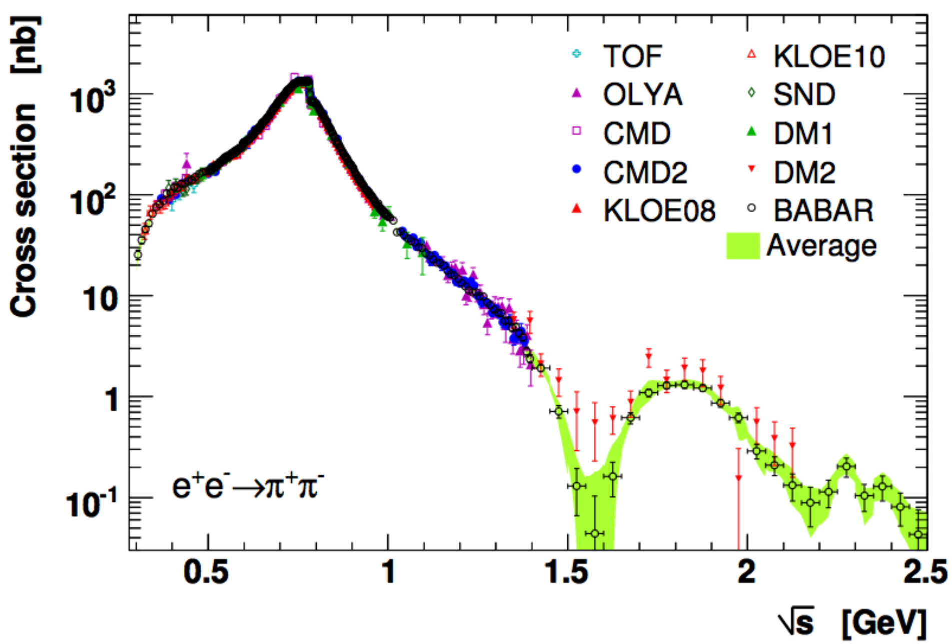

Davier *et al.*, Eur. Phys. J. C71, 1515 (2011)

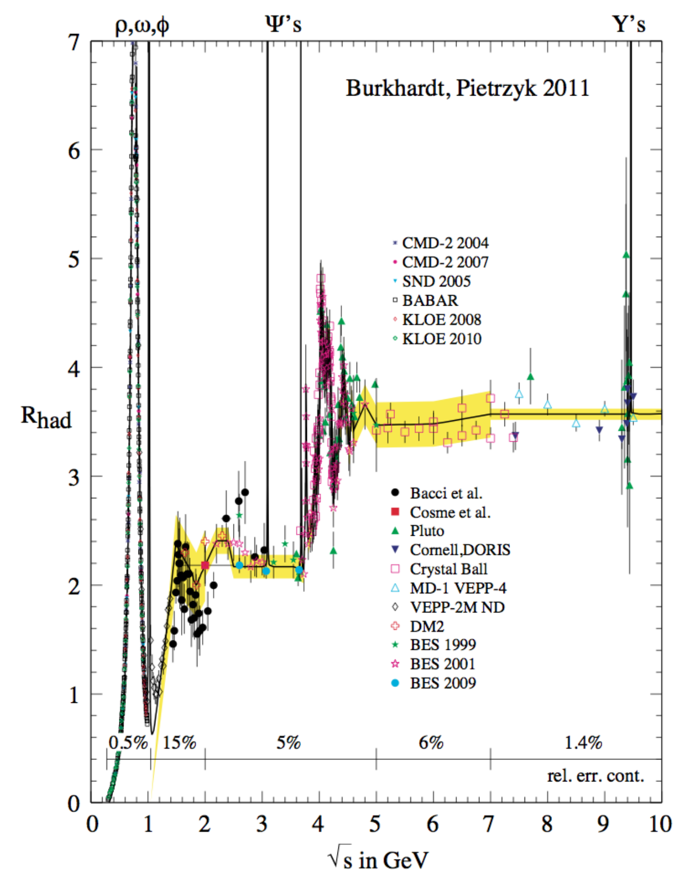

Burkhardt and Pietrzyk, Phys. Rev. D 84, 037502 (2011)

Definition of f_Z

To determine α and β we use the following strategy. Suppose $R_{EM}(E_0) = \alpha' E_0 + \beta'$, then:

$$M(Z) = \sqrt{2E(e_1)E(e_2)(1-\cos\omega)} \Rightarrow M(Z) \simeq \alpha' \times M_{true}(Z) + f_Z\beta' + \mathcal{O}(\beta'^2)$$

where

$$f_Z(true) = \frac{(E_0(e_1) + E_0(e_2))(1-\cos\omega)}{M_{true}(Z)}$$

Inspired by this observation, we fit templates of $m_{ee} \times f_Z$ for varying α and β against our Z sample.

Electron energy resolution

Electron energy resolution is driven by two components:
sampling fluctuations and constant term

Sampling fluctuations are driven by sampling fraction of CAL modules (well known from simulation and testbeam) and by uninstrumented material. As discussed before, amount of material has been quantified with good precision.

Constant term is extracted from $Z \rightarrow e\,e$ data (essentially fit to observed width of Z peak).

Result:

C = (2.00 ± 0.07) %

in excellent agreement with Run II design goal (2%)

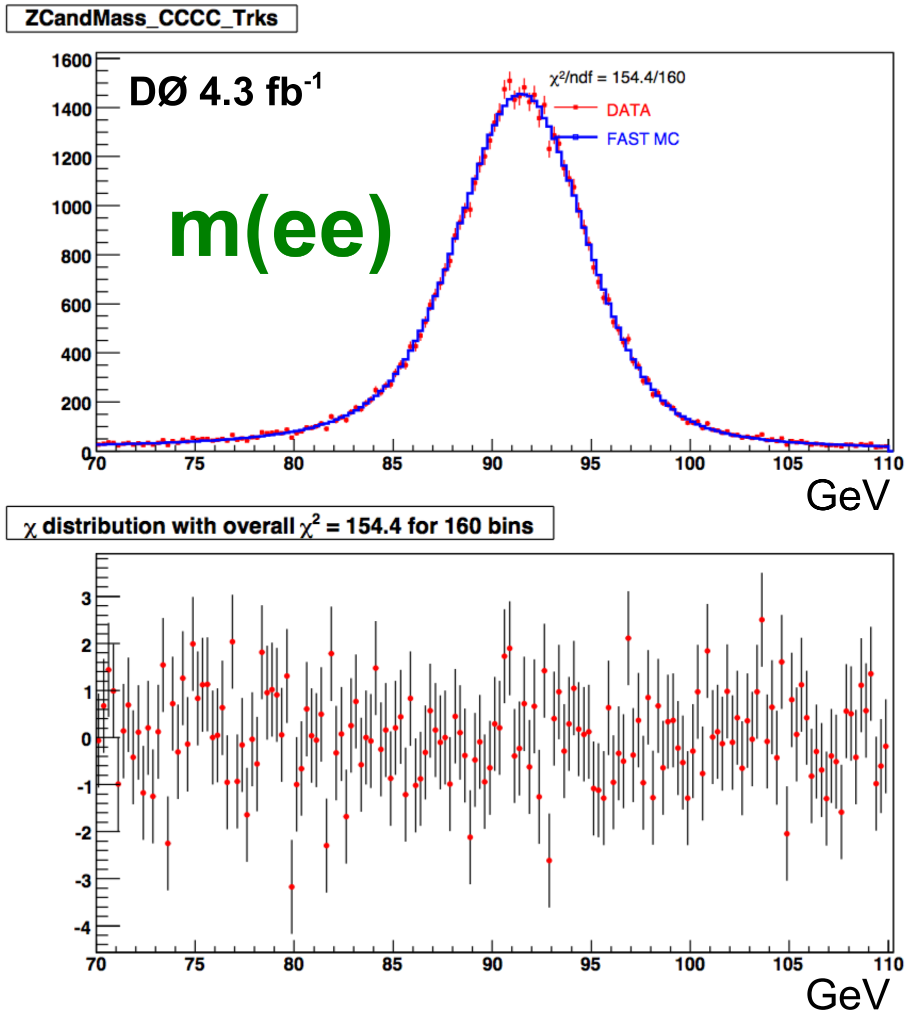

Z data

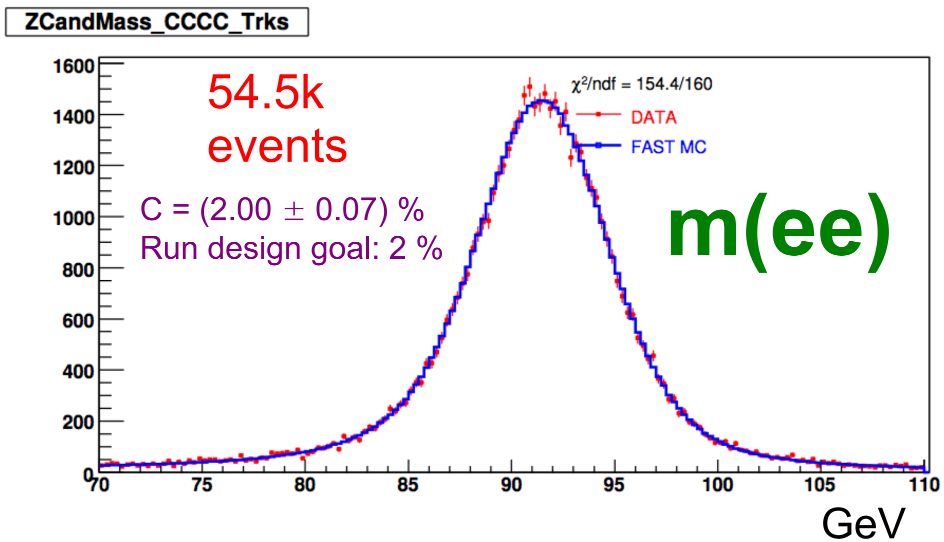

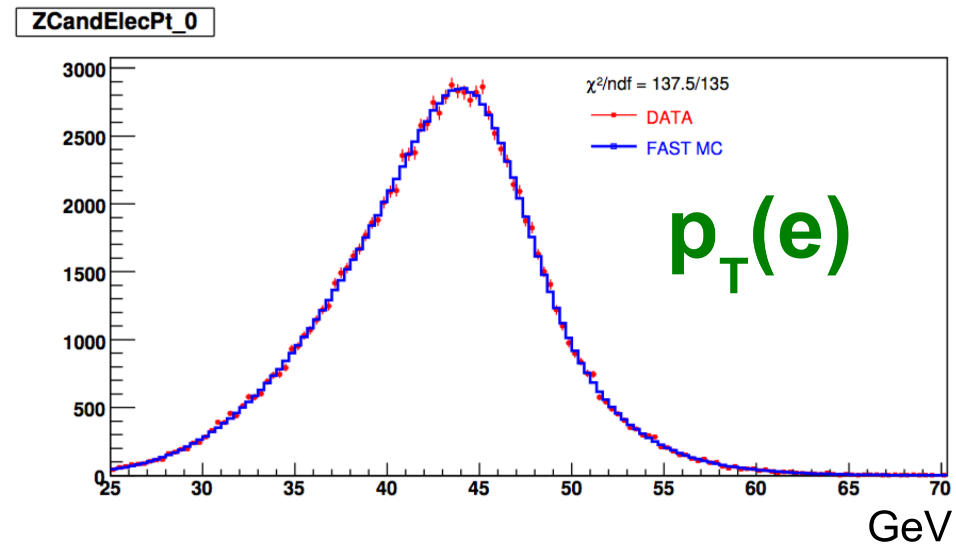

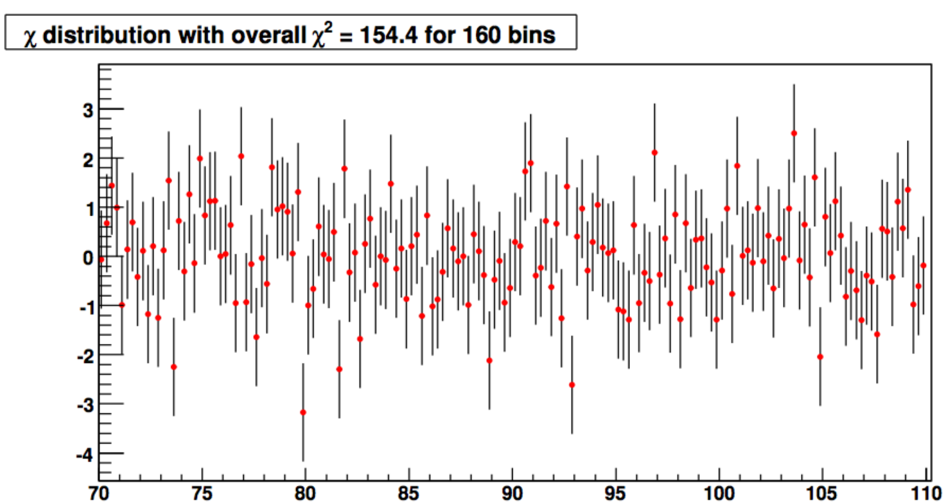

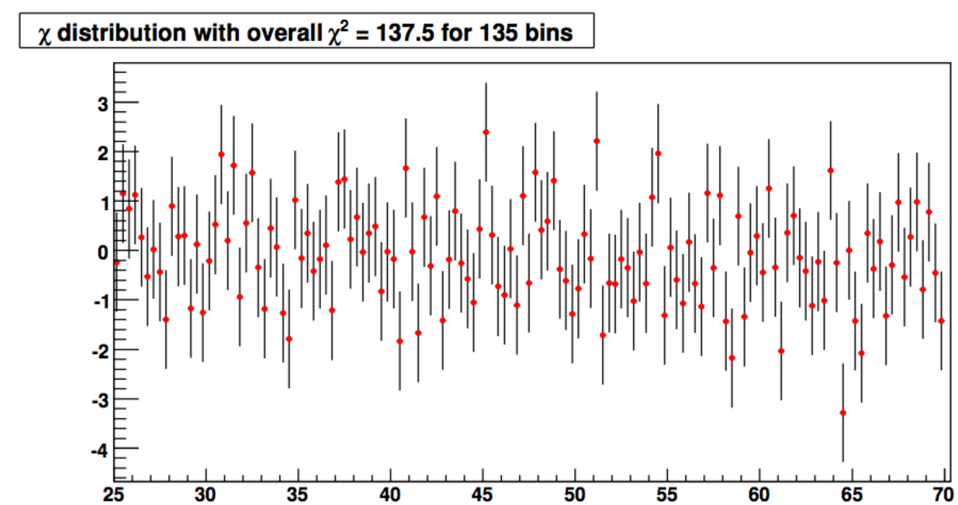

m(Z) = 91.193 ± 0.017 (stat) GeV

Good agreement between data and parameterised Monte Carlo.

Z data

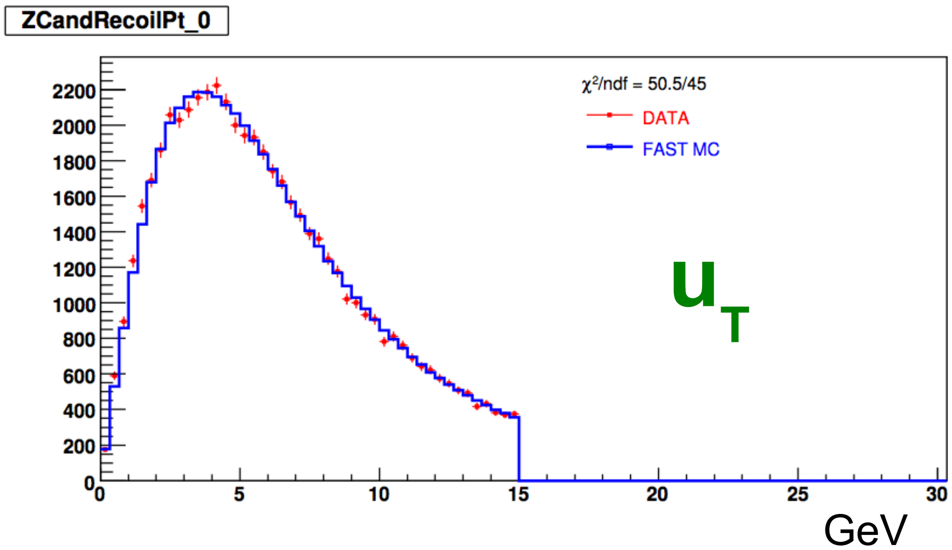

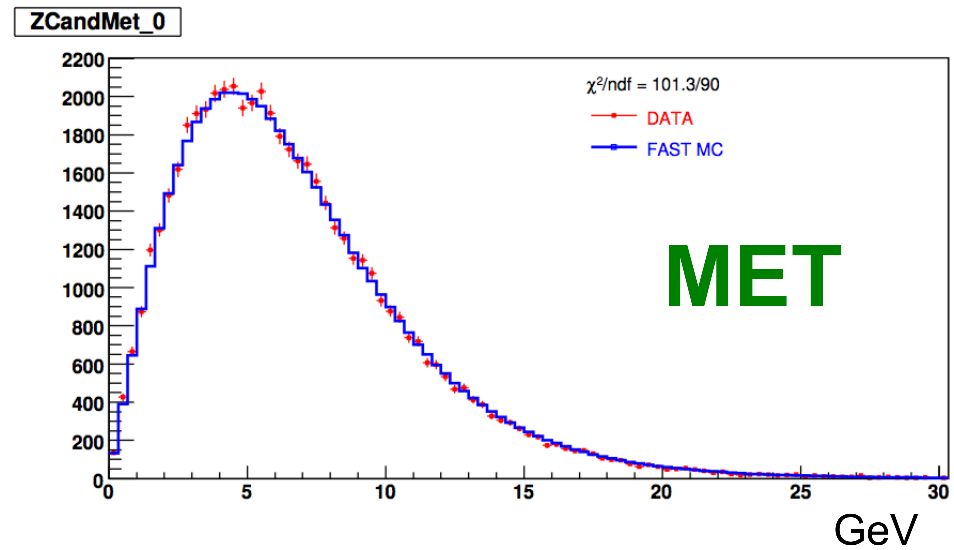

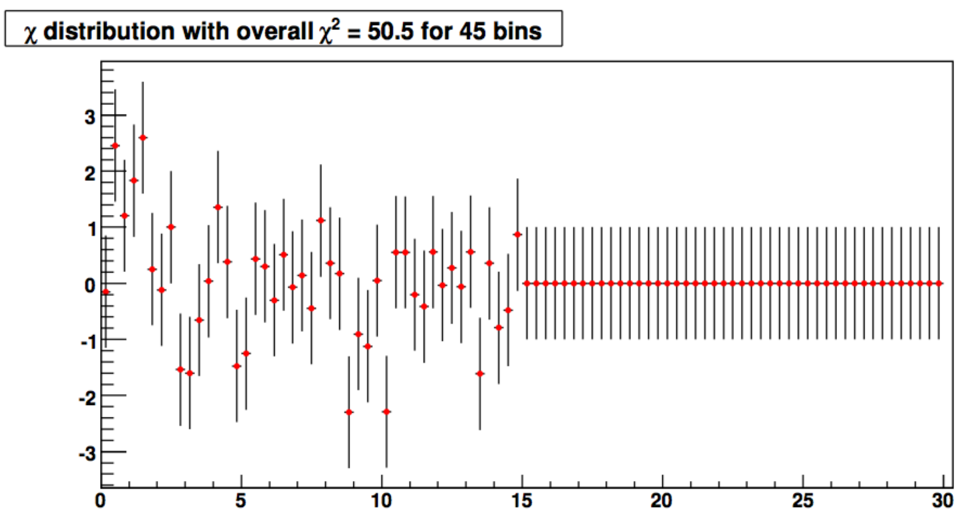

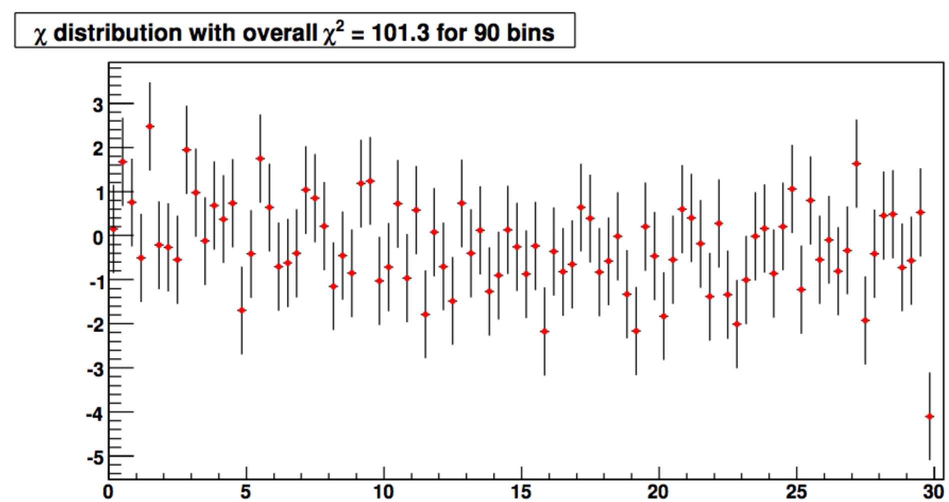

Good agreement between data and parameterised Monte Carlo.

Z data

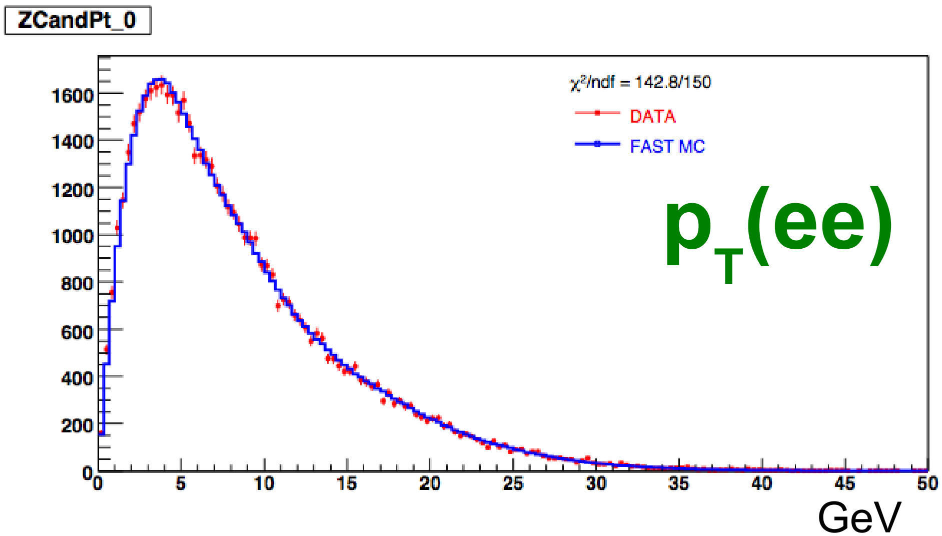

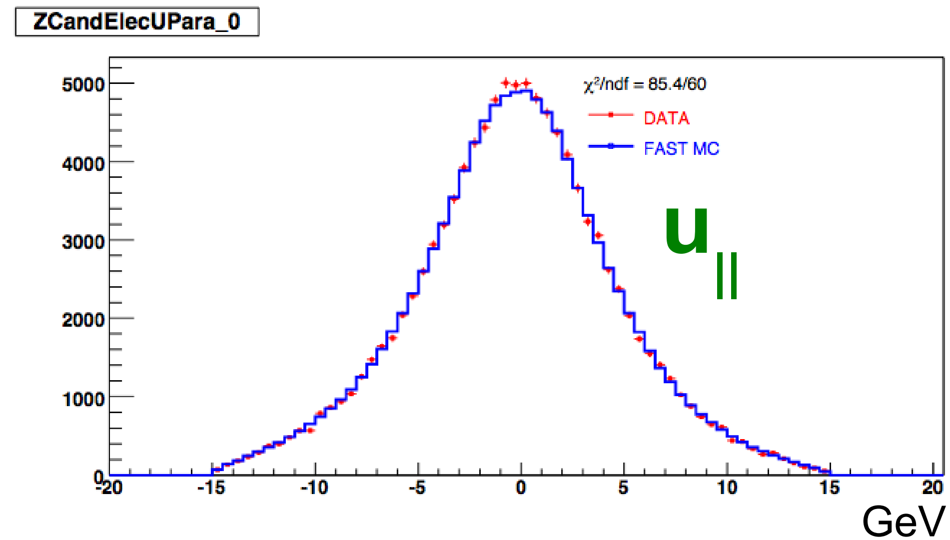

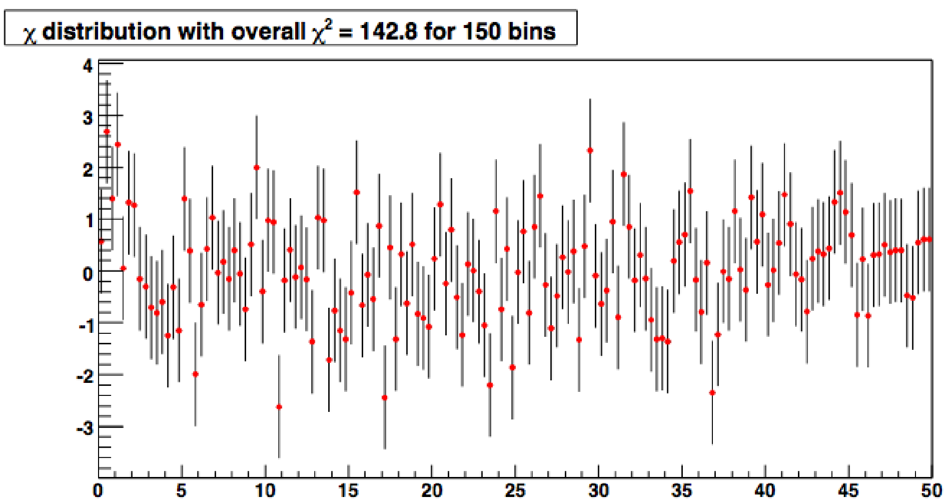

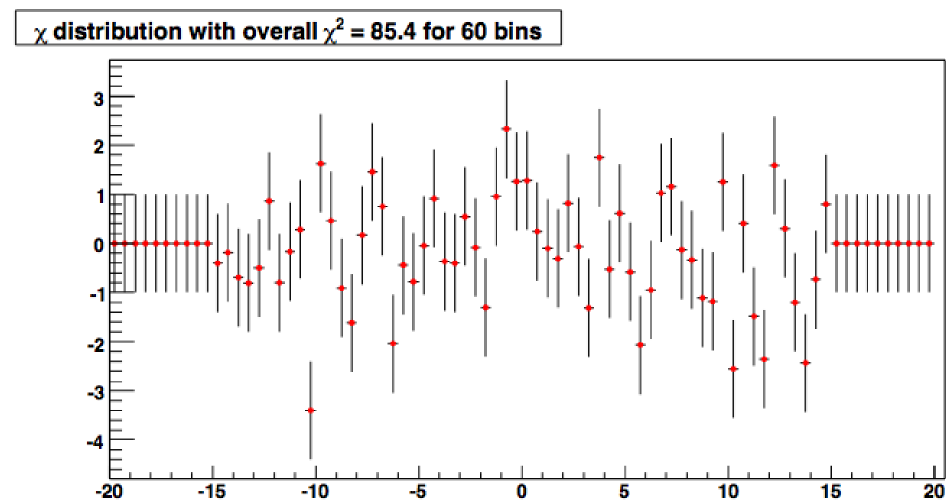

Good agreement between data and parameterised Monte Carlo.

W data

MET

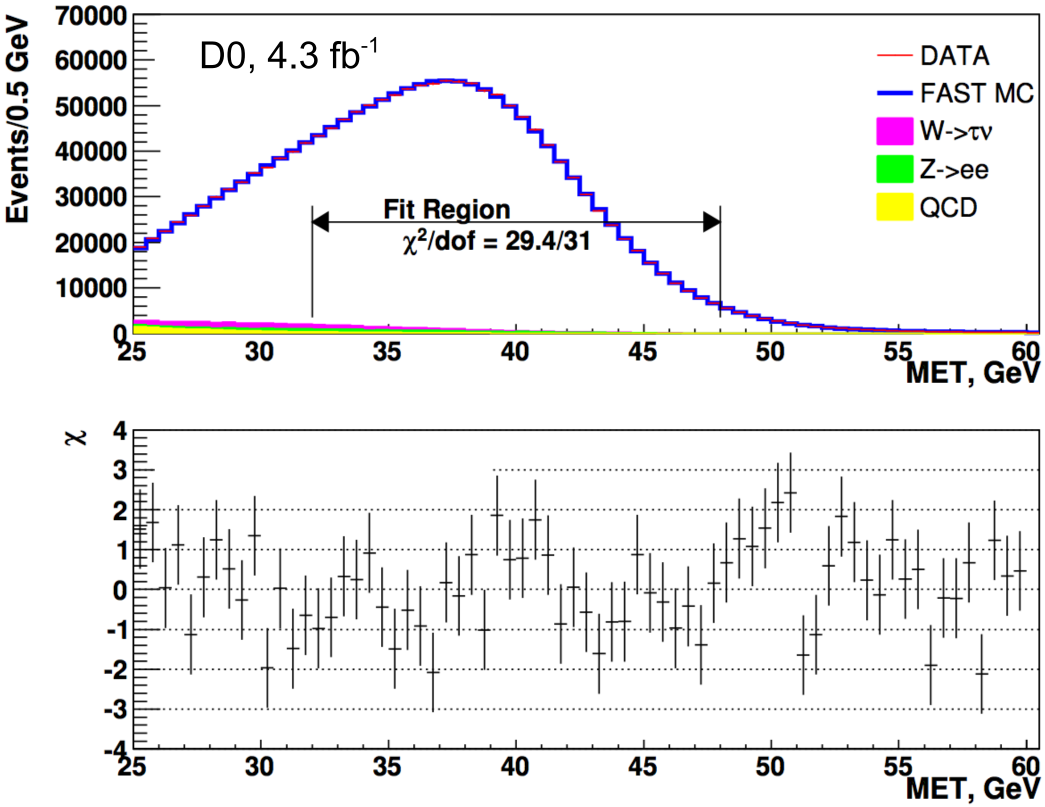

Fit results:

m(W) =
80355 ± 15 MeV (stat)

W data

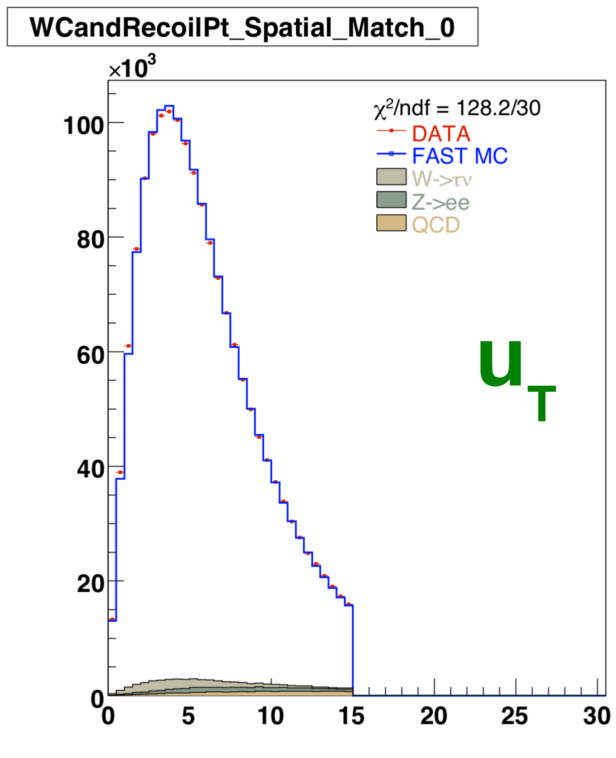

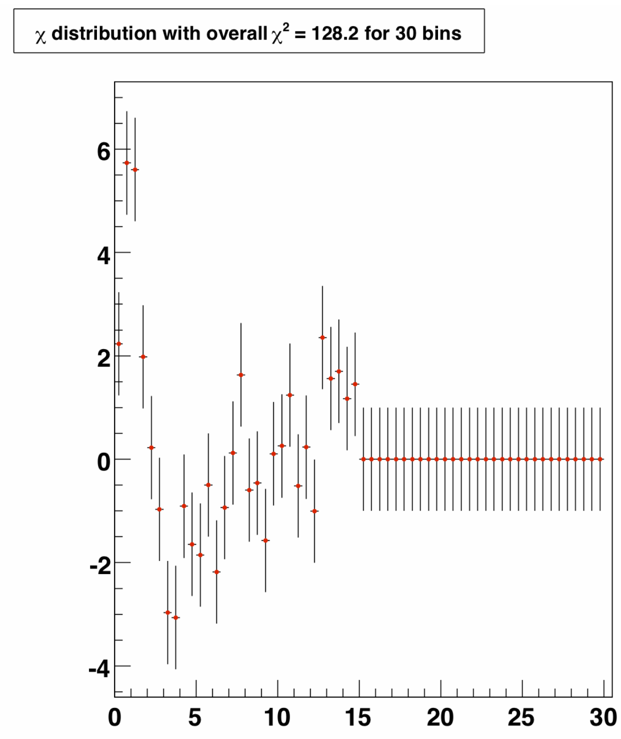

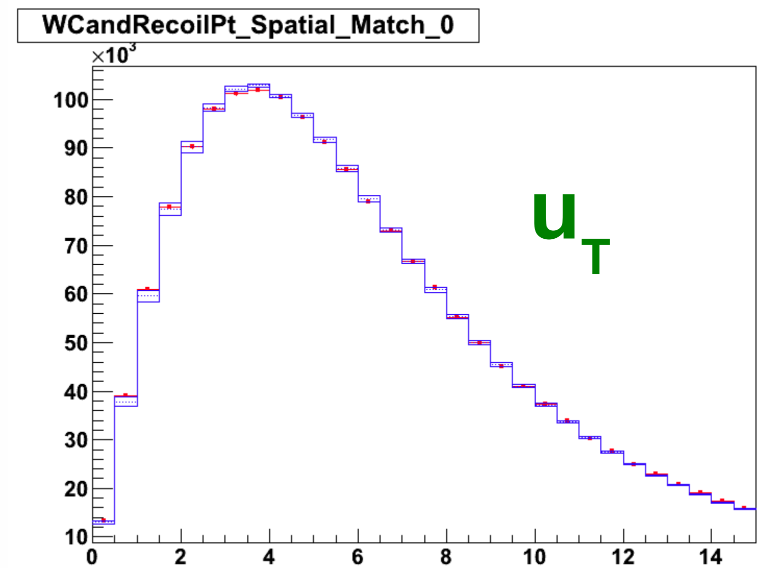

Here the error bars only reflect the finite statistics of the W candidate sample.

These are the same W candidates in the data. The blue band represents the uncertainties in the fast MC prediction due to the uncertainties in the recoil tune from the finite Z statistics.

Good agreement between data and parameterised Monte Carlo.